# Membrane Treatment of Agricultural Drainage Water: Recovery Enhancement and Brine Minimization

**Interagency Agreement 4600002097**

# DRAFT

**Final Report for the**

**Period 7/1/03 - 6/30/05**

Submitted to

**California Department of Water Resources**

By

**Yoram Cohen[1] and Julius Glater**
Department of Chemical Engineering
University of California, Los Angeles (UCLA)
Los Angeles, California 90095-1592

**Other UCLA Project Participants:**
Wen-Yi Shih, Anditya Rahardianto and Junbo Gao

September 9, 2005

[1] Author to whom correspondence should be addressed. E-mail: yoram@ucla.edu; Phone: (310) 825-8766; Fax: (310) 477-3868.

# TABLE OF CONTENTS


1.0 Synopsis ..... - 2 -
2.0 Background ..... - 3 -
3.0 Objectives ..... - 7 -
4.0 Suppression of Mineral Salt Crystallization by Antiscalants ..... - 8 -
4.1 Overview ..... - 8 -
4.2 Experimental ..... - 8 -
4.2.1 Reagents and selected antiscalants ..... - 8 -
4.2.2 Experimental System ..... 10
4.2.3 Antiscalant Ranking Methodology ..... 10
4.3 Results and Discussion: Suppression of Mineral Salt Crystallization by Antiscalants ..... 12
5.0 Impact of Mineral Salt Scaling and Antiscalant Action on RO Permeate Flux ..... 18
5.1 Overview ..... 18
5.2 Materials and Model Solutions ..... 19
5.3 Membrane Test System ..... 20
5.4 Gypsum Scaling Experiments ..... 22
5.5 Analysis of Flux Decline Experiments ..... 23
5.6 Analysis of Membrane Samples ..... 24
5.7 Establishment of Baseline Flux ..... 26
5.8 Results and Discussion: Membrane Scaling and Antiscalant Mitigation ..... 28
5.8.1 Effects of CP and Antiscalant Treatment on Permeate Flux Decline ..... 28
5.8.2 Effects of Membrane Type on Permeate Flux Decline ..... 32
5.8.3 Optical Imaging of Membrane Surface ..... 34
5.8.4 Total Surface Scale Coverage ..... 36
5.8.5 Effects of CP and Antiscalant on Local Surface Scale Coverage ..... 38
6.0 Precipitation Softening for Enhanced RO Recovery ..... 42
6.1 Overview ..... 42
6.2 Saturation Indices ..... 44
6.3 Effect of Product Water Recovery level on Mineral Salt Saturation Levels ..... 47
6.4 Calcium Removal Requirements for Scale Suppression and Enhanced Product Water Recovery ..... 52
7.0 Process Analysis and Laboratory Assessment of Enhanced Product Water Recovery with Integration of Accelerated Precipitation Softening with RO Membrane Desalination ..... 53
7.1 Overview ..... 54
7.2 Experimental ..... 55
7.2.1 Calcium Removal by Accelerated Precipitation ..... 55
7.2.2 Kinetic of Accelerated Precipitation ..... 55
7.2.3 Membrane scaling diagnostic tests ..... 56
7.3 Analysis of Recovery Limits Imposed by Gypsum and Osmotic Pressure ..... 56
7.4 Process Simulations of Integrated RO-Accelerated Precipitation Softening ..... 57
7.4.1 Overview of Simulations ..... 57
7.4.2 Single Step APS-Membrane Desalting ..... 61
7.4.3 Two-Step APS-Membrane Desalting ..... 61
7.5 Antiscalant Effectiveness ..... 66
7.6 Calcium Removal by Accelerated Precipitation Softening ..... 68
8.0 Summary and Recommendations ..... 73
9.0 References ..... 74

# Membrane Treatment of Agricultural Drainage Water: Tasks 9 through 18 – Recovery Enhancement and Brine Minimization

Amendment to DWR Agreement 4600002097

Submitted to

**California Department of Water Resources, San Joaquin District**

by

**Yoram Cohen**
University of California at Los Angeles

## 1. Synopsis

This report summarizes research conducted to: (a) refine and further demonstrate a methodology for rapid ranking of antiscalant effectiveness for suppressing mineral salt scaling based on crystallization induction time measurements; (b) develop diagnostic laboratory methods to evaluate membrane scaling propensity and scale control with antiscalants; (c) evaluate the strategies for enhanced product water recovery using accelerated precipitation softening. The present study builds on experience and knowledge gained at UCLA as part of tasks 1-8 under DWR Intra Agency Agreement 4600002097. The method developed to compare and rank antiscalant effectiveness was refined and also shown to be useful for assessing the impact of particulate matter on the induction of mineral salt crystallization. In order to quantify differences in membrane scaling propensities and antiscalant effectiveness, in suppressing membrane scaling, a series of laboratory diagnostic membrane scaling experiments and optical surface characterization techniques were developed. The approach of combining flux decline measurements due to scale formation along with optical observation of scaled membrane surfaces was shown to be effective for determining the antiscalant dose required for scale free operation. Following multi-ion analysis of the solubility of mineral salts of concern at different pH levels, the limit on product water recovery was calculated based on analysis of the saturation levels for the mineral salts of interest at various recovery levels. Based on the above analyses, a process design evaluation along with demonstrative laboratory bench scale study were undertaken to assess the technical feasibility for reaching high product water recovery via the integration of desalting by low pressure RO and nanofiltration (NF) in conjunction with chemical precipitation softening and antiscalant usage. The present study provides the basic scientific framework needed for the design of future field studies of membrane desalination of agricultural drainage water to test strategies of high product water recovery.

## 2. Background

Low pressure reverse osmosis processes offer a unique opportunity for membrane treatment of agricultural drainage water. Membranes that are specifically designed for brackish water desalting have been developed in recent years. Such membranes provide high salt rejection and flux at remarkably low operating pressures. However, in order to ensure efficient and cost-effective desalination with such membrane processes, one must combat membrane fouling and minimize the volume of concentrate (brine) generated.

Membrane fouling results from deposition and adhesion of particulate and colloidal matter (including growth of microorganisms) [1-7], adsorption of organics[8, 9], and mineral scaling [10-13]. Fouling and scaling can lead to significant reduction in membrane performance (flux reduction and salt rejection impairment) and shortening of membrane life. While various feed pretreatment technologies have been advanced in recent years for the removal of particulate and colloidal matter, mineral salt scaling remains a major impediment to successful implementation of high recovery inland water desalting. Control of surface scaling by pH adjustment has been successful for suppressing calcium carbonate scaling; however, this approach is not effective for the control of scale formation of calcium sulfate and barium sulfate salts due to negligible effect of pH on the solubility of these salts. Limited control of membrane scaling due to these sparingly soluble mineral salts, has been achieved to some degree by adding antiscalants to the feed stream [14-19]. However, the use of antiscalants is limited to relatively low levels of supersaturation of these salts and has not been extensively tested for agricultural drainage water and brackish groundwater in the San Joaquin Valley. San Joaquin groundwater has high concentrations of calcium, sulfate and carbonate (Table 2.1) and as a result these waters are at high level of saturation or may be supersaturated with respect to the mineral salts of calcium carbonate, calcium sulfate and barium sulfate.

Limited field studies conducted in the San Joaquin Valley (e.g., Buena Vista Water Storage District [2]) have been restricted to recoveries of 50-75% in order to avoid fouling and scaling problems. In the above product water recovery range the volume of concentrate (brine) stream is significant and thus brine disposal presents a major challenge. Clearly, it would be beneficial if recovery could be increased, thereby minimizing the volume of brine generated. It is important to recognize that membrane scaling and concentrate minimization are coupled. Increasing recovery will result in a higher level of concentration polarization, which in turn will increase the potential for mineral scaling of membrane surfaces.

Increased product water recovery and salt rejection both lead to greater concentration of the retentate stream relative to the feed streams as expressed by the concentration factor, CF,

$$CF = \frac{C_c}{C_F} = \left(\frac{1}{1\text{-}R_w}\right)\left[1\text{-}R_w\left(1\text{-}R_s\right)\right] \tag{2.1}$$

in which $C_C$ and $C_F$ are the retentate and feed concentrations, respectively, $R_S$ is the fractional salt rejection ($R_S$=1-$C_P$/$C_F$, where $C_P$ is the permeate concentration) and $R_W$ is the fractional product water recovery ($R_W$=$Q_P$/$Q_F$, where $Q_P$ and $Q_F$ are the permeate and feed flow rates, respectively). As an illustration, it is instructive to consider the desalination of brackish groundwater from the San Joaquin Valley using two specific water compositions (BVWSD and OAS-2548/Source B) shown in Table 2.1. The saturation indices for the above water sources with respect to the specific mineral salts of calcium sulfate (gypsum), calcium carbonate (calcite) and barium sulfate (barite) are 0.45, 12.5, 13.6 and 0.41, 6.3, 41 for the BVWSD and OAS-2548/Source B locations, respectively. These saturation levels with respect to the above mineral salts are high and can lead to concentrations (on the membrane feed-side) well above saturation under typical membrane desalting conditions. For example, for membrane desalination at product water recovery of 75% and salt rejection of 95% would result in a CF value of 3.85, with estimated saturation indices for calcium sulfate, barium sulfate and calcium carbonate for the BVWSD and OAS 2548/Source B water sources of 2.06, 57.3, 59.2 and 1.74, 28, 176.3, respectively. At the above level of product water recovery, crystallization of sparingly soluble mineral salts is expected to occur near or onto the membrane surface, leading to scale formation that results in permeate flux decline, and eventually shortening of membrane life [10, 11, 20]. Clearly, for the above water compositions and water recovery levels appropriate scale mitigation strategies would have to be implemented.

Control of membrane scaling is imperative if membrane desalination of brackish groundwater is to be adopted on a large scale. Previous studies at UCLA, with three leading commercial RO membranes, have clearly shown that various membranes scale to different degrees [11, 21, 22]. These studies have demonstrated that the two major operating parameters affecting mineral scaling are cross-flow velocity and transmembrane pressure. Surface scaling was found to increase with decreasing cross-flow velocity and increasing transmembrane pressure.

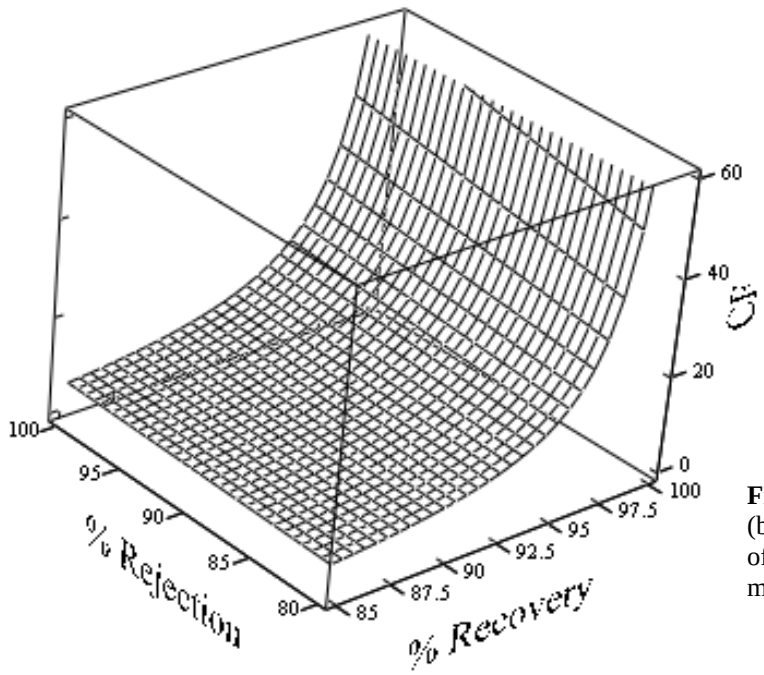


**Figure 2.1** Concentration of the retentate (brine) stream relative to the feed as a function of salt rejection and product water recovery for membrane desalting.

**Table 2.1** Examples of the concentrations of major ions in groundwater in the San Joaquin Valley

| **Major Ions** | **Concentration (mg/L)** | | |
|---|---|---|---|
| | **Buena Vista Water Storage District** [(a)] | **San Joaquin Valley OAS 2548** [(b)] | |
| | BVWSD | Source B | Source D |
| $Na^{+}$ | 1,150 | 1,080 | 2,830 |
| $Ca^{2+}$ | 555 | 224 | 430 |
| $Mg^{2+}$ | 60.7 | 104 | 249 |
| $Ba^{2+}$ | 0.17 | 0.25 | 0.5 |
| $Cl^{-}$ | 210 | 468 | 1,120 |
| $SO_4^{2-}$ | 1,020 | 2340 | 6,460 |
| $HCO_3^{-}$ | 291 | 291 | 211 |
| Total Alkalinity ($HCO_3^{-} + CO_3^{2-}$) | 238 | 239 | 173 |
| pH | 7.7 | 7.1 | 7.9 |
| TDS (mg/L) | 5,250 | 3,828 | 11,100 |
| Saturation Index with respect to calcite | 12.5 | 6.3 | 4.1 |
| Saturation Index with respect to gypsum | 0.45 | 0.41 | 0.94 |
| Saturation Index with respect to barite | 13.6 | 41 | 95.8 |

(a) Source: Lee et al. (2003); (b) Source: DWR San Joaquin Valley Drainage Monitoring Program Database (See also Table 6.1)

Studies at UCLA have shown that there is a significant difference among commercial antiscalants with respect to their effectiveness in retarding the onset of mineral salt crystallization. Limited pilot studies in California with brackish groundwater [2, 23] and with high salinity surface water [24-26] have shown that product water recovery may be limited even with the use of antiscalants. It has been suggested that one possible approach to enhancing product water recovery is to employ a strategy that involves accelerated precipitation softening (APS) to reduce the concentration of scale precursor ions from the primary RO feed, followed by filtration to remove formed crystals, acidification of the treated feed to reduce the saturation level of calcite, followed by secondary RO membrane desalting.

The use of APS to remove mineral salts from RO feed water was documented in a number of past studies [27-31]. For example, accelerated precipitation of calcium carbonate by seeding in a crystallization vessel and filtration of the outlet stream was proposed for treatment of river water [32-34], enabling recovery up to 80%. Another example, is the accelerated precipitation of calcium sulfate for desalination of mine water as demonstrated in the SPARRO process [35-37]. In the SPARRO process, in which tubular RO membranes were used, RO feed water was seeded directly to enhance bulk crystallization while minimizing surface crystallization. Although recovery levels in excess of 90% were achieved, membrane flux degradation of up to 40% (due to fouling or chemical degradation) was reported during various phases of the project. In-situ seeding as employed in the SPARRO process is impractical for spiral-wound membranes due to erosion damage of the membrane surface by bulk crystals. Therefore, the SPARRO process [35, 38] would be limited to small desalination facilities. It is interesting to note that in both of the above examples, feed water TDS was in the range of 2000-15,000 mg/*l*, which is within the TDS range observed for brackish groundwater in the San Joaquin Valley (DWR[2]; Tables 2.1).

In order to develop practical high recovery membrane processes for desalting of brackish San Joaquin Valley water, it is necessary to first develop diagnostic laboratory approaches to determine the necessary antiscalant dose and the feasibility of using accelerated precipitation softening to reduce scaling propensity. Accordingly, the present study focused on the following three major areas: (1) refinement of antiscalant effectiveness ranking via crystallization induction time measurements; (2) refinement of diagnostic membrane scaling experiments to quantify membrane scaling propensity and antiscalant dose effectiveness; and (3) demonstration of the feasibility of accelerated precipitation softening for reducing the potential for membrane scaling to enable water recovery enhancement.

[2] DWR San Joaquin Valley Drainage Monitoring Program Database

# 3. Objectives

The results from the present study along with previous diagnostic membrane desalination studies provide information needed for planning long-term field studies and for an economic assessment of drainage water reclamation by membrane desalination.

The major study tasks were intended to:

- Evaluate the kinetics of bulk (i.e., homogeneous) crystallization as impacted by antiscalant type, antiscalant dose and the presence of colloidal matter.
- Improve experimental membrane scaling diagnostics to evaluate and compare membrane scaling propensity.
- Develop an experimental protocol to quantify antiscalant treatment effectiveness and dose optimization for surpassing mineral salt scaling.
- Investigate the potential for enhancement of bulk crystallization by pH adjustment and crystal seeding.
- Evaluate potential strategies for high recovery membrane desalting via process analysis and laboratory demonstration experiments.
- Develop a framework for evaluating membrane desalting process feasibility to facilitate a rationale design field demonstration of high membrane desalting recovery.

# 4.0 Suppression of Mineral Salt Crystallization by Antiscalants

## 4.1 Overview

The effectiveness of different commercial antiscalants was evaluated based on measurements of the bulk (i.e., homogeneous) crystallization induction time for gypsum. Crystallization kinetics was monitored by on-line turbidity measurements and the impact of antiscalant dosage was quantified for selected antiscalants. The utility of the present approach for determining the relative impact of particulate matter on the crystallization induction time was evaluated using model colloidal silica particles. A direct diagnostic evaluation of the impact of antiscalant dosage on membrane surface scaling was subsequently evaluated as described in Chapter 5.

## 4.2 Experimental

### 4.2.1 Reagents and selected antiscalants

Bulk crystallization studies were carried out with aqueous model salt solutions prepared from reagent grade chemicals (Fisher Scientific, Pittsburgh, PA). De-ionized water was obtained by filtering distilled water through a Milli-Q water system (Millipore Corp., San Jose, CA). Reagent grade calcium chloride ($CaCl_2.2H_2O$), sodium chloride (NaCl), magnesium sulfate ($MgSO_4.7H_2O$), anhydrous sodium sulfate ($Na_2SO_4$) and aluminum sulfate octadecahydrate ($Al_2(SO_4)_3.18H_2O$) were obtained from Fisher Scientific (Pittsburgh, PA. Colloidal silica particles (100 nm diameter) were obtained from the PQ Corporation (South Gate, CA) and colloidal silica solutions were prepared from a stock silica particle suspension. Commercial antiscalants evaluated in the present study and in the 2001-2003 phase of the study are listed in Table 4.1. The content of non-volatile material (termed here “residual solids”) for the different antiscalants was determined by low temperature evaporation (50°C under vacuum) of 1 gram of antiscalant solution until no weight loss was observed. Ethylenediamine-tetraacetic acid (EDTA), supplied by Fisher Scientific (Pittsburgh, PA) was used as a cleaning agent for the turbidity probe and crystallization vessel and its components.

**Table 4.1.** Commercial antiscalants evaluated in the study

| Antiscalant | Chemical Description | Recommended Use | Supplier |
|---|---|---|---|
| Sokalan 30cL (S30) | Fully neutralized sodium salt of polyacrylic acid | Scale inhibitor | BASF |
| Sokalan 80sL (S80) | Polyacrylic acid | Sequestrant for calcium and magnesium | |
| KochTreat AsL 720sc | Hyperbranched dendrimer | NA | Koch Membranes |
| PreTreat 2000 | NA | Control $CaCO_3$, $CaSO_4$, $SrSO_4$ and $CaF_2$, Silica scale | King Lee Technologies |
| PreTreat 1100 | NA | Control $CaCO_3$, $CaSO_4$, $CaF_2$, $Al^{3+}$, Silica scale | |
| PreTreat 0300 | NA | Control $CaCO_3$, $CaSO_4$, $SrSO_4$ , $BaSO_4$, $CaF_2$ scale | |
| PreTreat 0400C | NA | | |
| PreTreat 0200-3 | NA | | |
| PreTreat NSF | NA | Control $CaCO_3$, $CaSO_4$, $SrSO_4$ $BaSO_4$, $CaF_2$, Silica scale | |
| PreTreat 0100 | NA | Control $Al^{3+}$, $Fe^{3+}$, $CaCO_3$, $CaSO_4$, $SrSO_4$ $BaSO_4$, $CaF_2$, Silica scale | |
| Flocon 100 | Polycarboxylic acid | Control $CaCO_3$, $CaSO_4$, $SrSO_4$ and $CaF_2$ scale | Biolab Water Additives |
| Flocon 260 (F260) | | Control $CaCO_3$, $CaSO_4$, $SrSO_4$ and $CaF_2$, iron and Silica scale | |
| BioLab DP 6000 | Phosphino carboxylic acid | NA | |
| BioLab DP 6001 | | NA | |
| Aquafeed 600 | Phosphorous acid and phosphonic acid | Inhibit the formation and growth of $CaCO_3$, $CaSO_4$ and disperse suspended solids and colloids. | Noveon, Inc. |
| Aquafeed 1000 | | Disperse suspended solids and colloids, stabilize metal ions, control $CaCO_3$, $CaSO_4$ scale. | |
| Aquafeed 1025 | | Inhibit the formation and growth of $CaCO_3$, $CaSO_4$, disperse suspended solids and colloids, stabilizes metal ions. | |
| Aquafeed 1405 | | Prevent silica fouling, disperse silica/silicate-based particulates, inhibit the formation and growth of $CaCO_3$, $CaSO_4$, disperse suspended solids and colloids, stabilizes metal ions. | |
| Phreedom 5200M | Organic phosphonate, Na salt | NA | Calgon Corp. |
| CL 4000 | NA | NA | |
| Vitec 2000 (V2000) | Phosphino-carboxylic acid polymer | Control $CaCO_3$, $CaSO_4$, $SrSO_4$ $BaSO_4$, colloid and silt scale | Avista Technologies |
| Vitec 3000 (V3000) | phosphonate-blend polymer | Control $CaCO_3$, $CaSO_4$, $SrSO_4$ $BaSO_4$, colloid and silt scale, coagulant compatible | |

### 4.2.2 Experimental System

Crystallization induction times were determined from bulk crystallization tests in a well-mixed 600 ml crystallization reactor (Figure 4.1). Mixing was accomplished using a stirring plate (1150049S, Fisher Scientific, Pittsburgh, PA) and a 2" octagonal Teflon-coated magnetic stir bar with the rpm measured using a laser stroboscope (Extech 461825, Extech Instruments Corporation, Waltham, MA). Turbidity was monitored with a back-light scattering turbidity probe (Analite 90$^{o}$) along with a turbidity meter (Analite 160) both manufactured by McVan Instruments (Mulgrave, Australia). Continuous on-line measurements of solution turbidity in the stirred crystallization reactor served to signal the onset of crystallization. Response time for the turbidity probe was essentially instantaneous, allowing accurate determination of observed crystallization induction times. Reproducibility errors for measured induction times were in the range of $\pm$5%.

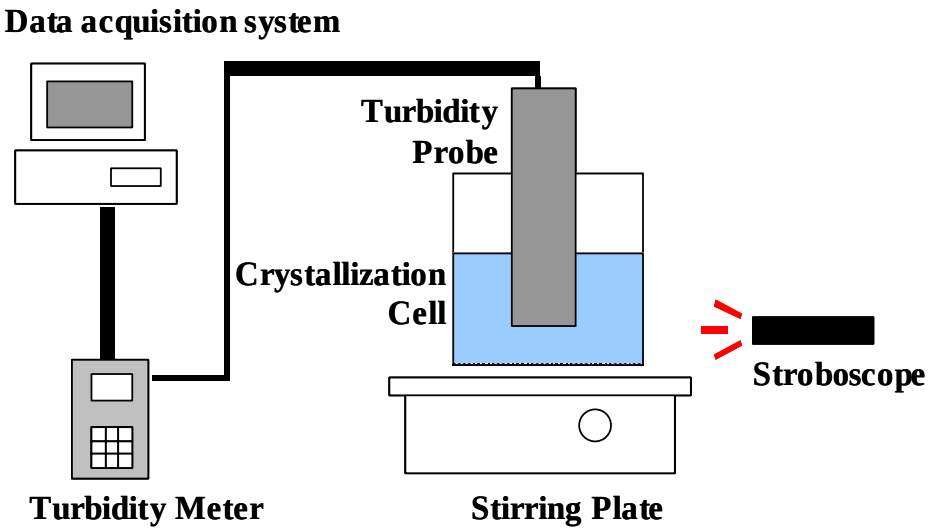


**Figure 4.1.** Crystallization system for antiscalant ranking

### 4.2.3 Antiscalant Ranking Methodology

Crystallization experiments were carried out with "model solutions" prepared from reagent grade chemicals dissolved in de-ionized water. Model solutions that contain the major ions found in San Joaquin Valley brackish groundwater were prepared. However, barium and carbonate ions were excluded in order to focus on gypsum crystallization. For the present study, the reference solution was from the Buena Vista Water Storage District (BVWSD) in the California San Joaquin Valley (Table 4.2) which had a TDS level of 5250. Chemical equilibrium

calculations indicate that the saturation index of gypsum for the reference solution is at a saturation level (S.I) of 0.450 (Table 4.2). Therefore, supersaturated solutions were prepared to enable measurements of the onset of crystallization. In preliminary studies, the onset of homogenous crystallization of gypsum (in a stirred beaker) was observed at a concentration factor (see Eq. 2.1) of CF=3.05 relative to the reference BVWSD solution only after an induction period of about 10 hours. Given the long induction time at the above CF level, it was more efficient to evaluate and rank antiscalant effectiveness for BVWSD water at a higher CF value to shorten the experimental time. Accordingly, for the BVWSD water, CF=5 and CF=6 ($SI_{gypsum}$ values of 2.93 and 3.5, respectively) were selected (Table 4.3) such that the induction time was less than 1 hour for these antiscalant-free solutions.

**Table 4.2.** Concentration of major ions present in the Reference Water Source

| Ion | Concentration | |
|---|---|---|
| | Buena Vista Water Storage District | |
| | (mg/L) | (mol/L) |
| **Cations** | | |
| $Na^+$ | 1150 | 0.05 |
| $Ca^+$ | 555 | 0.01 |
| $Mg^{2+}$ | 60.7 | 0.0025 |
| **Anions** | | |
| $Cl^-$ | 2010 | 0.06 |
| $SO_4^{2-}$ | 1020 | 0.01 |
| pH | 7.7 | |
| TDS (mg/L) | 5250 | |
| $SI_{gypsum}$ | 0.45 | |

**Table 4.3.** Model solution composition at CF5 and CF 6

| Salt | Concentration (M) | |
|---|---|---|
| | CF 5 | CF6 |
| $CaCl_2$ | 0.070 | 0.084 |
| $MgSO_4$ | 0.015 | 0.018 |
| $Na_2SO_4$ | 0.040 | 0.048 |
| NaCl | 0.170 | 0.204 |
| $SI_{gypsum}$ | 2.9 | 3.5 |

Saturation index in Tables 4.2 and 4.3 calculated using OLI Analyzer V. 2.0 [41].

Prior to each experiment, the turbidity probe was thoroughly cleaned in a sonicator with a 0.03M EDTA solution at pH 11 for a period of 0.5 hours. For each crystallization induction time determination two starting solutions were prepared. Solution #1 was prepared at CF=10 with all the required salts except for calcium chloride. Solution #2 contained only calcium chloride at a level of CF=10. For example, for the CF=5 solution, 200 mL of solution #1 was transferred to the 600mL beaker. The turbidity probe was then centrally located in the beaker so that the bottom of the probe was a distance of 4 cm from the bottom of the crystallization beaker. Subsequently, the rotational speed of the magnetic stirrer was adjusted to 800 rpm and data

acquisition was initialized. Solution #2 was then added to the 600 mL beaker, pouring along the wall in order to avoid entrainment of air bubbles. The selected antiscalant or colloidal silica were subsequently added to the solution mixture (ensuring the same total volume in all experiments) at exactly 1 minute after the addition of solution #2. The system was then covered with a black box to eliminate stray light and turbidity was monitored until it reached about 1000 NTU.

## 4.3 Results and Discussion: Suppression of Mineral Salt Crystallization by Antiscalants

Crystal nucleation begins early in the crystallization process, when a solution is at a sufficiently high supersaturation, as illustrated for gypsum crystallization in Figures 4.2 and 4.3 for a solution at CF=5 with antiscalant F260 and S30, respectively, at dosage range of 0.25-3 ppm. In the presence of the antiscalant, sequestration of calcium (ions and/or nuclei) by the polymeric antiscalant leads to a rise in the concentration of colloidal matter (calcium-bound antiscalant colloids). Consequently, there is a slow turbidity rise region which is followed by fast increase in turbidity upon the onset of rapid crystallization as the sequestration capacity of the antiscalant for calcium and/or gypsum nuclei is exhausted. With increased antiscalant dosage, there is a greater antiscalant capacity per unit volume of solution for sequestration of gypsum nuclei and adsorption onto bulk crystals. Therefore, the onset of rapid crystallization is retarded with increased antiscalant dosage. Antiscalant effectiveness can be quantified in terms of the time elapsed from the formation of the supersaturated solution to the onset of crystallization induction time; this time period is known as the crystallization induction time.

The induction time, $t_{ind}$, can be estimated from the turbidity-time curve by fitting a straight line to the linear portion of the rapid crystallization region, and further extrapolating that line to the time axis, thereby identifying the induction time [15]. The above approach was shown to be consistent with induction times obtained from more tedious calcium depletion experiments [15]. As an additional check of the reliability of the present approach, gypsum crystallization induction times were measured for the a $CaCl_2$-$Na_2SO_4$-NaCl solution, at an initial saturation index of 3.02 with respect to calcium sulfate dihydrate. The above system was previously studied by He et al. [39] who reported an induction time of 761 seconds in excellent agreement with the present determination of 763 seconds.

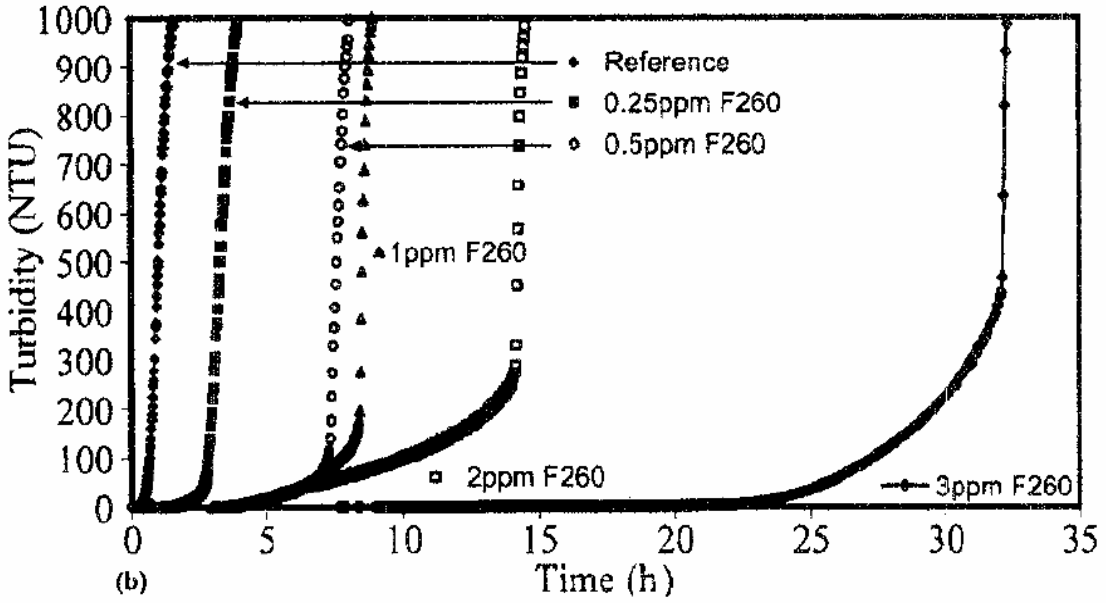


**Figure 4.2.** Gypsum bulk crystallization curves for a model solution at CF=5 (Table 4.3) in the presence of the antiscalant F260.

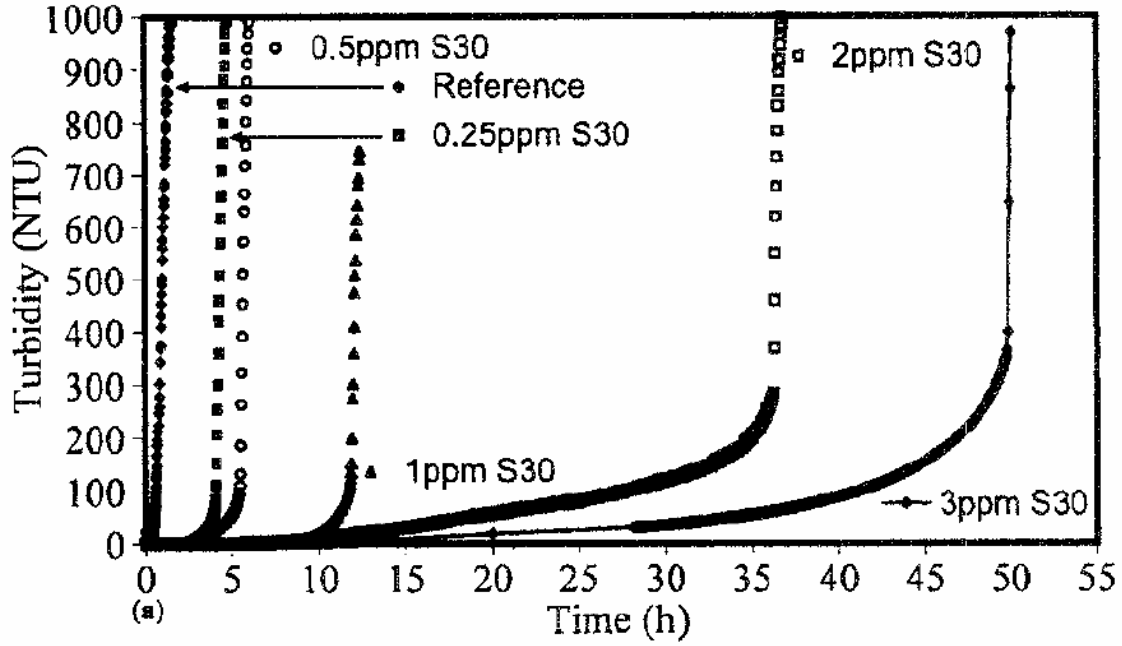


**Figure 4.3.** Gypsum crystallization curves for model solution (Table 4.3) at CF=5 in the presence of the S30 antiscalant

Crystallization induction times, in the absence of antiscalant treatment, decreased with increasing level of gypsum saturation index ($SI_{gypsum}$) as indicated in Table 4.4. For example, as the gypsum saturation index increased from 2.9 to 3.5 (Table 4.3), the crystallization induction time decreased from 0.6 hr to 0.2 hr. Similarly, antiscalant effectiveness, at a given dose, was reduced as $SI_{gypsum}$ increased, as illustrated in Table 4.4 for a dose of 1 ppm of the S30 antiscalant. It is noted that the variation of crystallization induction time on antiscalant dosage can be non-linear as illustrated in the study of Shih et al. [15]. Therefore, prior to testing antiscalant effectiveness in membrane field studies, it is imperative to first evaluate the sensitivity of antiscalant scale suppression capability with respect to the applied dose.

In an earlier UCLA study [11, 21, 22], it was clearly shown that gypsum crystallization suppression capability of different antiscalants can vary by more than an order of magnitude depending on the specific antiscalant used (Figure 4.4). Antiscalants are commercially available in various formulations (mostly in the liquid form) but the actual content of the active ingredients is often unknown. Moreover, specifications by suppliers regarding recommended applied dose are typically on a volume basis or mass of the formulation mixture without specification of the actual concentrations of the active ingredients. An illustration of percent of residual solids in the various available antiscalant formulations along with the gypsum crystallization induction times for 1 ppm dose is provided in Figure 4.4. Clearly, antiscalants differ in heir residual solids content and thus comparison of antiscalants on the basis of residual solid content is a better approach of comparing antiscalant effectiveness, which is the approach utilized in the present study.

**Table 4.4** Crystallization induction time for selected antiscalants (1 ppm dose) and model solutions.

| Antiscalant (Dosage, 1ppm) | Base Model Solution | CF[(b)] | Crystallization Induction Time (hr) |
|---|---|---|---|
| Reference Soon (No AS) | BVWSD | 5 | 0.6 |
| | | 6 | 0.2 |
| S30 | BVWSD | 5 | 11.8 |
| | | 6 | 2.1 |
| S80 | BVWSD | 5 | 1.7 |
| F260 | BVWSD | 5 | 8.5 |
| | | 6 | 1.5 |
| V2000 | BVWSD | 5 | 20.6 |
| V3000 | BVWSD | 5 | 1.7 |

(b) Concentration factor (CF) with respect to the reference model solution of Table 4.2 (see also Table 4.3)

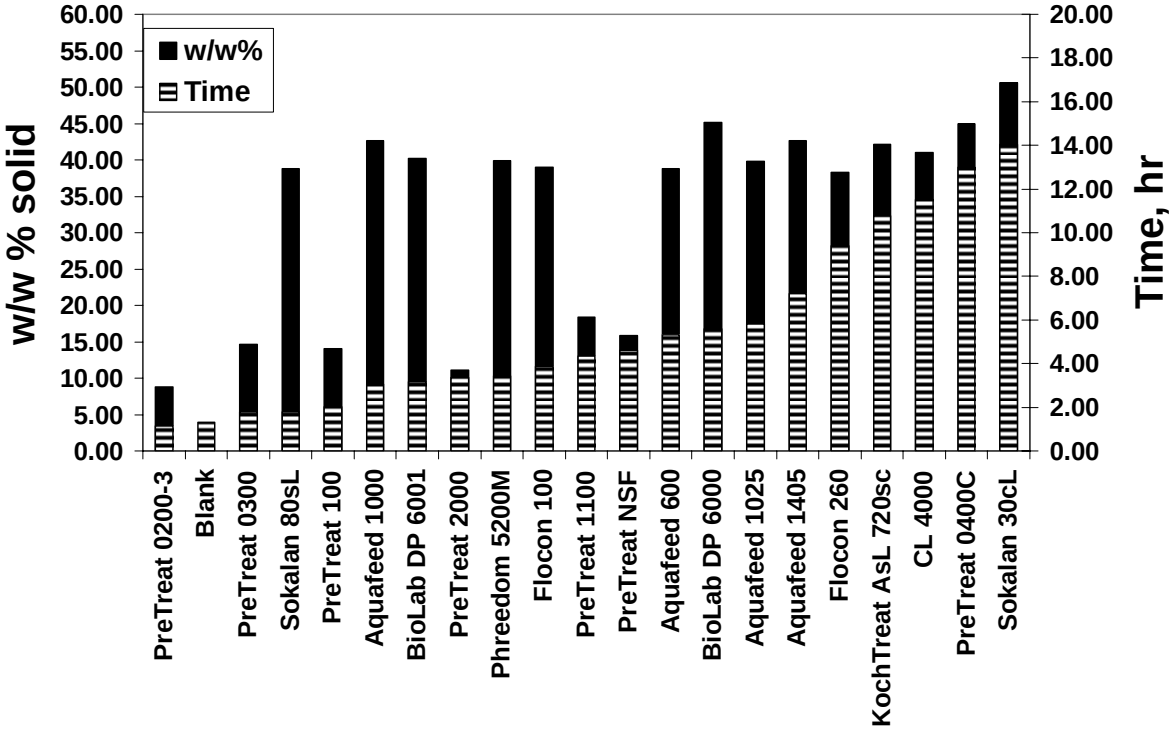


**Figure 4.4.** Gypsum crystallization induction time for different antiscalants at a dose of 1 ppm and residual solids content for various antiscalant formulations.

The potential impact of colloidal and particulate matter on membrane mineral scaling has not been previously considered in the literature. While feed filtration can remove the bulk of particulate matter and microorganisms, particles in the nanometer range are not removed. As a first step to evaluating the potential effect of nano-particles on gypsum crystallization, a series of bulk crystallization experiments were carried out in the presence of 100 nm silica particles at a concentration range of 25 mg/L – 625 mg/L. The turbidity-time plots for the silica-dosed model solutions (Figure 4.5) indicate that the onset of crystallization was retarded in the presence of silica. The induction time increased from 62 minutes (25 mg silica/L), to 580 minutes (625 mg silica/L) (Figure 4.6). It is apparent that gypsum nuclei may be adsorbed by or complex with the negatively charged silica nano-particles and those silica particles could also adsorb and/or deposit onto crystal surface, thereby suppressing gypsum crystallization.

In closure, the present study demonstrated an effective experimental approach to ranking antiscalant effectiveness on the basis of crystallization induction time measurements with a back-light scattering turbidity probe. The present approach allows rapid relative ranking of antiscalant effectiveness with respect to type and dosage. This approach is useful for antiscalant selection and assessment of the range of effectiveness with respect to antiscalant dose. Once candidate antiscalants are identified following the above approach, final antiscalant selection for specific water feed chemistry must be followed by diagnostic membrane scaling experiments as described in Chapter 5.

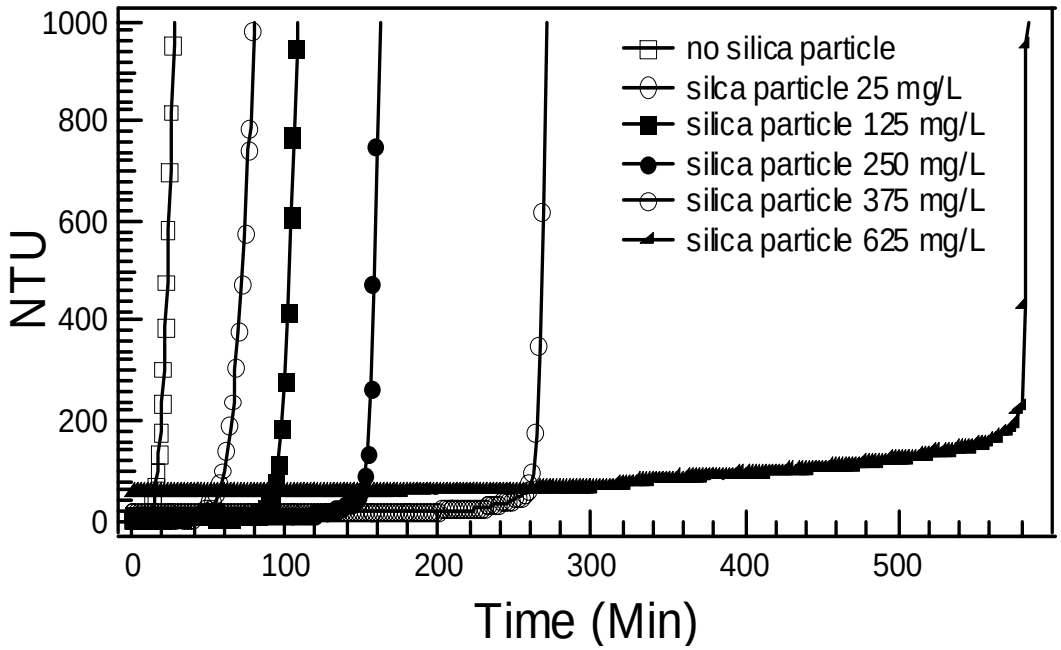


**Figure 4.5.** Effect of colloidal silica concentration on gypsum crystallization induction time. (Solution composition set at CF=5 relative to the reference solution composition given in Table 4.3).

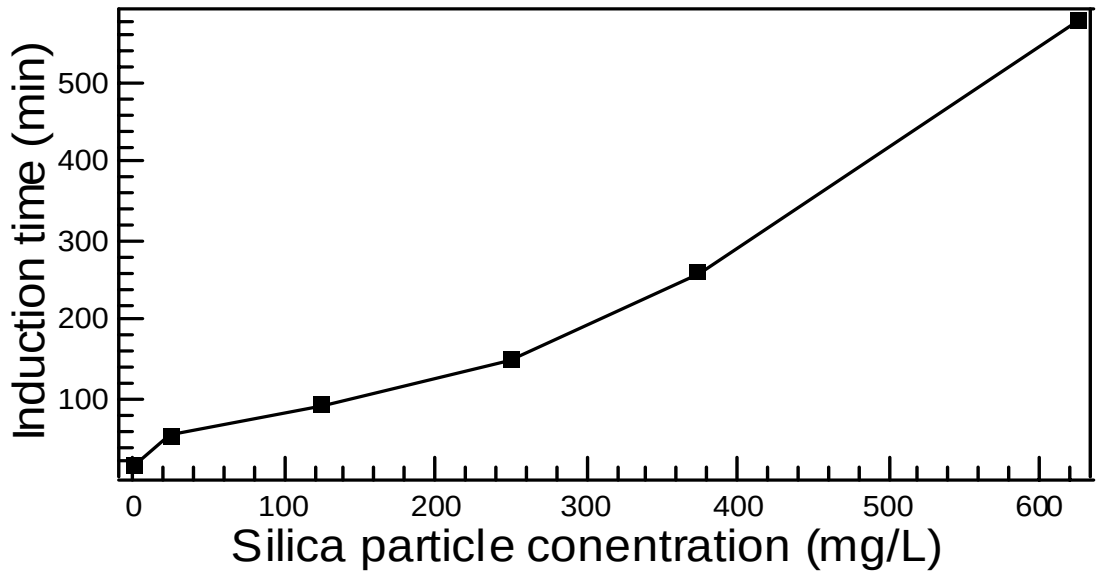


**Figure 4.6**. Correlation of gypsum crystallization induction time with colloidal silica concentration (Solution composition same as in Figure 4.5)

# 5. Impact of Mineral Salt Scaling and Antiscalant Action on RO Permeate Flux

## 5.1 Overview

Membrane desalting of brackish groundwater and agricultural drainage water is hampered by the presence of high concentration of mineral ions scale precursors. Membrane scaling by mineral salts results in flux decline and ultimately the shortening of membrane productive life. In order to evaluate the potential impact of membrane desalting process conditions (including the effectiveness of feed pretreatment strategies) on mineral scale formation, there is a need for a quantitative diagnostic membrane scaling analysis that will provide information needed for membrane plant design and operation. Previous work at UCLA has established the basis for scale characterization based on studies in a laboratory plate-and-frame RO unit using a number of leading low pressure RO membranes. The extent of membrane scale coverage was determined by low resolution optical scanning.

In the present study, an improved high resolution imaging and digital image analysis was developed to quantify the extent of scale coverage. This imaging method, along with flux decline measurements, were utilized to demonstrate the impact of process conditions and antiscalant treatment on scale suppression. Gypsum was selected as the model scalant given the greater difficulty in mitigating gypsum scaling relative to the common calcium carbonate mineral salt scalant [11, 15, 22, 27]. Studies were carried out with model solutions and the degree of supersaturation, with respect to gypsum, of the model feed solution and at the membrane surface (due to concentration polarization) was quantified in terms of the gypsum Saturation Index ($SI_{gypsum}$), defined as:

$$SI_{gypsum} = \frac{(Ca^{2+})(SO_4^{2-})}{K_{sp}} \tag{5.1}$$

where $(Ca^{2+})$, $(SO_4^{2-})$ are the activities of the calcium and sulfate ions, respectively, and $K_{sp}$ is the solubility constant (product) for gypsum. The SI for gypsum was determined via multi-electrolyte thermodynamic solubility calculations using the OLI Analyzer software [41].

## 5.2 Materials and Model Solutions

Four aromatic polyamide composite low-pressure RO membrane types, Hydranautics LFC-1 (Oceanside, CA), Koch Membrane Systems TFC-ULP and TFC-HR (San Diego, CA), and Trisep Corporation X-20 (Goleta, CA) were used. The former three membranes have been previously shown to have a low biofouling potential [2]. Water permeability, solute rejection, and surface roughness of these membranes are listed in Table 5.1. Solute rejection was determined based on conductivity measurements of RO feed and permeate from desalination of a non-scaling model solution. Surface roughness of the native membranes were obtained from AFM analysis using a Veeco Multimode atomic force microscope (Veeco Instruments, Inc., Woodbury, NY), operated in the tapping mode. De-ionized (DI) water was obtained by filtering distilled water through a Milli-Q water system (Millipore Corp., San Jose, CA). Inorganic salts, obtained from Fisher Scientific (Pittsburgh, PA), were calcium chloride dihydrate (certified A.C.S), magnesium sulfate heptahydrate (crystalline, certified A.C.S), and sodium sulfate anhydrous (granular, certified A.C.S). The antiscalant used in the gypsum scale retardation experiments was Vitec 2000 (Avista Technologies, San Marcos, CA) containing a phosphino-carboxylic acid polymer as the active ingredient.

**Table 5.1.** Commercial low-pressure reverse osmosis membrane characteristics

| **Type (Material)** | **Manufacturer** | **Lp $\times 10^7$ (m bar$^{-1}$s$^{-1}$)** | **Nominal Rejection (Model Solution)** | **RMS surface roughness (nm)** |
|---|---|---|---|---|
| LFC1 (polyamide) | Hydranautics | 9.8 ± 0.3 | 98% | 65.5 |
| TFC-HR (polyamide) | Koch Membrane Systems | 9.9 ± 1 | 98% | 66.5 |
| TFC-ULP (polyamide) | Koch Membrane Systems | 12.3 ± 0.7 | 97% | 54.2 |
| X-20 (polyamide-urea) | Trisep Corporation | 13 ± 1 | 96% | 77.2 |

Membrane scaling experiments were conducted using a model solution (Table 5.2) prepared using the mineral salts of $CaCl_2$, $MgSO_4$ and $Na_2SO_4$. This model solution was slightly supersaturated with respected to gypsum ($SI_{gypsum}$=1.01). Bicarbonate, trace metals (e.g. barium), and natural organic matter were excluded to avoid co-precipitation of calcite and other mineral salts with gypsum during the diagnostic membrane scaling experiments. Sodium and chloride concentrations in the reference solution were adjusted to ensure a charge balance. For the antiscalant effectiveness experiments, a stock solution was freshly prepared prior to each experiment by diluting a weighed amount of concentrated antiscalant solution in 500 mL of DI water.

**Table 5.2.** Composition of reference and model solutions.

| Mineral Salt | **Model Solution** |
|---|---|
| [$CaCl_2$] | $1.64 \times 10^{-2}$ M |
| [$MgSO_4$] | $1.05 \times 10^{-2}$ M |
| [$Na_2SO_4$] | $1.45 \times 10^{-2}$ M |
| Saturation Index (SI) | 1.01 |

## 5.3 Membrane Test System

Membrane scaling experiments were conducted using a laboratory plate-and-frame RO membrane recirculation unit (Figure 5.1a). This unit consisted of two test cells (Industrial Research Machine Products, El Cajon, CA) arranged in parallel, each cell with active membrane surface area of 19.76 $cm^2$ (2.6 cm × 7.6 cm) and a channel height of 2.66 mm. The distance between the fluid entrance and exit of the channel, depicted as $L_i$, was 6.9 cm (Figure 5.1b). The feed reservoir was a magnetically stirred 18-L polyethylene tank. A cooling water recirculator (Model 625, Fisher Scientific, Pittsburgh, PA) served to maintain a constant reservoir temperature. A positive displacement pump (Hydra-Cell, Wanner Engineering, Minneapolis, MN) was used to deliver up to $6.94 \times 10^{-5}$ $m^3/s$ of feed solution. Transmembrane pressure was adjusted using a back-pressure regulator (US Paraplate, Auburn, CA). A digital flow meter (Model 1000, Fisher Scientific, Pittsburgh, PA), interfaced with a PC, provided for continuous monitoring of permeate flux and accumulated volume of product water. Feed and permeate

conductivities were monitored with a conductivity meter (model WD-35607-30, Oakton Research, Vernon Hills, IL). A 0.45 μm polypropylene microfiltration cartridge (Flotrex PN pleated Filter, Osmonics, Minnetonka, MN) was used to remove bulk crystals from the continuously recycled retentate stream. Previous studies demonstrated that the use of a microfilter in this manner minimized bulk crystal deposition onto the membrane surface, making surface crystallization the dominant mode of surface scaling [11].

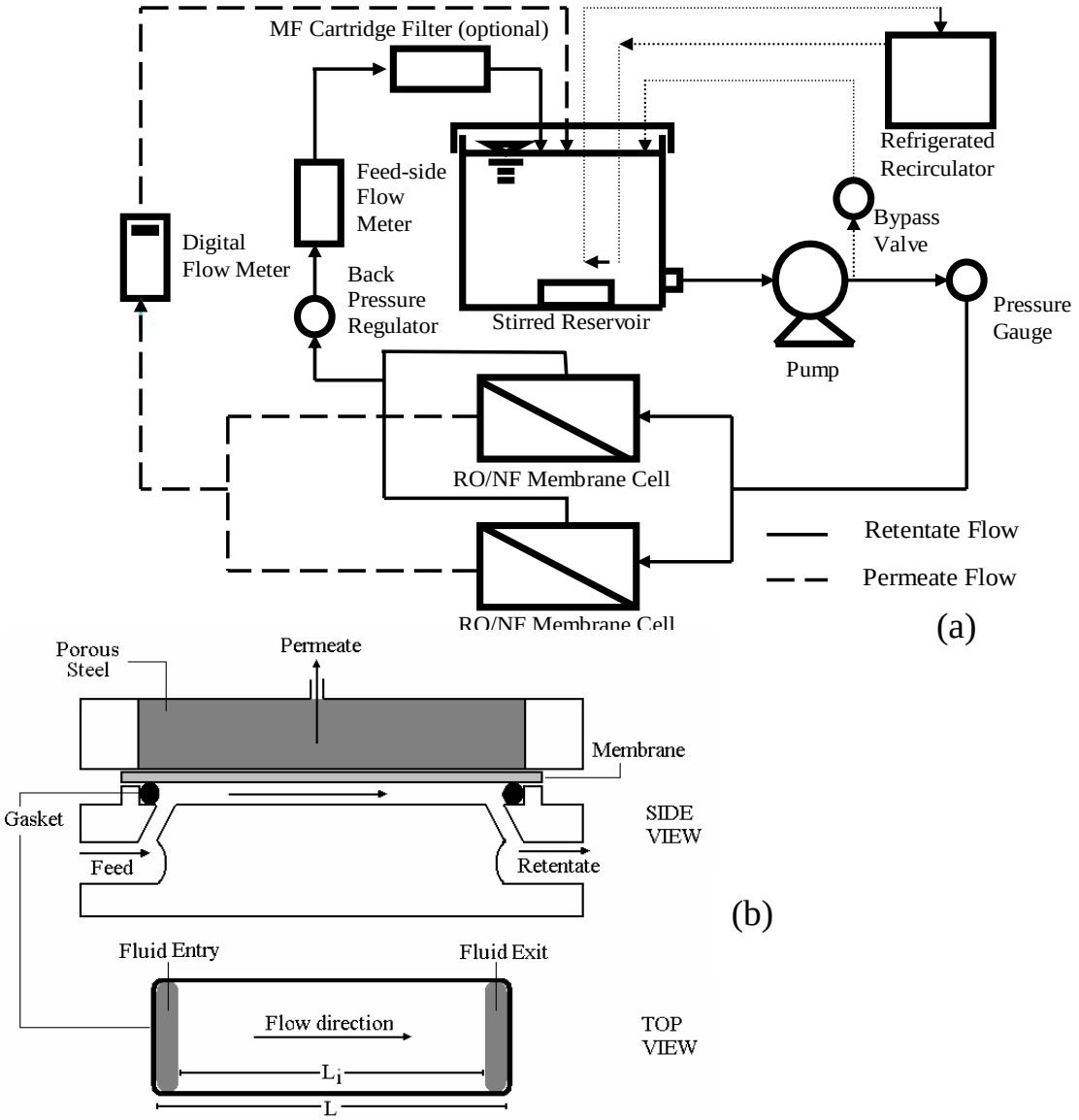


**Figure 5.1.** (a) RO membrane diagnostic system. (b) Details of a single membrane RO cell.

## 5.4 Gypsum Scaling Experiments

Gypsum scaling experiments were conducted by circulating the feed solution through the membrane channel in a total recycle mode (i.e., permeate and retentate streams were continuously recirculated to the feed reservoir) for a 24 hr period. Prior to each scaling experiment, two membrane coupons were conditioned in the RO cells by recirculating DI water through the system at a cross-flow velocity of 0.11 m/s and permeate flow rate of about 3.1 mL/min for 2 hours. This was followed by the addition of a portion of the model solution (sodium sulfate and magnesium sulfate solutions) for another 2 hours at the desired cross-flow velocity (0.1 – 0.3 m/s) and permeate flow rate of 2.4 mL/min to allow for conditioning of the membranes. At the end of the 4-hour period, the remainder of the model solution (calcium chloride solution) was added to the feed reservoir to initiate the membrane scaling experiment. Experimental runs with antiscalant addition were conducted by adding a weighed amount of the antiscalant stock solution 5 minutes prior to the addition of the calcium chloride solution.

All scaling experiments were conducted with a feed solution that was supersaturated with respect to gypsum such that $SI_{gypsum}$=1.01. For this solution, bulk crystallization was not observed even under intense mixing for a period of 3 days. Therefore, over the 24 hr duration of the membrane scaling experiments bulk crystallization would not be expected to occur in the feed reservoir. Previously it was shown [11] that the mass of gypsum scale formed on membranes, for the present plate-and-frame RO cells, was less than 10 mg for identical scaling conditions. Given the above information and the fact that in the present membrane cells product water recovery was less than about 0.3%, the feed solution composition was essentially constant during the 24 hr scaling runs. All membrane-scaling experiments were carried out at the same initial permeate flow rate of 2.25 mL/min. However, cross-flow velocity for different experiments was varied in the range of 0.1 – 0.3 m/s (500 < Re < 1350) to establish different initial concentration polarization levels and thus different solution supersaturation levels with respect to gypsum at the membrane surface.

The degree of concentration polarization (*CP*) was estimated using the classical film model [40],

$$CP = \frac{C_m}{C_b} = (1 - R_o) + R_o \exp(\frac{J}{k}) \tag{5.2}$$

in which $C_m$, $C_p$, and $C_b$ are solute concentrations near the membrane surface, in the permeate stream, and in the bulk solution, respectively. The observed/nominal salt rejection is given as $R_o=1-C_p/C_b$, $J$ is the permeate flux, and $k$ is the solute mass transfer coefficient that can be estimated from a number of available empirical correlations [22]. Equation 5.2 is an approximation since it does not account for axial development of the concentration polarization layer along the membrane channel. Numerical studies with the present RO channel geometry have shown that the CP value obtained from Eq. 5.2 is a reasonable representation of the average CP along the membrane surface. Due to concentration polarization, solution saturation with respect to gypsum will be higher near the membrane surface relative to the feed solution. The saturation index for gypsum, $SI_{gypsum}$, was calculated using the OLI aqueous thermodynamic simulation software [41]. The reported saturation index for gypsum for the scaling experiment is the value at the membrane surface at the beginning of a run, $SI_{m,0}$, calculated based on a solution concentration at the membrane surface ($C_m$) obtained based on the CP value calculated from Eq. 5.2 (i.e., $C_m = CP \cdot C_f$ ) at the observed membrane salt rejection.

## 5.5 Analysis of Flux Decline Experiments

In the absence of mineral scaling, the initial permeate flow rate ($Q_o$) is given by the classical flux expression

$$Q_o = J_o \cdot A_o = L_p(\Delta P - \Delta\Pi)A_o \tag{5.3}$$

where $J_o$ is the initial permeate flux, $A_o$ is the total membrane area, $L_p$ is the pure water permeability, $\Delta P$ is the applied pressure drop across the membrane, and $\Delta\Pi$ is the osmotic pressure difference across the membrane. It has been suggested in the literature that mineral surface scale reduces permeate flux via a pore blockage mechanism [42-45] such that the permeate flow rate ($Q$) at any given time is given as $Q = J_{free} \cdot A_{free}$, where $J_{free}$ is the permeate flux over the membrane area free of scale crystals ($A_{free}$). Thus, the fractional permeate flux decline ($FD$) is related to the fraction of membrane surface area covered by gypsum scale ($\phi$) by:

$$FD = 1 - \frac{Q}{Q_o} = \frac{J_{free} \cdot A_{free}}{J_o \cdot A_o} = \frac{A_{xtal}}{A_o} = \phi \tag{5.4}$$

Here, $A_{xtal}$ is the membrane surface area covered by crystals and assumed not available for permeate flow (i.e. impermeable scale layer assumption). The pore blockage model states that permeate flux over the membrane surface area free of crystals is equal to the initial permeate flux ($J_o$) and is not affected by scale deposit elsewhere on the membrane. Accordingly, permeate flux decline is the result of decreasing membrane surface area available for permeate flow and not due to increasing permeation resistance of a "cake" layer.

## 5.6 Analysis of Membrane Samples

Optical images of the dried membranes were obtained using a high resolution digital camera (Nikon model D100, Nikon Corp., Japan) with a 28-105 mm lens and a 4+ macro lens attachment. High contrast imaging of the scaled surface was obtained using a low angle dark-field illuminator (Model DF-200-1, Northeast Robotics, NH). The 6.2 Megapixel RAW format color digital images were converted to a 16-bit gray-scale images for subsequent image analysis. The pixels representing the scaled membrane surface area were identified by digital image analysis software (Fovea Pro, Version 3.0, Reindeer Graphics, Asheville, NC). The analysis proceeded by first applying a series of image filters to the grayscale image (Figure 5.2a) to identify crystal edges and thus determine the projected crystal surface areas. The final processed image consisted black and white pixels (Figure 5.2b) representing scaled and scale-free areas, respectively. The above image analysis consistently overestimated the scaled membrane surface area by up to about 5% as verified from application of the image analysis method to membrane surface area covered by objects of known dimensions.

The fraction of membrane surface area covered by gypsum scale, at the end of the 24-hr period (total surface scale coverage, $\Phi_{24}$), was estimated as the fraction of the black pixels relative to the total pixels (black and white). Significant amount of scale was present around the edges of the membrane in the proximity of the edge of the flow channel due to: (a) the complex flow configuration in this region, and (b) significant concentration variations near the channel edges. Therefore, in order to appropriately assess the axial variation of gypsum scaling in the direction of fluid flow, these edge effects were not included by considering only a subsection of the processed image that represented a rectangular dimension of 6.9 cm × 1.4 cm in the middle section along the membrane. This portion of the membrane image was divided into approximately 2600 rectangular slices perpendicular to the flow direction. Each slice

corresponded to a dimensionless axial location defined as $X = x/L_i$, in which $x$ is the distance measured from the middle of the slice to the channel entrance and $L_i$ is the channel length. The local surface scale coverage ($\phi_{24}$) at a given axial location $X$ was estimated as the fraction of black pixels in a given slice and noise in the $\phi_{24}$ versus $X$ data was minimized using a moving average filter with a span of about 100 slices. The limit of detection of the above method of determining the total and local measures of fractional scale coverage ($\Phi_{24}$ and $\phi_{24}$) was estimated to be about 0.01-0.02.

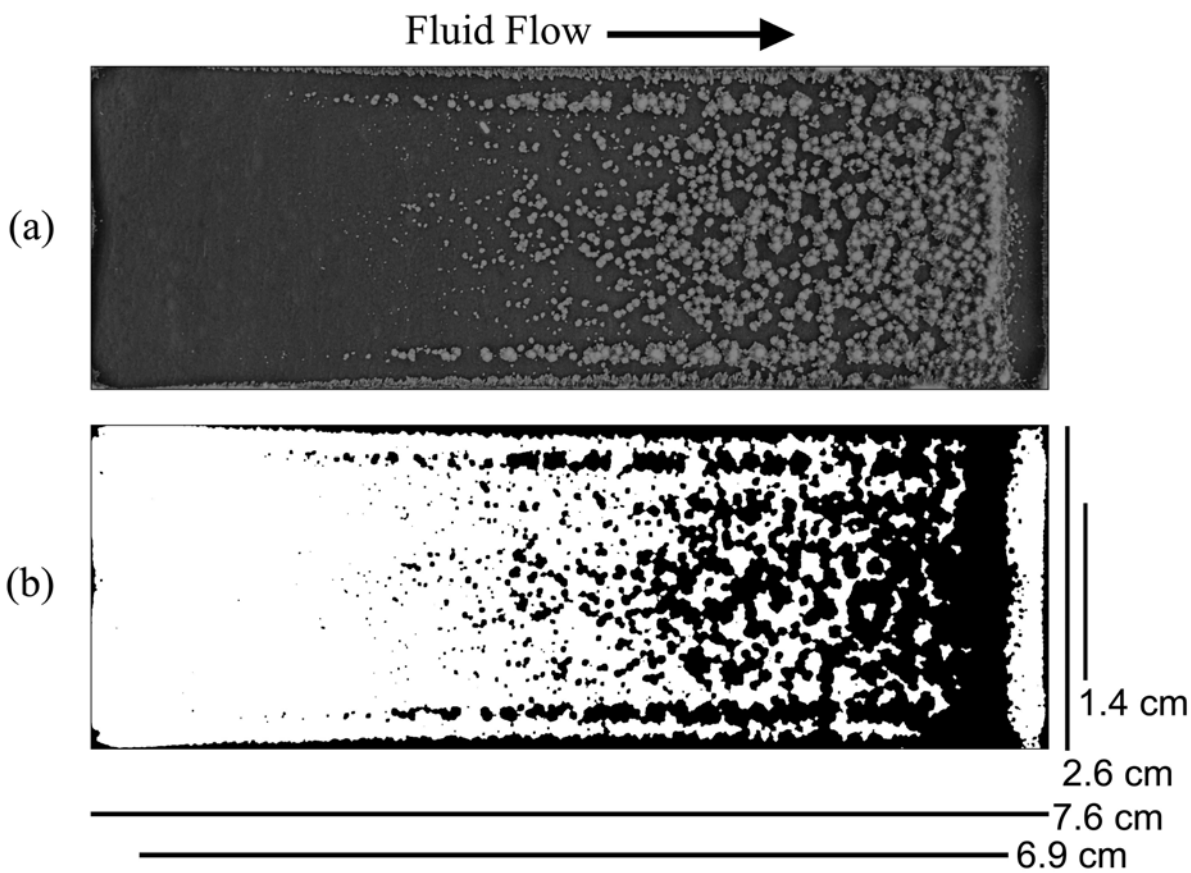


**Figure 5.2.** Optical images of scaled LFC1 membrane: (a) original gray-scale image, (b) processed image for calculation of surface scale coverage. The axial profile of surface scale coverage was determined for the central region measuring 6.9 cm x 1.4 cm.

## 5.7 Establishment of Baseline Flux

Measurements of flux decline provide an indirect measure of the buildup of scale on the membrane surface. However, it is important to recognize that there is usually a flux decline of up to about 5% (at steady state) due to membrane conditioning. In order to assess the above contribution to flux decline, a test solution was prepared similar to the scaling model solution (Table 5.2) but with equimolar amount of $MgCl_2$ substituted for the $CaCl_2$ portion of the model solution. Flux measurements (Figure 5.3a) for the four test membranes demonstrated up to about 7% flux decline (at steady state). A small degree of flux decline (up to about 5%) that was also observed (at steady state) even for 24 hr scaling runs with 5 ppm dosage of Vitec2000 antiscalant (Figure 5.3b), despite the fact that surface gypsum crystals were not observed. This flux decline trend was similar to that observed for the non-scaling solution suggesting that antiscalant adsorption, if it occurs, is not affecting flux decline. Since the degree of flux decline was different for the different membranes, the baseline flux under non-scaling conditions was taken to be the flux obtained with the use of 5 ppm of the Vitec 2000 antiscalant. This approach enabled a more accurate characterization of the contribution of scale formation to flux decline relative to the scale-free condition for the same solution composition under scaling and non-scaling conditions. Accordingly, for each membrane type, the measured permeate flux at time $t$, in the run with sufficiently high antiscalant dosage (5ppm), was taken as the baseline flux ($F_{bt}$ ). The permeate flux at time $t$, $F_t$, relative to the corresponding baseline flux at the same time, $F_{bt}$, for the given membrane, was then expressed as the flux ratio $RF_t = F_t/F_{bt}$. The fractional flux decline due to membrane surface blockage by gypsum at the end of a 24-hr period ($FD_{24}$) was defined as $FD_{24}=1-RF_{24}$. Based on the accuracy of the permeate flow meter, the experimental $FD_{24}$ values were determined within an error of $\pm$ 3 %.

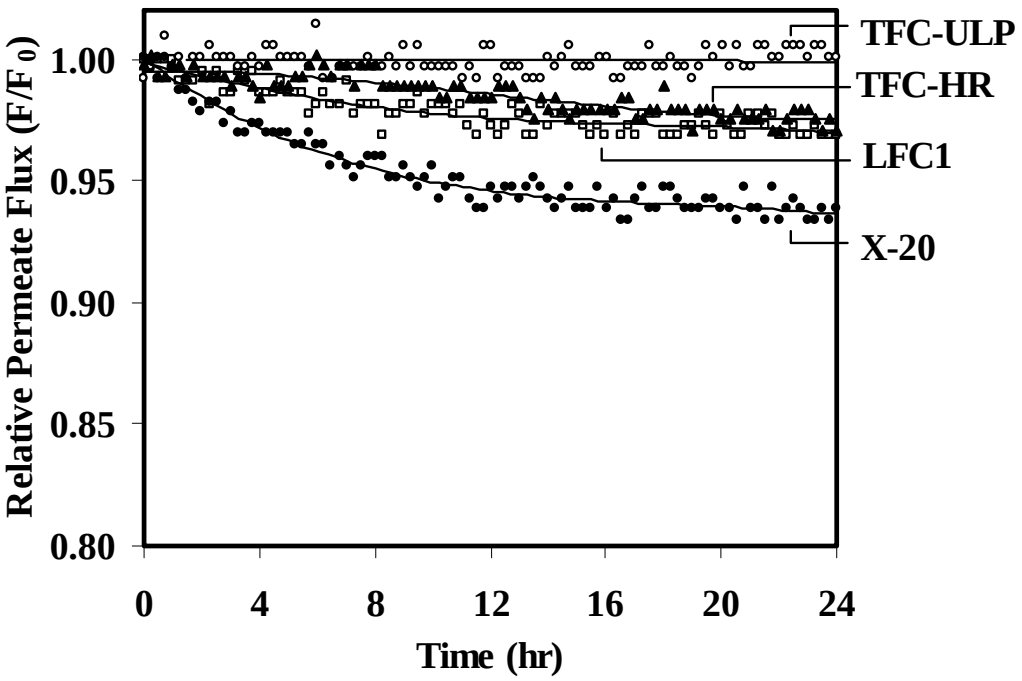


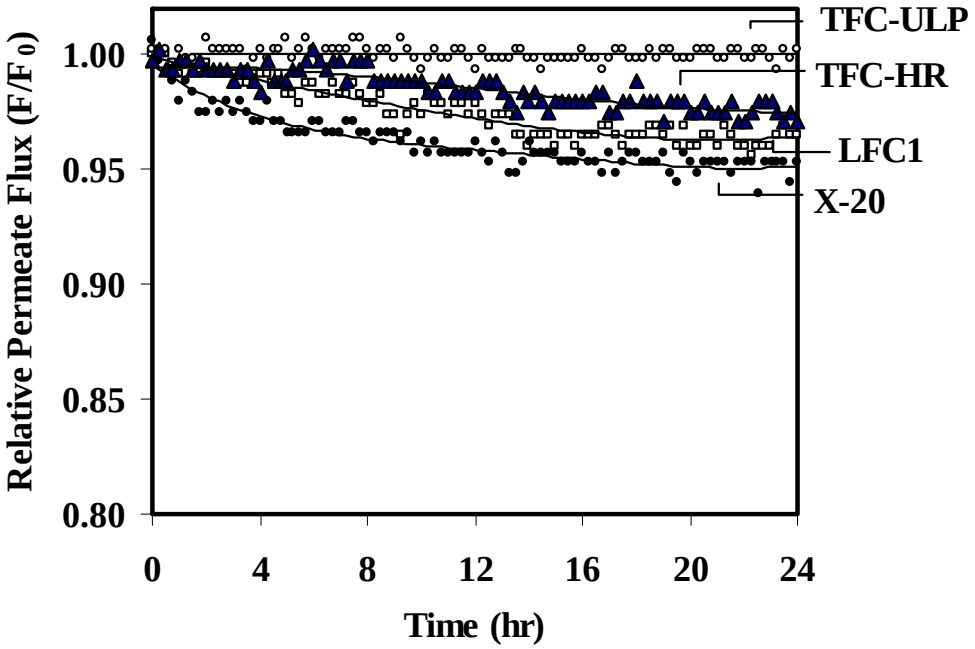


**Figure 5.3.** Relative permeate flux in non-scaling desalting experiments using: (a) non-scaling test solution (magnesium sulfate); (b) model solution (calcium sulfate) with 5 ppm VITEC 2000 antiscalant,

## 5.8 Results and Discussion: Membrane Scaling and Antiscalant Mitigation

### 5.8.1 Effects of CP and Antiscalant Treatment on Permeate Flux Decline

Permeate flux decline is the immediate and apparent consequence of surface crystallization and deposition of mineral salt crystals on the membrane surface. The driving force for surface crystallization and bulk precipitation of mineral salt in solution near the membrane surface [45] is difference between the supersaturated concentration and the concentration at equilibrium [42, 43] (i.e., solubility of the mineral salt). In most cases, given the relatively short convective residence time in RO modules, scale formation is primarily via surface crystallization. Therefore, flux decline should correlate with the saturation index for the mineral salt at the membrane surface. This behavior is demonstrated in Figures 5.4a and 5.4b for gypsum scaling of LFC-1 and TFC-HR membranes, respectively. As the gypsum saturation index, $SI_{gypsum}$, increased from 1.86 to 2.30 there was a noticeable increase in the fractional permeate flux decline from 0.04 to 0.27 and 0.04 to 0.2 for the LFC1 and TFC-HR membranes, respectively. With increasing magnitude of at the membrane surface, permeate flux decline became increasingly sensitive to small changes in the initial value of $SI_{gypsum}$ at the membrane surface where concentrations at the membrane surface were estimated based on Eq. 5.2. For the $SI_{m,0}$ range investigated (1.8-2.3) in the present work, there was a definitive correlation of $FD_{24}$ and $SI_{m,0}$ (Figure 5.5) demonstrating an exponential rise in fractional flux decline with the initial level of gypsum saturation index at the membrane surface.

Antiscalants have been known to effectively retard the onset of homogenous crystallization and slow the growth gypsum crystals, even at antiscalants doses lower than 10 ppm [11, 14, 15, 17, 19]. Indeed, as demonstrated for the LFC-1 membrane (Figure 5.6), the addition of 0.5 ppm antiscalants to the feed solution reduced flux decline by suppressing scale formation. For the LFC-1 scaling runs at initial gypsum saturation index values of 1.95, 2.08, and 2.30 resulted in the corresponding 24-hr fractional permeate flux decline ($FD_{24}$) of 0.16, 0.07, and essentially no flux decline (Figure 5.6), respectively, compared to $FD_{24}$ levels of 0.27, 0.12, and 0.04, for the same initial conditions, in the absence of antiscalant treatment (Figure 5.4a). At the given dosage of antiscalants, the retardation of gypsum scale growth, as implied by the reduction in the fractional flux decline ($FD_{24}$) strongly depended on the level of gypsum supersaturation near the membrane surface.

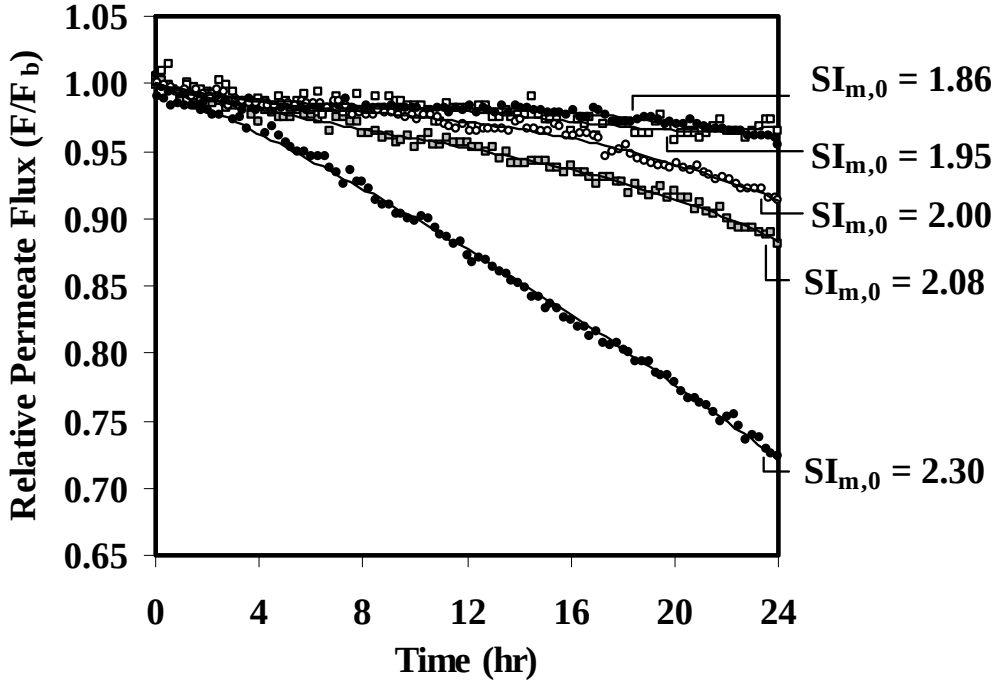


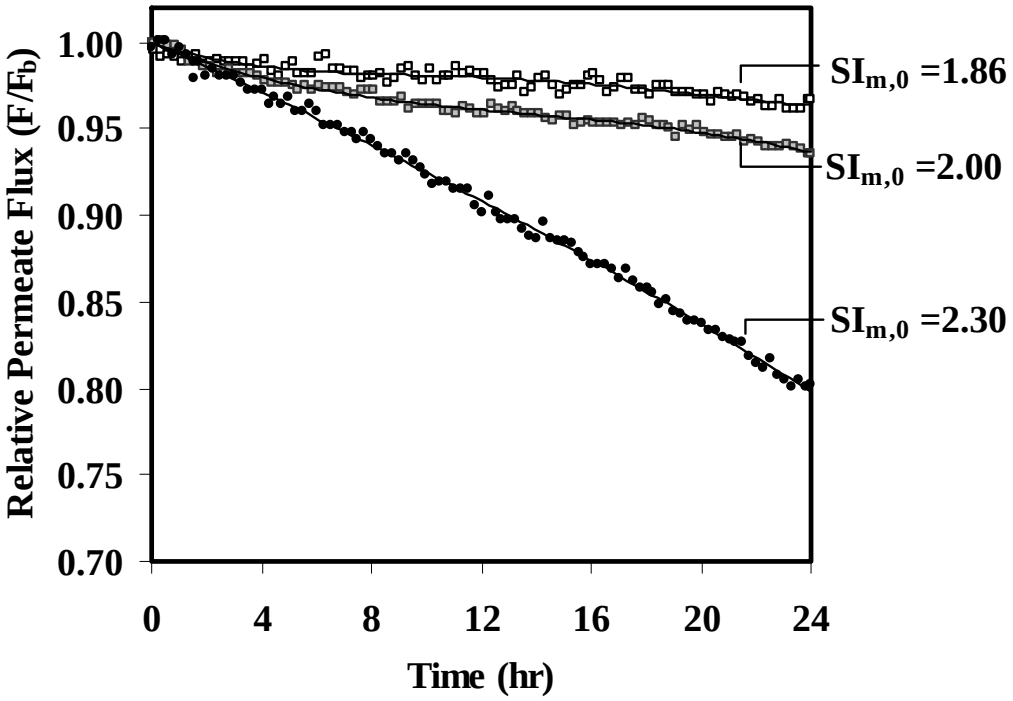


**Figure 5.4.** Relative permeate flux decline for (a) LFC1 and (b) TFC-HR membranes in desalting scaling experiments at various initial solution saturation index ($SI_{m,0}$) in the absence of antiscalant feed treatment.

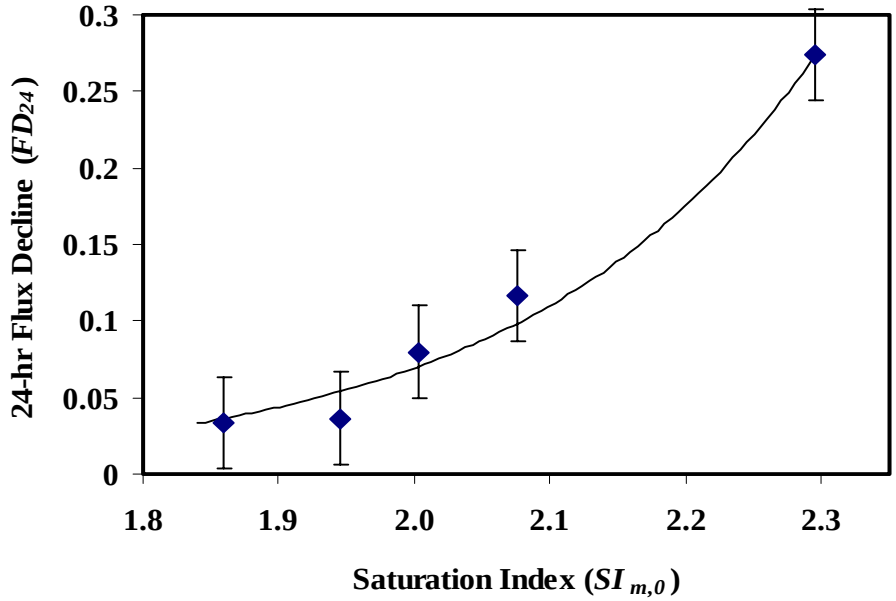


**Figure 5.5.** Permeate flux decline over 24-hr period as a function of initial solution saturation index ($SI_{m,0}$) at the membrane surface for the LFC1 membrane scaling experiments conducted without antiscalant feed treatment.

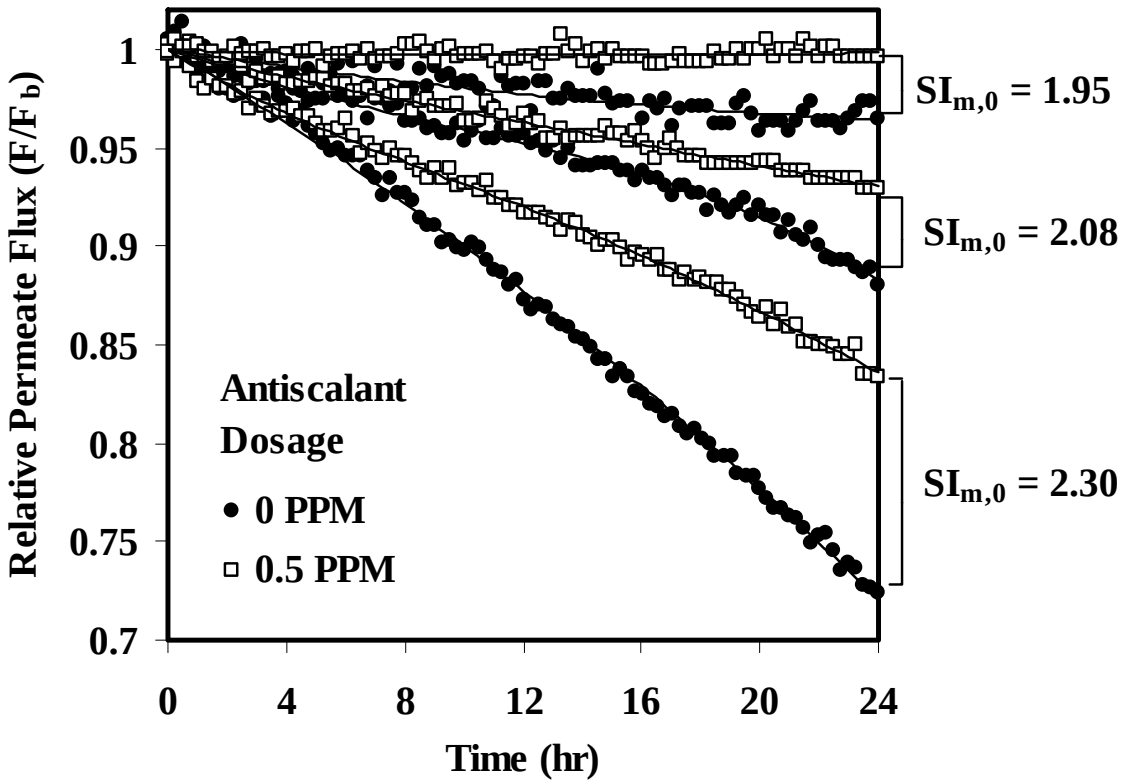


**Figure 5.6.** The effect of 0.5 ppm antiscalant addition to RO feed on the relative permeate flux decline for LFC1 membrane scaling experiment at various initial surface gypsum saturation levels ($SI_{m,0}$).

The fractional flux decline, $FD_{24,}$ at a given initial gypsum saturation index at the membrane surface (i.e., $SI_{m,0}$) decreased nonlinearly with antiscalant dose as illustrated in Figure 5.7 for scaling results with the LFC-1 membrane. In the $SI_{m,0}$ range tested (1.95-2.3), flux decline due to scaling was completely eliminated at antiscalants dosage of $\gtrsim 3\,\text{ppm}$, for the present range of $SI_{m,0}$ levels. This inhibition of flux decline suggests either a complete retardation of the onset of gypsum crystallization or extremely slow growth of gypsum crystals on the membrane surface. It is important to recognize that, the present experiments were conducted in a total recycle mode for a fixed volume of solution feed. Therefore, it was expected that, given sufficient time, eventually gypsum crystals would grow to an extent that would be manifested by a measurable level of permeate flux decline. In other words, in the present experiments the residence time of the feed stream over the membrane surface was as long as the experiment itself. In contrast, in field operations of RO desalting the solution residence time in the membrane module is equal to the convective residence time of the feed solution in the membrane module. Therefore the present approach, in which the exposure of the membrane to the scaling solution is much longer than the convective residence time in the membrane, provides a much more stringent test of membrane scaling potential and antiscalant effectiveness.

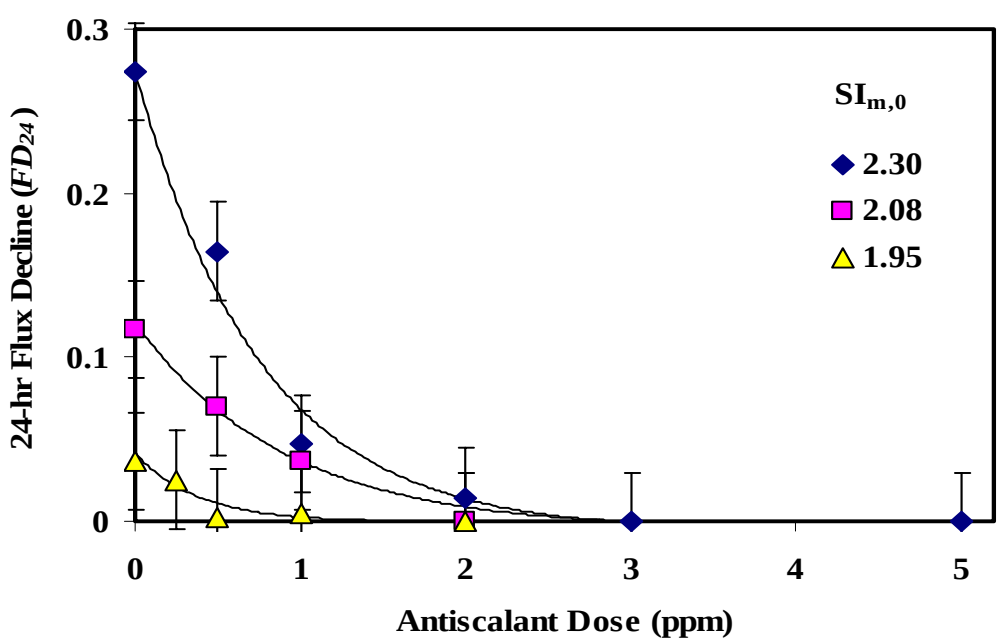


**Figure 5.7.** Permeate flux decline, for 24 hr LFC1 membrane scaling experiments, as a function of initial surface gypsum saturation index ($SI_{m,0}$) for various Vitec 2000 antiscalant dosages.

### 5.8.2 Effects of Membrane Type on Permeate Flux Decline

The scaling propensity of the four different membranes studied (Table 5.1) was compared by evaluating the fractional flux decline for scaling runs that were all carried out at identical initial gypsum saturation index of about 2.3 ± 0.02 at the membrane surface. The results for the fractional flux decline, in the absence of antiscalant addition and for a 1 ppm antiscalant dose, are shown in Figures 5.8a and 5.8b, respectively. The X-20 membrane exhibited the lowest scaling tendency (Figure 5.8a) quantified by a fractional flux decline of $FD_{24}$=0.17, followed by the TFC-HR ($FD_{24}$=0.20), TFC-ULP ($FD_{24}$=0.23), and the LFC1 ($FD_{24}$=0.27) membranes. Upon the application of 1 ppm of the antiscalant Vitec2000 the impact of gypsum scaling was reduced as indicated by the lower level of fractional permeate flux decline (Figure 5.8b). However, for this latter case, the greatest flux decline was observed for the TFC-ULP membrane ($FD_{24}$= 0.17), followed by TFC-HR ($FD_{24}$=0.13), X-20 ($FD_{24}$=0.07), and LFC1 ($FD_{24}$=0.05) membranes. The above results demonstrate that the order of membrane scaling propensity, with respect to membrane type, changes under the scale suppression action of the antiscalant. For example, the LFC1 membrane, which had the highest scaling propensity in the absence of antiscalant treatment ($FD_{24}$ = 0.27), had the lowest scaling propensity ($FD_{24}$ = 0.05) when 1 ppm of antiscalants was added to the feed solution. It is plausible that surface nucleation, adhesion and growth of surface gypsum crystals and complexation of the antiscalant with mineral salt nuclei and crystal surfaces, as well as the membrane surface, are all affected by a complex interplay of membrane topology and surface chemistry. Clearly, studies with well controlled topology and chemistry of surrogate surfaces would be needed to better understand the above observed scaling behavior.

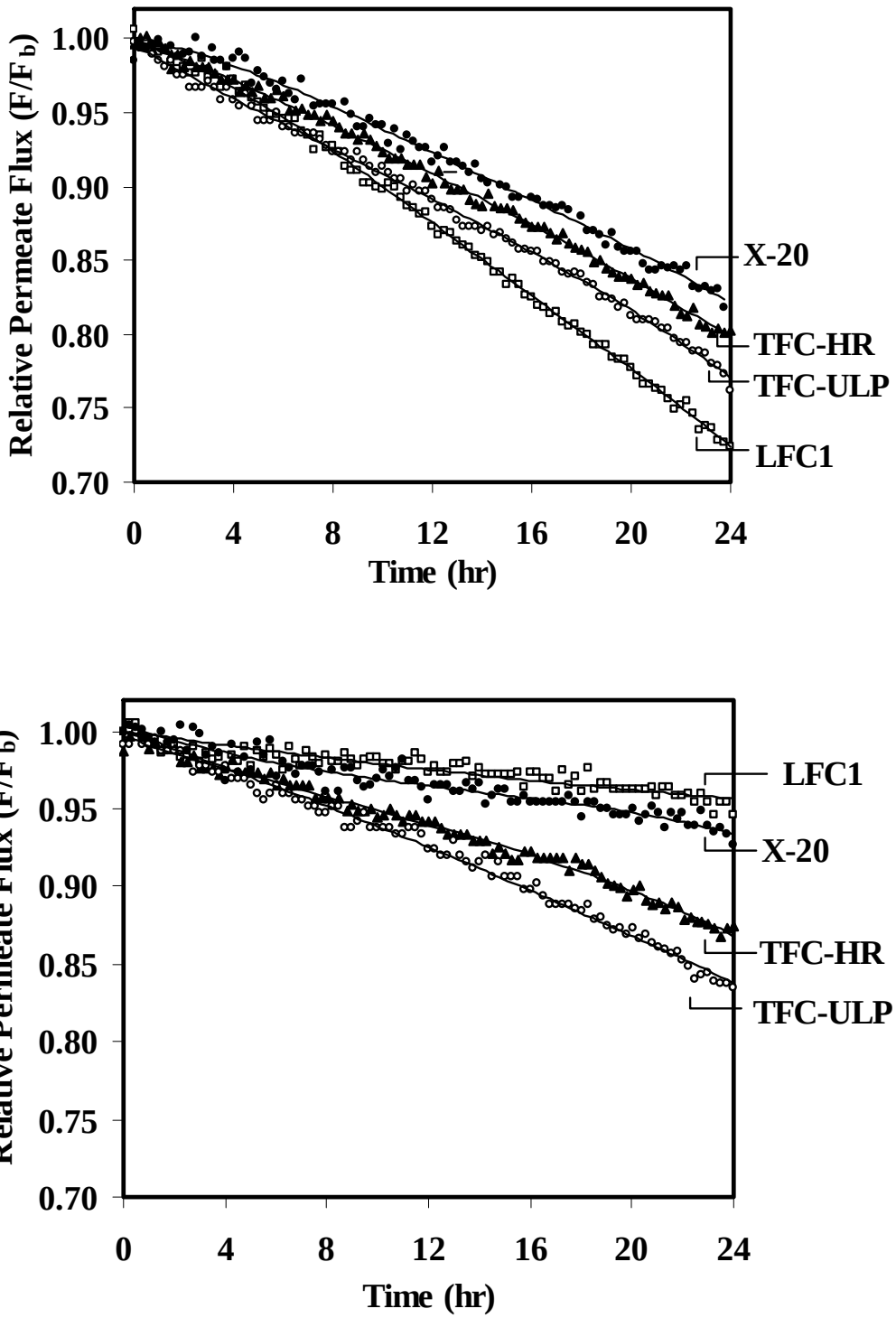


**Figure 5.8.** Relative permeate flux decline in LFC1, TFC-ULP, TFC-HR, and X-20 membrane scaling experiments at an initial surface gypsum saturation index ($SI_{m,0}$) of 2.30: (a) without antiscalant addition, (b) with 1 ppm Vitec 2000.

### 5.8.3 Optical Imaging of Membrane Surface

Analysis of optical images of scaled membranes surfaces is a direct method of examining and quantifying the extent of membrane scaling. An illustration of the approach is provided in Figure 5.9a for the LFC-1 membrane, at different initial levels of gypsum saturation index at the membrane surface, in the absence of antiscalant treatment. The optical images reveal that the extent of gypsum scaling increases with increasing supersaturation with respect to gypsum (5.9) which is consistent with flux decline measurements (Figures 5.4 and 5.5). The optical images also clearly depict an increase in scale coverage along the membrane as one approaches the exit region. The flow field, which is more uniform in the central region of the channel, becomes more complex near the channel edges and near the exit and entrance, in part, due to the protruding gaskets and placement of the exit and entrance slits (inward from the channel edges) , resulting in non-uniform distribution of surface scale traverse to the flow direction.

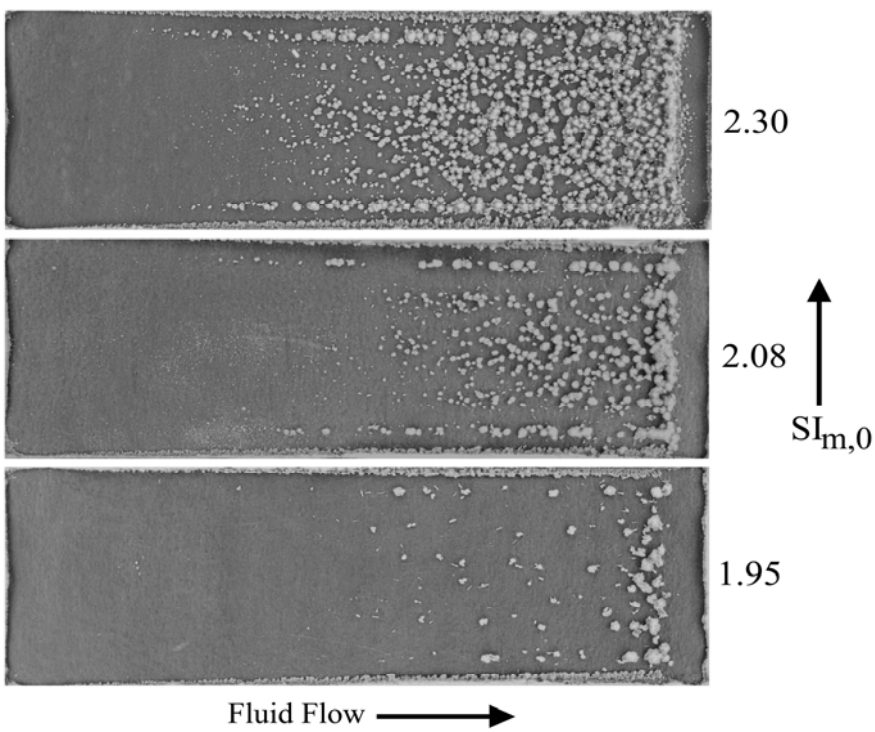


**Equation 5.9.** Optical images of LFC1 membrane scaled at initial gypsum saturation index (at membrane surface) values of 1.95 to 2.30 in the absence of antiscalant treatment.

The impact of antiscalant addition on gypsum scale formation can be observed directly via surface imaging as shown in the example of Figure 5.10 for the LFC-1 membrane in which the feed was treated the Vitec 2000 antiscalant. The scaling runs were conducted at an initial

surface gypsum saturation index of 2.3. Clearly, as the antiscalant dose increased the extent of membrane area coverage by scale also decreased. At a dose of $\gtrsim 3$ ppm the membrane surface appears to be free of gypsum crystals. It is also apparent that the formation of scale becomes progressively more restricted to the exit region as the applied antiscalant dosage increases.

Given that surface scale density is highest at the membrane exit region, it is most convenient to visually compare membrane scaling propensity based on scale coverage in that region. Accordingly, a comparison of the extent of gypsum scale coverage for the four different membranes is shown in Figure 5.11, at the same level of initial surface gypsum saturation index (2.3±0.02). The images depict noticeable differences in scaling propensity among the different membranes. It appears that the LFC1 and the X-20 membranes responded more favorably to 1 ppm antiscalants treatment relative to the TFC-ULP and TFC-HR membranes. A similar trend was also observed at an anticipant treatment dose of 3 ppm in which trace of gypsum scale was still apparent on TFC-HR and TFC-ULP membranes. As the antiscalant dose was raised to 5 ppm and above (not shown), optical images of the membranes (Figure 5.11) suggest that surface mineral scale was completely suppressed for all the membranes.

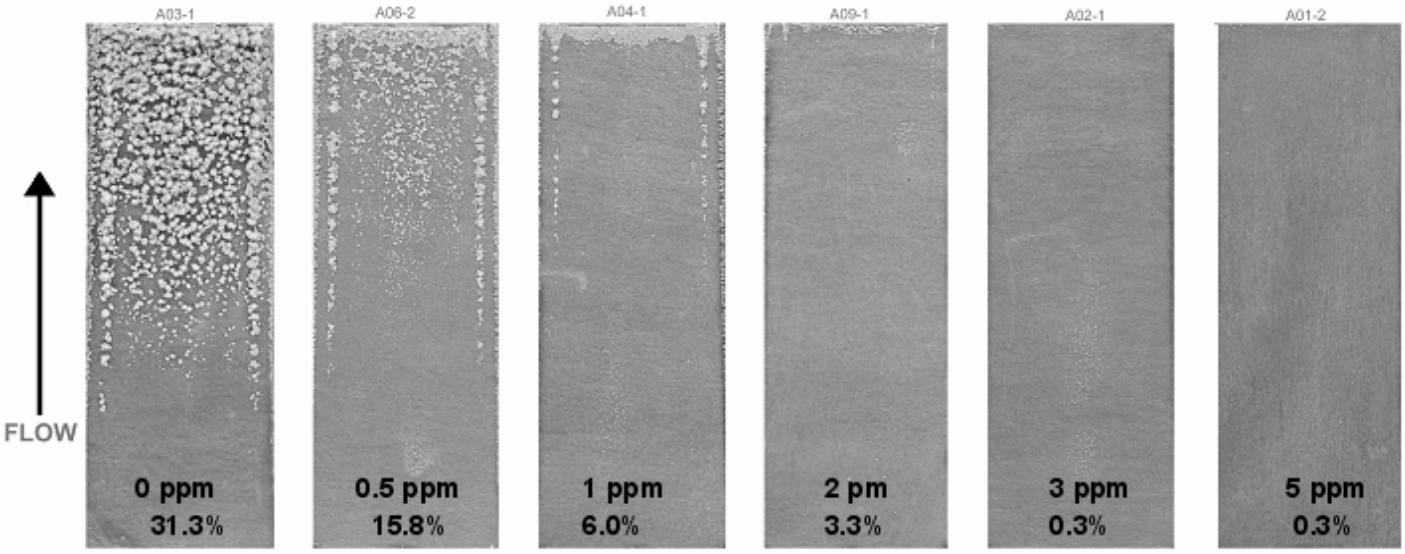


**Equation 5.10.** Optical images illustrating the impact of antiscalant (Vitec 2000) treatment on gypsum scaling of LFC-1 membrane. All runs were for initial surface gypsum saturation index of 2.3.

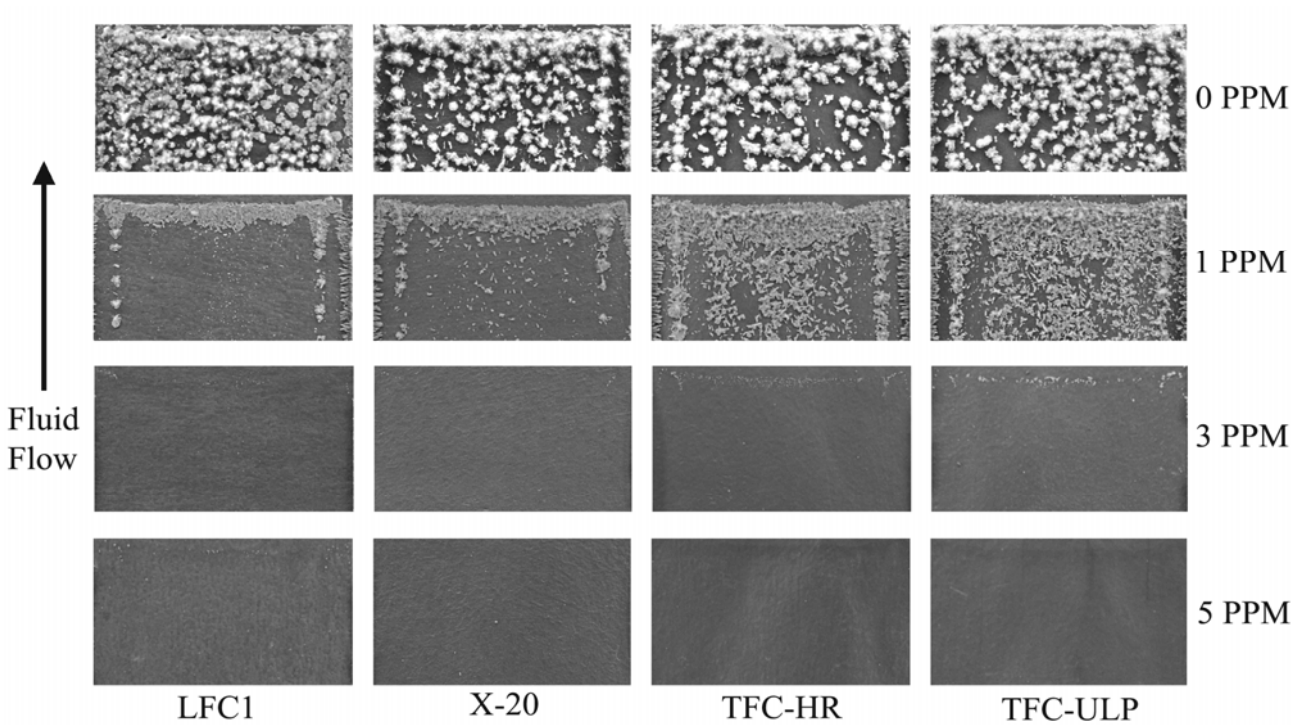


**Figure 5.11.** Optical images of LFC1, TFC-ULP, TFC-HR, and X-20 membrane surfaces (channel exit region) scaled in desalting experiments conducted at initial surface gypsum saturation index ($SI_{m,0}$) of 2.30 and for an antiscalants dose in the range 0-5 ppm.

### 5.8.4 Total Surface Scale Coverage

The imaging approach utilized in the present work enabled detailed analysis of high resolution images (6.2 megapixel image) to obtain the total, axial and traverse profiles of the surface area covered by mineral salt scale. Using the image analysis approach described in Section 5.6, the fraction of total surface area covered by scale, $\Phi_{24}$, was determined for the various scaling runs (i.e., for different initial values of the surface gypsum saturation index) and found to correlate nearly linearly with the fractional permeate flux decline, $FD_{24}$, as shown in Figure 5.12. The fractional flux decline was lower (by up to 30%) than the fractional surface area covered by scale. This suggests that the scaled layer does not completely blocks the membrane pores. This conclusion is in contrast to the study of Hasson and co-workers [42, 45, 46] who proposed that scaled areas can be modeled via the surface blockage model. In the Hasson and co-workers studies, however, measurements were conducted by casting a section of the scaled membrane with a polyester resin, which could have reduced the accuracy measurements by destruction of fragile arms of surface gypsum rosettes [11] or biasing the

imaging due to the polymeric matrix. In contrast, the present approach is non-destructive and enables a high resolution analysis of surface scale coverage. It is emphasized that the scaled layer should not be considered as a "Cake layer" in the traditional definition; however, there is some permeation through the scaled areas. Gypsum scale on the membrane surface is primarily in the form of three-dimensional rosette structures (Figure 5.12b; [11]), whereby permeation can take place through the interstitial spaces between the rosette arms. Surface morphology of surface gypsum crystals (Figure 5.12b) suggests that only the base of the rosettes makes intimate contact with the membrane surface where pore-plugging occurs.

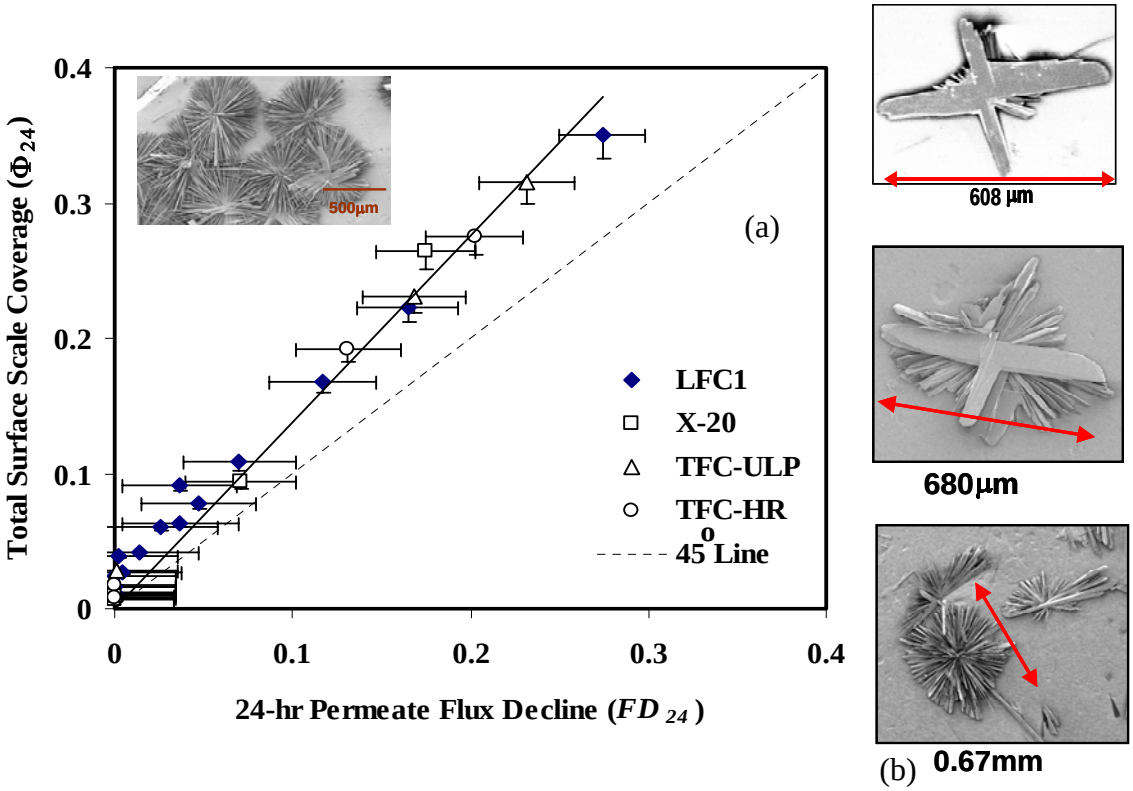


**Figure 5.12.** (a) Correlation of fractional of surface covered by gypsum scale with the measured fractional flux decline due to surface gypsum scaling. (b) Images of single surface gypsum crystals [11].

### 5.8.5 Effects of CP and Antiscalant on Local Surface Scale Coverage

Axial development of gypsum scale (SEM) was observed (Figure 5.2. 5.9 and 5.10) even for the relatively short axial length (6.9 cm) of the active membrane area. Optical images of the scaled membranes revealed that gypsum scale coverage increased toward the channel exit. This behavior can be rationalized by the well-accepted kinetic model for gypsum crystallization that describes the rate of change of surface scale mass, *m*, by $dm/dt = k\left(C_m - C_s\right)^n$, where *k* is the growth rate constant, $C_m$ *a*nd $C_s$ are the gypsum concentration and equilibrium solubility, respectively, at the membrane surface and *n* is an kinetic order which varies from a value of 1 for diffusion-controlled crystallization to a value of 2 for surface reaction process. According to the above model, given that CP and thus $C_m$ both increase with axial position, it can be inferred that the rate of surface scale formation should increase as the membrane exit region is approached [11]. This behavior, which is pictorially demonstrated in the images of Figures 5.9 and 5.10, is depicted quantitatively in Figure 5.13 by the local fractional surface scale coverage ($\phi_{24}$) for the different membranes. These local scale profiles are snapshots of gypsum scale development along the membrane surface. Therefore, it can be inferred that gypsum scale progressed with time starting from the region of high (channel exit) to low (channel entrance) solution supersaturation.

The rate of gypsum surface crystal growth and thus the percent of local surface scale coverage should increase with increasing initial surface gypsum saturation index ($SI_{m,0}$). Indeed, this is the case as illustrated for the LFC-1 membrane (Figure 5.14) by the axial profiles of gypsum fractional surface coverage, $\phi_{24}$, for scaling runs at three different levels of initial surface gypsum saturation indices. For $SI_{m,0}$= 1.95, at which the overall crystal growth rate was expected to be relatively low, the distribution of surface scale was primarily confined to the region near the membrane channel exit ($X$>0.9). More of the gypsum scale was distributed towards the membrane channel entrance as $SI_{\mathrm{m,0}}$ was increased to 2.30.

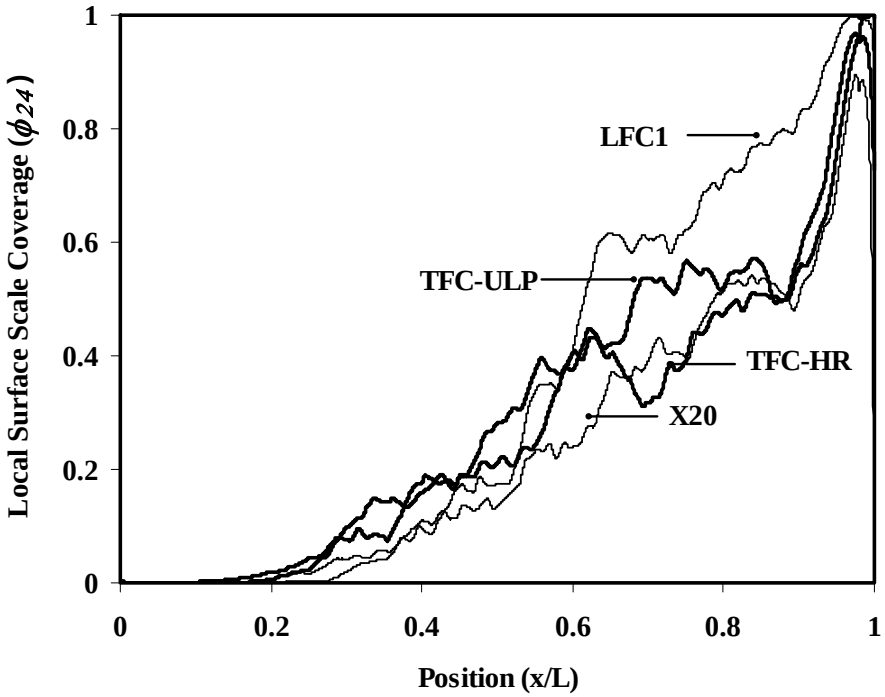


**Figure 5.13.** Local surface scale coverage ( $\phi_{24}$ ) of LFC1, TFC-ULP, TFC-HR, and X-20 membrane types obtained from experiments conducted at $SI_{m,0}$ of 2.30.

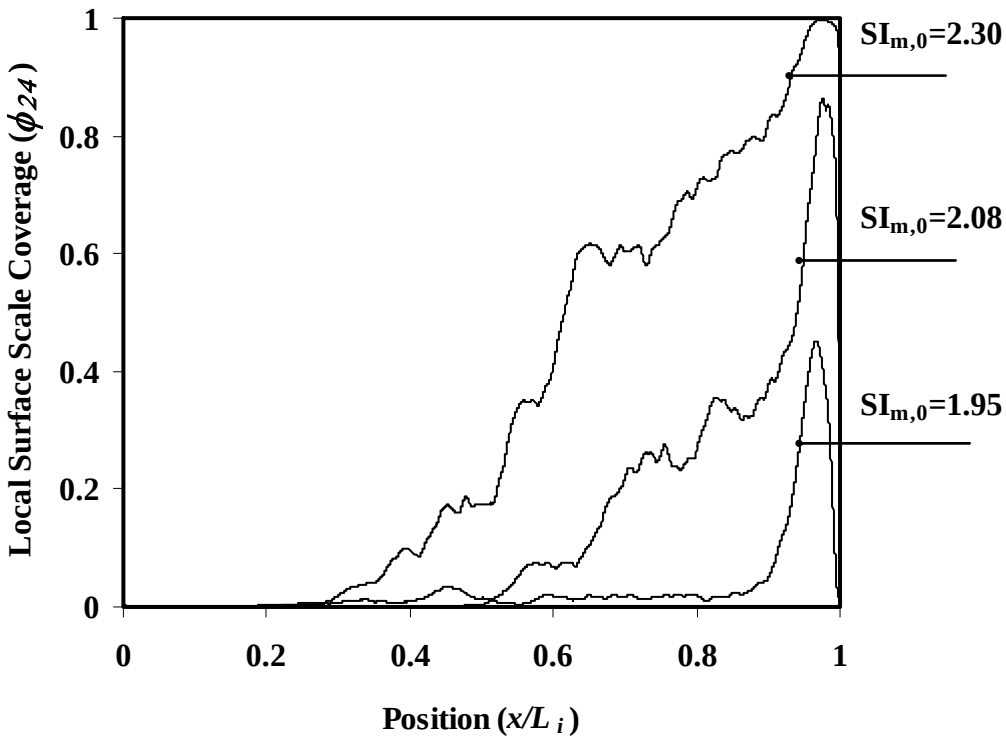


**Figure 5.14.** Local surface scale coverage ( $\phi_{24}$ ) of LFC1 membrane obtained from RO desalting experiments conducted at various initial surface gypsum saturation index values ($SI_{m,0}$).

The suppression of gypsum scale growth by antiscalant addition is indicative by the decrease in local fractional surface scale coverage ($\phi_{24}$) with increasing antiscalant dosage as illustrated for the LFC-1 membrane in Figure 5.15, at a fixed $SI_{m,0}$ of 2.08. It is clear that antiscalant addition to the RO feed results in retardation of gypsum surface scale development at every axial position along the membrane. Given that the rate of surface crystallization is higher near the membrane channel exit, the impact of antiscalants dosage is also more pronounced in that region. The rise in of $\phi_{24}$ in the channel exit region (X>0.9) is indicative of the rapid increase in the local gypsum saturation index as the membrane channel exit is approached. In this region suppression of gypsum scale formation was minimal until a sufficiently high antiscalant dosage was applied ($\gtrsim 3\,\text{ppm}$). This clearly demonstrates that the required antiscalant dosage for effective scale suppression strongly depends on the local level of solution supersaturation.

The present results suggest that the effectiveness of antiscalant treatment will differ depending on the specific membrane type. This behavior is illustrated in Figure 5.16 in which four different membranes are compared at the same initial membrane surface gypsum saturation index, $SI_{m,0}$ =2.30±0.02 and antiscalant dosage of 1 ppm. Clearly, there are noticeable differences in the local fractional surface scale coverage profiles according to the following order of decreasing membrane scaling propensity: TFC-ULP, TFC-HR, X-20 and LFC1. It is noted that differences in scaling propensity were also observed in the absence of antiscalant treatment (Figure 5.13). For this case, at the same experimental conditions as those of Figure 5.15, the following order of decreasing scaling propensity was obtained: LFC1, TFC-ULP, TFC-HR, and X-20. However, differences in scaling propensities among the membranes were more pronounced when antiscalant was added to the RO feed below the minimum amount required for complete scale suppression.

In closure, a detailed diagnostic approach for scale characterization was developed that enables one to compare the scaling propensity of RO membranes, evaluate antiscalant effectiveness, and optimize antiscalant dosage based on direct observation of scale coverage and flux decline measurements. The present study provides a framework for a systematic approach to assess optimal process conditions and membrane selection for desalting operations at which sufficiently high levels of solution supersaturation are expected with respect to scale forming mineral salts.

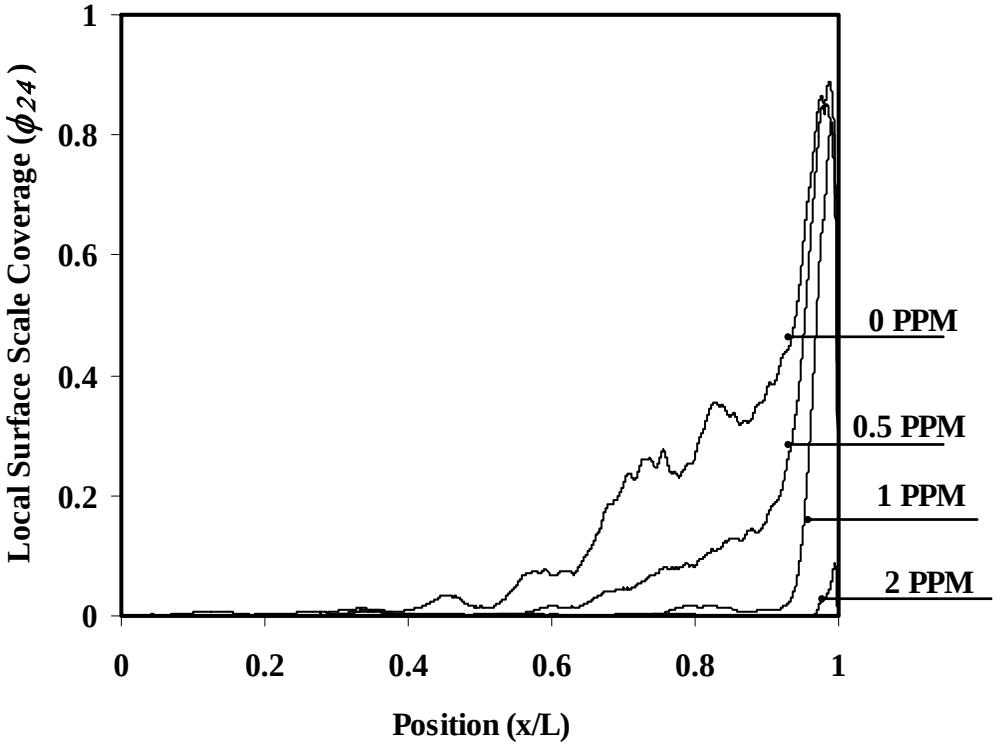


**Figure 5.15.** Local surface scale coverage ($\phi_{24}$) for LFC1 membrane scaled in RO desalting experiments conducted at initial surface gypsum saturation index ($SI_{m,0}$) of 2.08 and antiscalants dosage of 0-2 ppm.

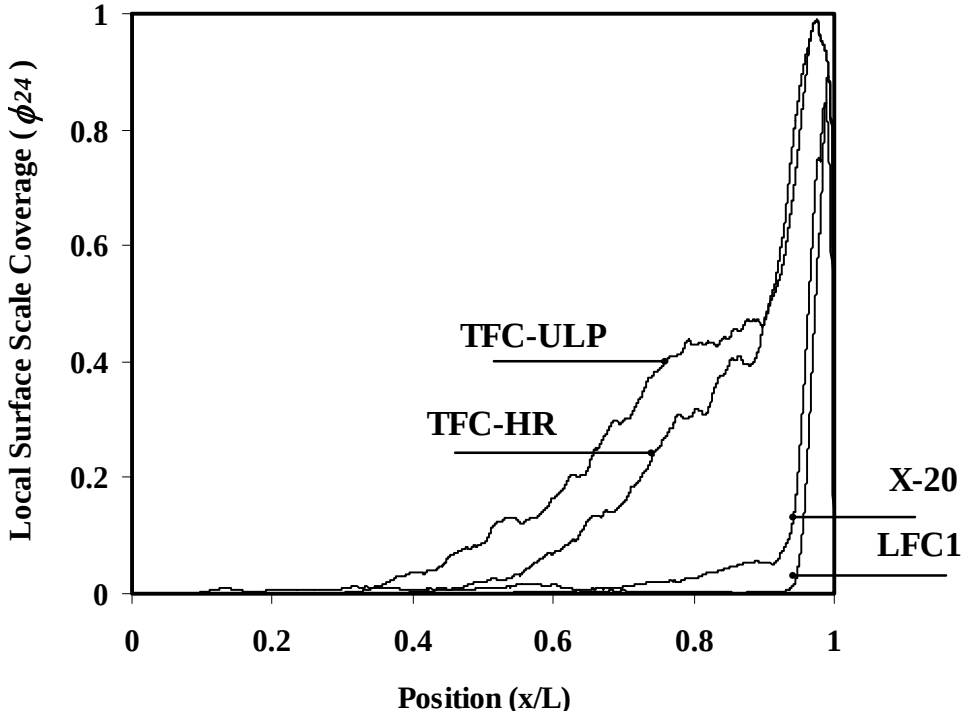


**Figure 5.16.** Local surface scale coverage ($\phi_{24}$) for LFC1, TFC-ULP, TFC-HR, and X-20 membranes obtained from RO desalting experiments conducted at $SI_{m,0}$ of 2.30 and antiscalants dose of 1 ppm.

# 6.0 Precipitation Softening for Enhanced RO Recovery

## 6.1 Overview

In order to increase product water recovery from membrane desalting of brackish groundwater and agricultural drainage water it is necessary to carefully evaluate the limits on product water recovery due to mineral salt scaling. Groundwater in the San Joaquin Valley contains high concentrations of divalent cations such as calcium, magnesium, barium and similarly high concentrations of carbonate and sulfate anions. At the prevailing concentrations of the above ions, their level of saturation with respect to mineral salt scalants can often be close to or above saturation. Moreover, upon concentration of the salts in the RO brine stream further increase in the saturation level occurs, thereby increasing the potential for mineral salt precipitation and thus membrane scaling. While it is beyond the scope of the present study to survey the extensive groundwater monitoring data from the San Joaquin Valley, the typical examples provided in Tables 2.1 and 6.1 clearly demonstrate the high TDS levels and variability in water chemistry in San Joaquin Valley (SJV) groundwater.

In order to evaluate product water recovery limit in membrane desalting of SJV brackish water, an analysis process was developed based on thermodynamic solubility calculations using the OLI software [41] for multi-ion systems (Section 5.4). The results are presented in Sections 6.2-6.5. Following solubility analyses for the of mineral salts of concern at different pH levels, the limit on recovery was calculated by evaluating the expected saturation levels, expressed in terms of the saturation indices for the mineral salts of interest, at various recovery levels. The theoretical recovery limit is reached when the saturation index of the mineral salt of concern reaches unity. Based on the above analyses, a process design analysis along with demonstrative laboratory bench scale experiments were undertaken to assess possible approaches to reaching high product water recovery. The present analysis considered integration of desalting by low pressure RO with nanofiltration (NF), chemical precipitation softening and antiscalant addition to reduce the potential for membrane scaling.

**Table 6.1** Selected examples of San Joaquin Valley groundwater quality[(a)]

| Station | BVWSD | OAS 2548 | | | | |
|---|---|---|---|---|---|---|
| | | Source A | Source B | Source C | Source D | Source E |
| Date | | 7/14/2003 | 9/9/2003 | 11/12/2003 | 1/12/2004 | 3/22/2004 |
| | Composition (mg/L) | | | | | |
| $Na^+$ | 1,150 | 1,810 | 1,080 | 2,320 | 2,830 | 2,310 |
| $SO_4^{2-}$ | 1,020 | 3,990 | 2,340 | 5,550 | 6,460 | 5,630 |
| TDS | 5,250 | 5,864 | 3,828 | 9,344 | 11,100 | 9,576 |
| $Cl^-$ | 210 | 779 | 468 | 952 | 1,120 | 847 |
| Total Alkalinity | - | 271 | 239 | 160 | 173 | 146 |
| $HCO_3^-$ | 291 | 330 | 290 | 195 | 211 | 178 |
| EC | - | 9,030 | 5,610 | 10,760 | 13,160 | 11,010 |
| Hardness | - | 1,362 | 988 | 1,793 | 2,099 | 2,052 |
| $Ca^{2+}$ | 555 | 283 | 224 | 385 | 430 | 454 |
| $Mg^{2+}$ | 61 | 159 | 104 | 202 | 249 | 223 |
| $K^+$ | - | 3.4 | 2.7 | 5 | 5 | 10 |
| B | - | 18.4 | 9.3 | 19.4 | 23 | 19.8 |
| $Ba^{2+}$ | 0.17 | 0.50 | 0.25 | 0.5 | 0.5 | 0.5 |
| Se | - | 0.099 | 0.061 | 0.144 | 0.171 | 0.149 |
| | | | | | | |
| pH | 7.7 | 7.6 | 7.1 | 7.9 | 7.9 | 7.9 |
| Temp, $^oC$ | - | 22 | 21 | 18 | 14 | 15 |
| Gypsum SI | 0.45 | 0.57 | 0.41 | 0.83 | 0.94 | 0.98 |
| Calcite SI | 12.5 | 6.32 | 6.3 | 3.92 | 4.12 | 3.99 |
| Barite SI | 13.6 | 89.5 | 41 | 94.8 | 95.8 | 95.5 |

[(a)] DWR San Joaquin Valley Drainage Monitoring Program Database.

SI – saturation index, TDS – total dissolved solids (mg/L).

## 6.2 Saturation Indices

The first step to assessing the limits imposed by mineral salt scaling on product water recovery is to determine the saturation indices of mineral salts of concern as a function of pH. Such an analysis provides information on feasibility of feed pH adjustment to reduce scaling potential, primarily with respect to calcium carbonate scaling since calcite solubility is pH sensitive. In order to illustrate the approach, the saturation indices for calcite, gypsum and barite were determined as a function of pH for the BVWSD and OAS-2548/ B and E water compositions (Table 6.1). The latter two water compositions had the lowest and highest gypsum saturation, respectively, of the four OAS-2548 compositions listed in Table 6.1. The saturation indices for calcite, gypsum and barite are defined as follows:

$$\mathrm{SI}_{calcite} = \frac{(Ca^{2+})(CO_3^{\ 2-})}{K_{sp_{calcite}}} \qquad (6.1)$$

$$\mathrm{SI}_{gypsum} = \frac{(Ca^{2+})(SO_4^{\ 2-})}{K_{sp_{barite}}}$$

$$\mathrm{SI}_{barite} = \frac{(Ba^{2+})(SO_4^{\ 2-})}{K_{sp_{barite}}}$$

where $(Ca^{2+})$, $(Ba^{2+})$, $(SO_4^{\ 2-})$ and $(CO_3^{\ 2-})$ are the activities of the calcium, barium, sulfate and carbonate ions, respectively, and $K_{sp_{calcite}}$, $K_{sp_{gypsum}}$ and $K_{sp_{barite}}$ are the solubility constants (products) for calcite, gypsum and barite, respectively. The variation of the above saturation indices with pH are shown in Figures 6.1 and 6.2. It is clear that calcite is most sensitive to pH while the solubilities of calcium sulfate and barium sulfate are pH insensitive. Although barite has the highest saturation index it is a metastable mineral salt with a slow nucleation kinetics [27]. Moreover, barium concentration is $\lesssim 0.5$ mg/L and thus the amount of barite scale (per unit surface area) that could form would be lower by about two orders of magnitude relative to gypsum. It is generally accepted that at $\mathrm{SI}_{barite} \lesssim 60$ barite is not expected to precipitate over the course of typical residence times in commercial RO modules. In contrast, precipitation kinetic of calcite and gypsum are relatively rapid and therefore these two scalants are generally of primary concern. For the water compositions given in Table 6.1, the saturation index for gypsum is below unity for all three water compositions (see also Figures 6.1 and 6.2), while calcite is

already above saturation at the native pH of these various feed water sources. Therefore, calcite is the primary limiting scalant for RO desalting of the above water feed compositions. The critical pH levels for which $SI_{calcite}$ will reach unity for the BVWSD and the OAS-2548/B and E water compositions are 6.78, 7.15 and 7.25, respectively. Membrane RO desalting of these waters would require adjustment of feed water pH to a level at which the calcite saturation index would be below unity. However, even with successful control of calcite scaling, gypsum concentration could rise above saturation with the increased RO recovery.

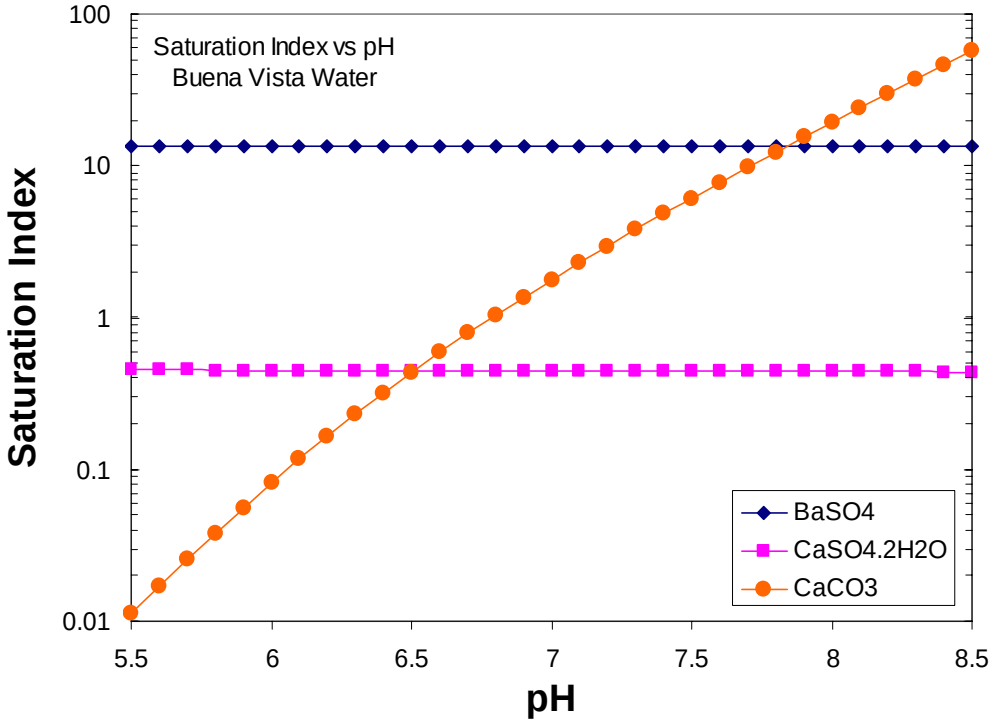


**Figure 6.1.** Variation of Saturation indices for calcite, gypsum and barite for the BVWSD source water given in Table 6.1.

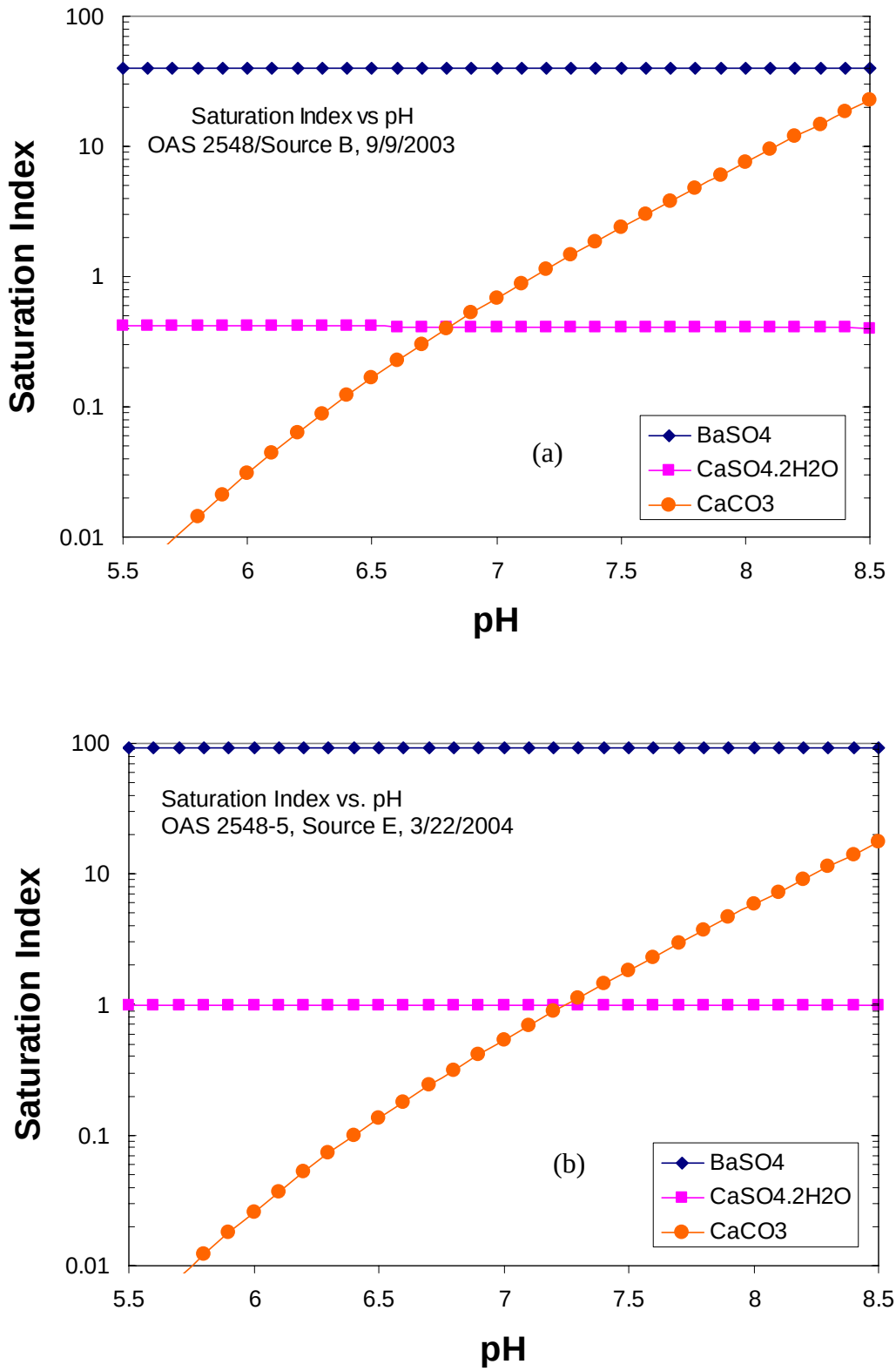


**Figure 6.2.** Saturation indices for calcite, gypsum and barite for the (a) OAS-2548 source B and (b) OAS-2548/Source E water compositions (Table 6.1)

## 6.3 Effect of Product Water Recovery level on Mineral Salt Saturation Levels

Operation of RO desalting at high product water recovery results in increased concentration of the retentate (brine) stream (see Eq. 2.1 and Figure 2.1). As a result the saturation levels with respect to the various mineral salts increase along the membrane channel. The critical recovery limit is dictated when the saturation index for the mineral salt of concern reaches unity. It is noted, however, that the crystallization kinetics of certain mineral salts can be extremely slow such that their supersaturated solutions can exist in a metastable state for long periods. As discussed in Section 6.2, crystallization kinetics of calcite and gypsum are fast relative to the rate of crystallization of barium sulfate, in part, due to trace level presence of barium in San Joaquin Valley brackish water. Since calcite scaling can be controlled by pH adjustment, gypsum is likely to be the scalant that imposes the upper limit on product water recovery. An illustration of the approach of arriving at a reasonable first order upper limit on product water recovery, analysis of saturation indices was carried out, as a function of product water recovery, for the BVWSD and OAS-2548/B and E water sources. Analysis for the OAS-2548 feed water source was carried out water compositions with the lowest (Source B) and highest (Source E) gypsum saturation levels (Table 6.1). The analysis was carried out at pH=6 to simulate a reasonable level of calcite precipitation control. As an illustration of the effect of pH adjustment, analysis for the BVWSD water source was also carried out at its native pH of 7.7.

The results of the above analyses, for the BVWSD and the OAS-2548/B and E water compositions are shown in Figures 6.3-6.4. In all cases the saturation indices for calcite, gypsum and barite increase as water recovery increases. It is also apparent that the saturation indices for calcite and barite are much higher than for gypsum. The saturation index for barite is in the order of magnitude range of $10\text{-}10^2$ and although its crystallization kinetics is slow, there is a concern that above barite saturation index values of about 50 barite scaling may become a problem. Calcium carbonate scaling is also an issue since its crystallization kinetics is rapid. For example, for desalting of the BVWSD feed water at about 99% salt rejection, the value of $SI_{gypsum}$ will increase from its initial value of about 0.5 to unity (saturation) at a product water recovery level of about 50%. Therefore, even with pH adjustment to control calcite precipitation, gypsum will place an additional limit on recovery. Adjustment of the feed water to pH of 6 would enable operation that is free of calcite scaling up to about a product water recovery of

80% for the BVWSD water and in excess of 90% for OAS-2548/Source B and E water compositions. However, the saturation index for calcium sulfate would reach unity at product water recoveries of about 50% and 55% for the BVWSD and OAS-2548/Source B water compositions, respectively. The OAS-2548/Source E water is saturated with respect to gypsum and therefore desalination would not be feasible without first reducing the saturation level with respect to gypsum or the use of scale suppressing additives. It is also noted that the saturation index with respect to barite exceeds the typical recommended upper limit of about 60 at water recoveries of about 75% for the BVWSD water and 30% for the OAS-2548/Source B water. The barite saturation index is at a level of nearly 100 and above for the feeds solution and at all recovery levels. The above examples suggest that calcite scaling control by pH adjustment is insufficient and additional control of gypsum and barite scaling is necessary to achieve reasonable levels of product water recovery (~ 70% or higher).

It is important to recognize that the required pH level for calcite scale suppression will be lower with increased product water recovery. Figures 6.5 and 6.6 indicate the pH level of the retentate which is required in order to ensure that calcite will not precipitate for desalting of BVWSD and the OAS-2548/B feed water compositions. The pH-recovery curves represent lines of calcite saturation whereby above the line calcite precipitation will occur. Although one can achieve calcite scale control for recoveries in excess of 90%, this would require additional process and chemical cost for pH control. Scale suppression additives (i.e., antiscalants) can be used either in the primary RO feed or between intermediate RO stages. In this manner acid dosing can be used for the first stage of recovery and antiscalants can be used with a smaller brine stream for additional recovery. Clearly, the strategic use of pH adjustment and antiscalants must be determined based on process optimization with respect to the target recovery, permeate quality and overall water production cost.

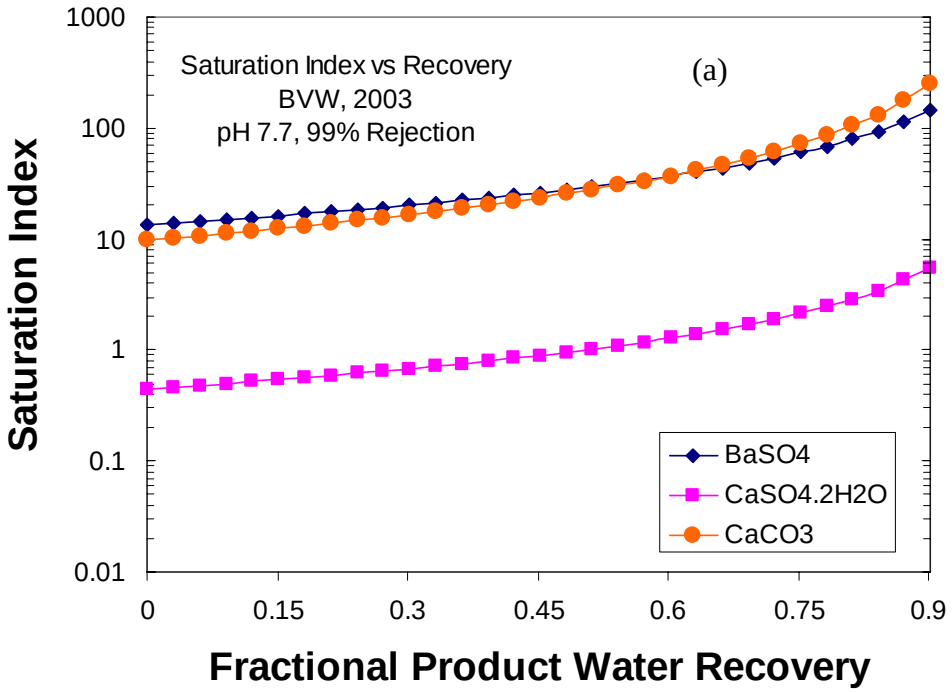


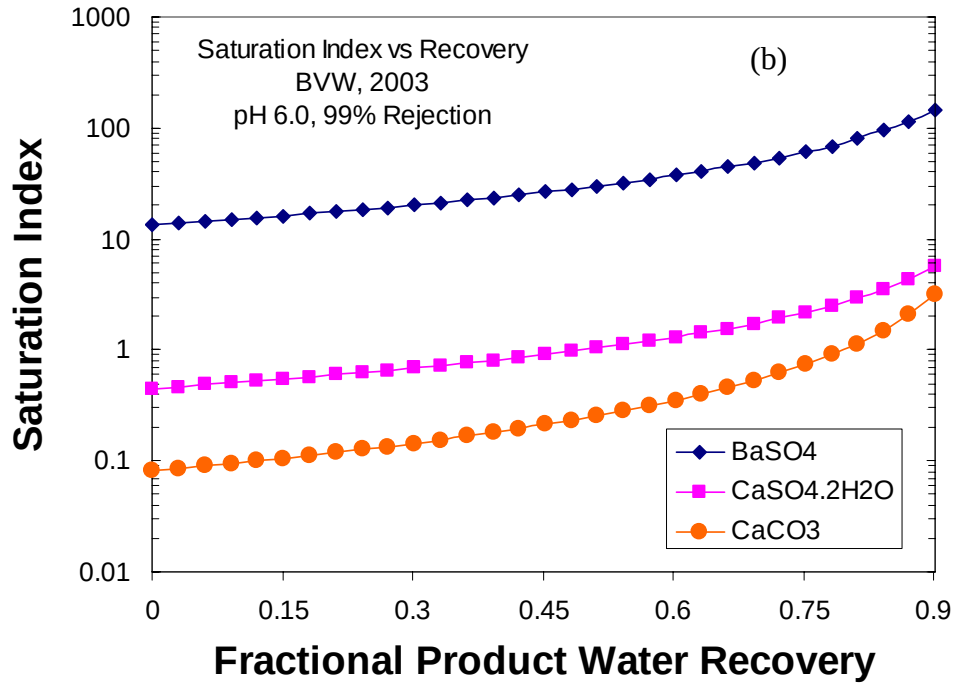


**Figure 6.3.** Dependence of mineral salt saturation indices on the level of product water recovery for membrane desalting (at 99% salt rejection) for the BVWSD water composition . (a) Simulations at the native pH of 7.7; (b) Simulations at pH= 6.

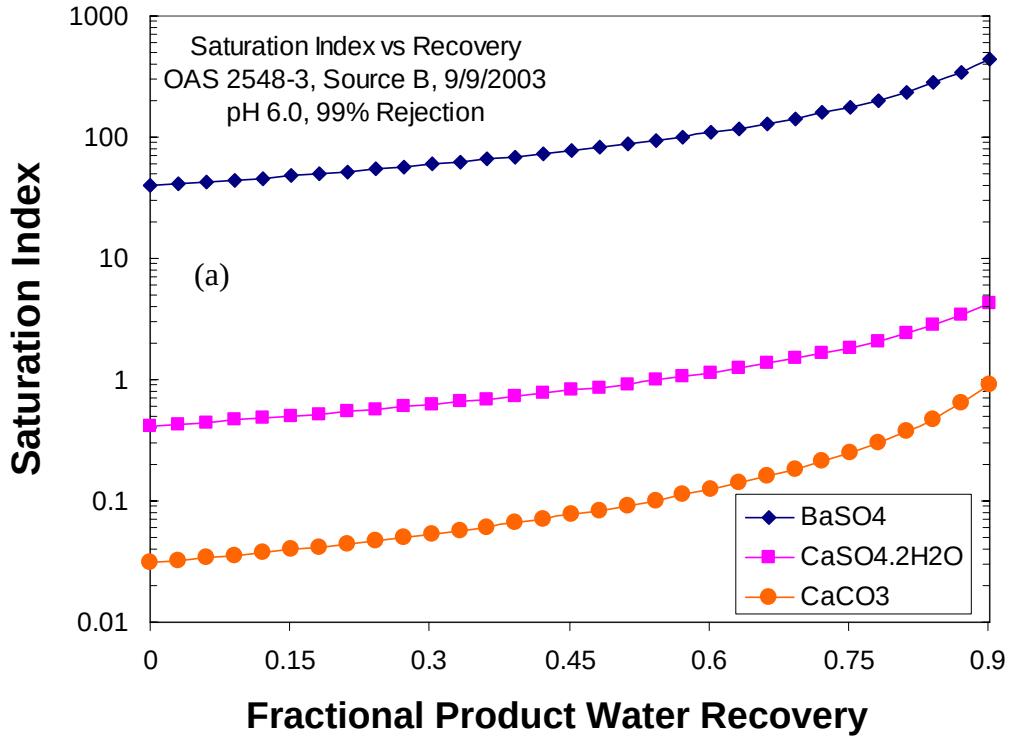


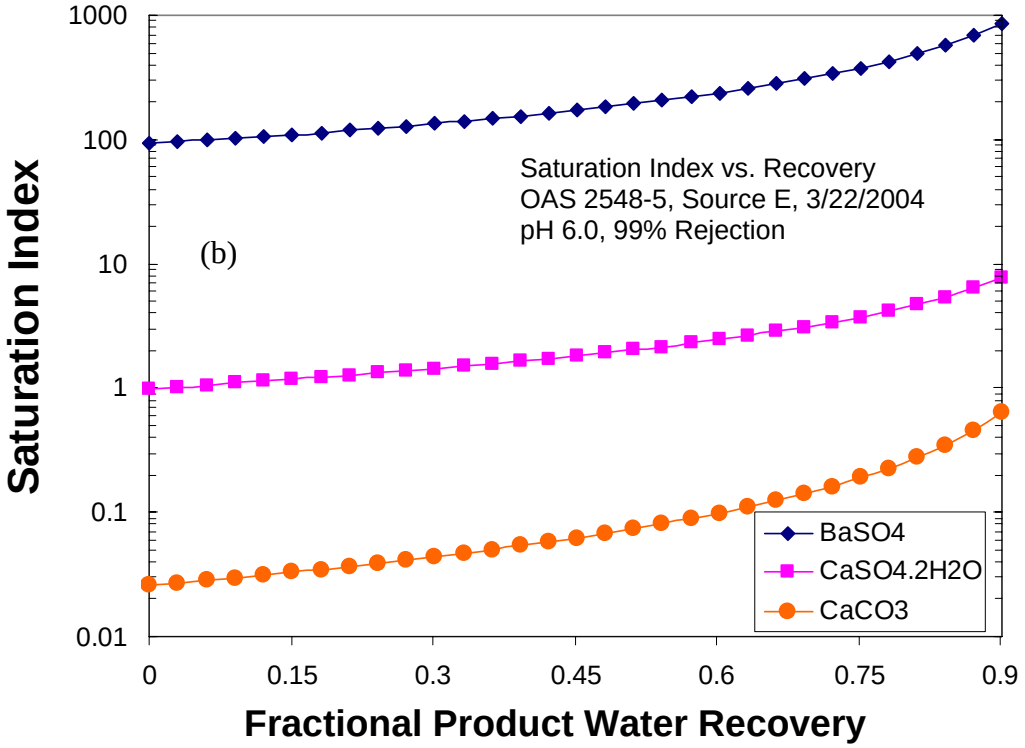


**Figure 6.4.** Dependence of mineral salt saturation indices on the level of product water recovery for membrane desalting (at 99% salt rejection) of brackish groundwater from location OAS 25485 (Table 6.1): (a) Simulations for water composition B at pH=6; (b) Simulations for water composition E at pH=6.

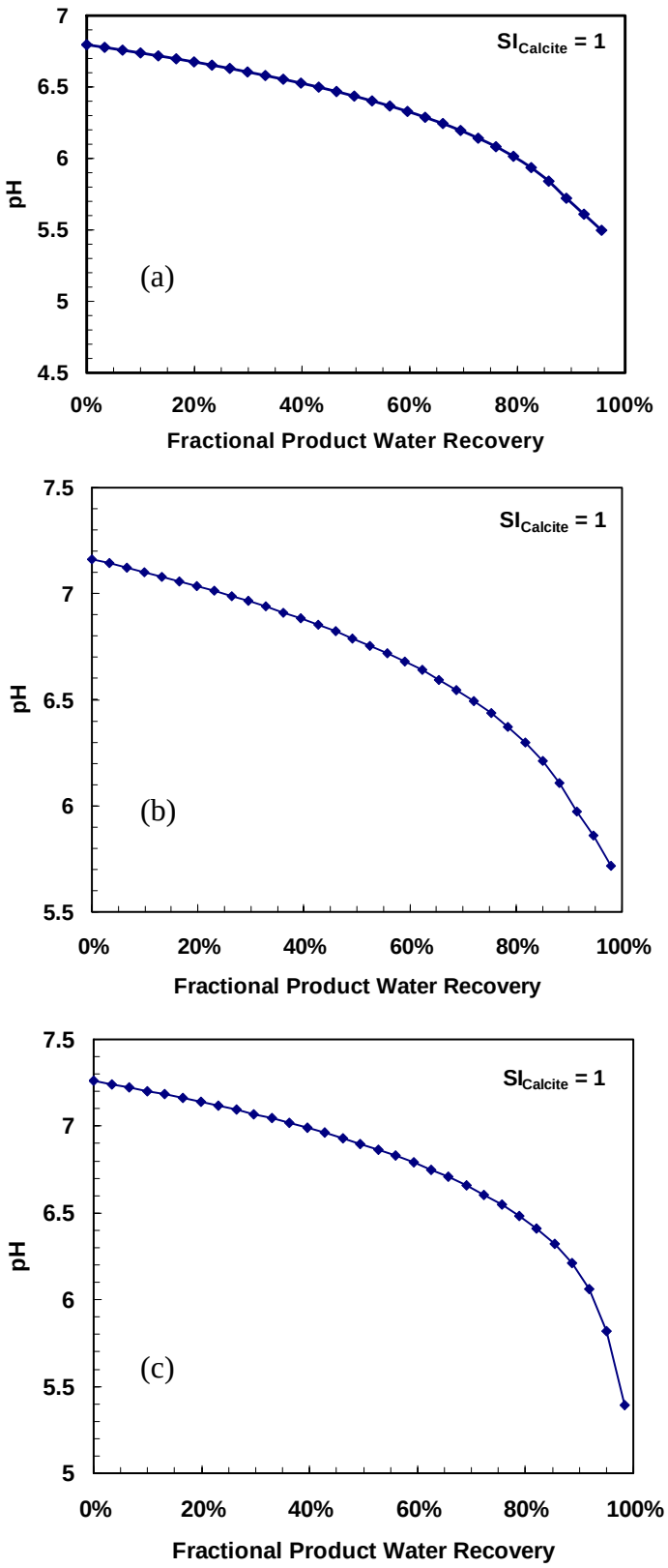


**Figure 6.5.** Feed pH adjustment at various product water recovery levels needed to keep the saturation index of calcite at unity. (a) BVWSD water; (b) OAS-2548/Source B; (c) OAS-2548/Source E.

## 6.4 Calcium Removal Requirements for Scale Suppression and Enhanced Product Water Recovery

One alternative to enhancing product water recovery is by accelerated precipitation softening (APS) under alkaline conditions. This can be achieved by raising the pH of the primary RO concentrate to a level of about 10-10.5 [27] and using calcium carbonate or calcium sulfate seeding to accelerate the kinetics of mineral salt crystallization. The goal is to reduce the supersaturation level of mineral salts scalants in the primary RO concentrate as a pre-treatment prior to a second RO desalting stage. Subsequently, the APS treated concentrate is filtered and further desalted in a secondary RO stage with the feed pH adjusted to acidic condition and with the option of adding additional makeup antiscalant to reduce the potential for calcite scaling. As an illustration, the required APS removal of calcium for the BVSWD and OAS-2548/B source water compositions are given in Figures 6.6a and 6.6b, respectively. The primary RO desalting can be carried out to a level of about 55% and 51% for the BVSWD and OAS-2548/Source B water feeds, respectively, due to limitations placed by gypsum scaling (i.e., saturation index for gypsum reaches unity). Clearly, the above analysis is a conservative one since antiscalant addition can be utilized to suppress scale formation to some extent and thus enable a higher recovery relative to the above thermodynamic-based estimate. For example, since the gypsum saturation index is at or greater than unity for the feed water at the composition of OAS-2548/Source D, this water can be desalted directly only through the use of antiscalants and/or precipitation softening treatment of the primary RO feed.

It is often recommended that, with the use of antiscalants, it may be possible to desalt up to a recovery level at which where the gypsum saturation index reaches a value of about 2.5. If such an approach is adopted then product water recovery in a primary RO stage would be about 84%, 76% and 69% for the BVWSD and OAS-2548/B and E water compositions, respectively. It is recognized that the use of antiscalants and APS would add to the cost of water desalination. Therefore, it is imperative to optimize the integration of both processes for maximizing product water recovery given constraints with respect to both process cost and the cost of concentrate handling.

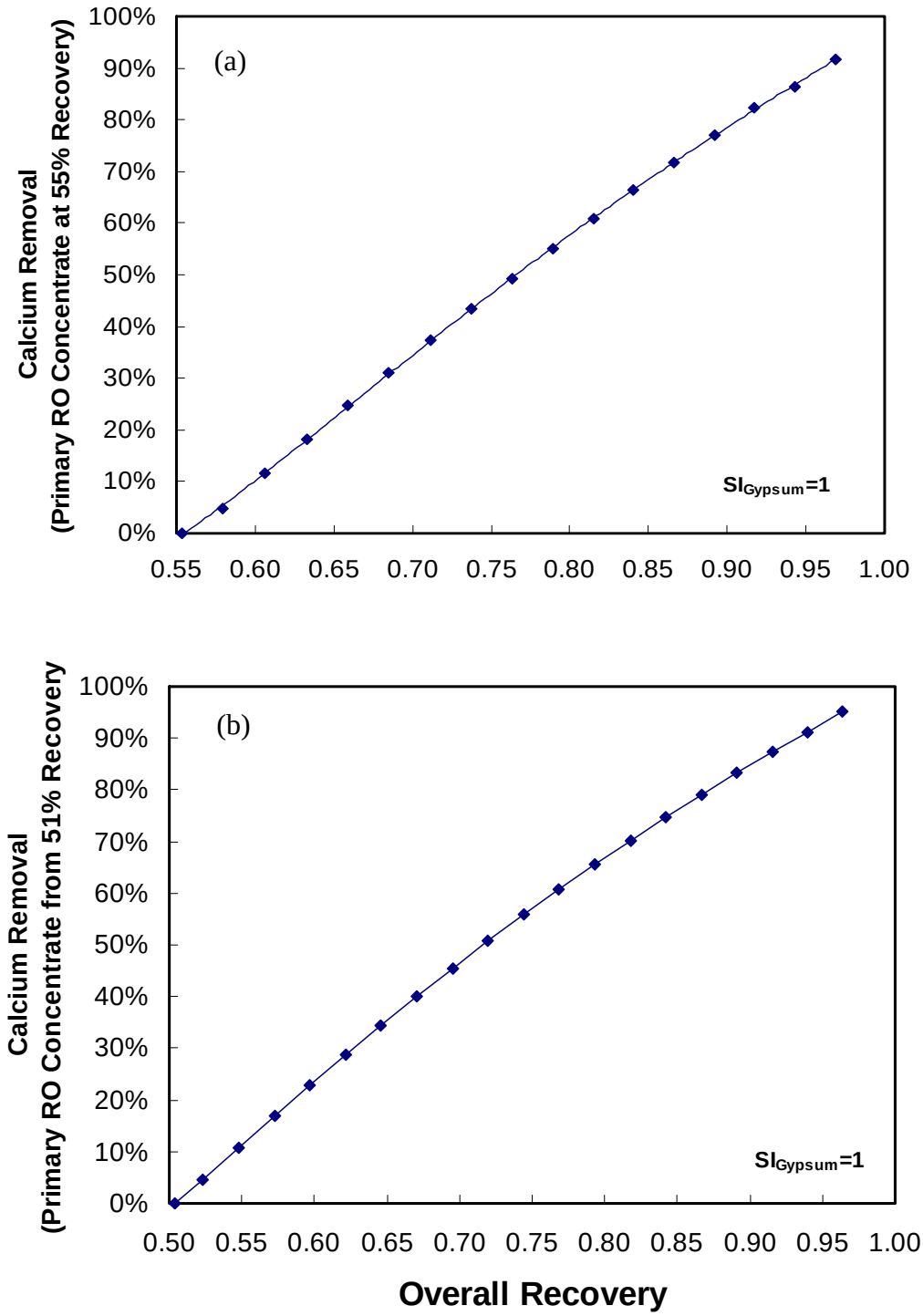


**Figure 6.6.** Required percent of calcium removal from primary RO concentrate produced from desalting (at 99% salt rejection) of (a) OAS-2548/B source water desalted at 55% recovery; (b) OAS-2548/E source water desalted at 51% recovery.

# 7.0 Process Analysis and Laboratory Assessment of Enhanced Product Water Recovery with Integration of Accelerated Precipitation Softening with RO Membrane Desalination

## 7.1 Overview

The thermodynamic analysis presented in Chapter 6 indicates that high recovery desalting would only be possible through reduction of the level of supersaturation the mineral salt sealants of concern. As discussed in Chapter 6, this reduction could be achieved either by softening the primary RO feed or the concentrate from primary RO desalting which would then be further desalted in a secondary RO stage. San Joaquin Valley water with composition similar to that of the OAS location is of the greatest concern since the TDS level is in the neighborhood of 10,000 mg/L TDS for significant portion of the year as revealed by the monitoring data for the period 2003-2004 monitoring period[3]. Desalination of such water (see Figs. 6.2b, 6.4b, 6.5c and 6.6b) would first require removal of scale ion precursors prior to membrane RO desalting. Accordingly the technical feasibility of two specific strategies was evaluated. The first was a single-stage membrane desalination consisting of an accelerated precipitation softening of the feed water followed by membrane desalination. The second alternative was a two-stage membrane desalination consisting of primary RO desalination followed by accelerated precipitation of the concentrate and a subsequent second stage RO desalting.

The highest saturation index for gypsum was encountered at the OAS source water location for the 3/22/2004 sample (Table 6.1). Therefore, the water composition from the OAC site that had the highest gypsum saturation index (Fig. 6.2b) was selected for assessment of this challenging water desalination. The technical feasibility and limitations on RO membrane desalting were investigated via both thermodynamic equilibrium calculations, RO process analysis using ROPRO (Koch Membrane Systems) and bench-scale experiments to assess the effectiveness of accelerated precipitation softening in averting membrane scaling.

[3] DWR San Joaquin Valley Drainage Monitoring Program Database

## 7.2 Experimental

### 7.2.1 Calcium Removal by Accelerated Precipitation

The extent of calcium removal by accelerated precipitation softening was conducted using OAS source E (Tables 6.1) model solutions (Table 7.1) representing RO feed water (Table 7.1) and primary RO concentrate (see Section 7.6). The model solution for the primary RO concentrate were dosed with 6 ppm of antiscalant (Flocon 100) in order to evaluate the impact of antiscalants on the APS process. For each model solution type (feed and concentrate), five APS runs were conducted in 50-mL capped vials immersed in a temperature-controlled water bath (20$^{o}$C), using 1.4 g/L calcite seed loading and varying amounts of sodium carbonate or sodium hydroxide dosage. The precipitation reaction was allowed to proceed for a period of ~30 hours (to ensure that equilibrium was reached). At the termination of the APS treatment the solution was filtered using a 0.1-micron filter and the pH and the calcium ion potential were measured.

**Table 7.1**. Reconciled water quality data of agricultural drainage from OAS monitoring site (3/22/2004 sample date).

| *Ions* | *Concentration (mg/L)* | *Mineral Saturation Index:* | |
|---|---|---|---|
| Sodium | 2,379 | Gypsum | 0.98 |
| Barium | 0.5 | Calcite | 3.97 |
| Calcium | 454 | Barite | 95 |
| Potassium | 10 | TDS | 9,703 |
| Magnesium | 223 | pH | 7.8 |
| Sulfate | 5,630 | | |
| Chloride | 847 | | |
| Nitrate | 45 | | |
| Bicarbonate | 178 | | |

*Basis temperature is 20$^{o}$C

### 7.2.2 Kinetic of Accelerated Precipitation

The kinetic of the APS process was assessed using OAS/Source E model solutions representing RO feed water and primary RO concentrate (Table 4). The precipitation reaction was carried out using 500-mL of the model solution in a 600 mL a magnetically-stirred beaker. The precipitation process was induced by dispersing a charge of calcite seeds, followed by the

addition of a predetermined amount of either 1-M sodium carbonate stock solution. Precipitation kinetics was followed by continuous monitoring of both pH and calcium ion potential until steady was reached. It is noted that the model solution for the primary RO concentrate contained 6 ppm of antiscalant (Flocon 100).

### 7.2.3 Membrane scaling diagnostic tests

Membrane scaling tests were conducted to assess the scaling potential for the primary and APS treated water. All tests were conducted using the LFC-1 membrane in the dual-cell plate-and-frame RO system (Section 5.3). Scaling tests are conducted with pre-washed membranes (Hydranautics LFC1) that were first conditioned in the RO cells by recirculating DI water through the system at a cross-flow velocity of 0.11 m/s and permeate flow rate of about 3.1 mL/min for 2 hours. A 0.752 M $CaCl_2$ solution was then circulated through the membrane system at a cross-flow velocity 0.11 m/s and permeate flow rate of 2 mL/min for a 24-hr period to allow for compaction of the membranes. The system was subsequently washed and DI water was circulated through the system for a period of 1-hr to remove $CaCl_2$ from the system. The membrane scaling test was initiated by charging the system with the model solution (Table 5) to which an antiscalant (Flocon 100) was added to yield a concentration of 3 ppm. The system was operated at a total recycle mode for a period 8.5 days at a constant cross-flow velocity of 0.11 m/s and an initial permeate flow rate of 2 mL/min. All experiments were conducted at 20$^{o}$C.

## 7.3 Analysis of Recovery Limits Imposed by Gypsum and Osmotic Pressure

In order to proceed with solubility analysis of source water OAS/E, the reported water quality data (Table 6.1) were first reconciled using the OLI software (Table 7.1). The OAS/E water was near saturation with respect to gypsum. However, it is generally recommended that antiscalants treatment can be applied to prevent gypsum and barite scaling provided that the saturation indices for gypsum and barite do not exceed about 2.3 and 60, respectively [47]. Accordingly, with the use of antiscalants, water source OAS/E can be desalinated up to a recovery level of 61% (see Fig. 6.4), provided that barium sulfate scaling is also mitigated by antiscalants treatment. It must be recognized, however, that osmotic pressure of the concentrate may also limit the achievable water recovery level. For example, at 90% recovery the osmotic pressure would reach about 600 psi (Fig. 7.1). It is noted that commercial vessels for

nanofiltration (NF) and ultra-low pressure RO (ULP-RO) are typically rated for 350 psi maximum pressure limit. Low pressure RO (High rejection (HR-RO) and extra high rejection (XR-RO) modules are generally rated for a 600 psi pressure limit, while seawater desalination RO module are usually made to withstand pressure of up to about 1200 psi. Clearly, if low pressure/high rejection RO desalting is the process of choice for the OAS/Source E brackish water desalination, then water recovery would be limited to 90% (Fig. 7.1). Higher recovery (>90%) may be possible if seawater RO modules are considered.

In order to achieve product water recovery beyond that which is possible with antiscalants treatment (i.e., 61% recovery), the concentration of calcium would have to be reduced so as to reduce the saturation level with respect to gypsum. The percent calcium removal required to maintain the concentrate at just the saturation level with respect to gypsum can be determined based on multi-ion thermodynamic solubility analysis. The results of such analysis (Fig. 7.2.) demonstrate that achieving 90% product water recovery would require about 90% calcium removal. It is interesting to note that the percent calcium removal required for the specific OAS/E water source is nearly equal to the percent of sought water recovery.

## 7.4 Process Simulations of Integrated RO-Accelerated Precipitation Softening

### 7.4.1 Overview of Simulations

In order to assess the technical feasibility of high recovery RO desalting two alternative process integration alternative (PIAs) that combine accelerated precipitation softening (APS) with RO membrane desalting were considered: (1) a single step RO desalination in which the feed is treated by accelerated precipitation softening (APS) followed by membrane RO desalting (Fig. 7.3a).; and (2) a two-step membrane RO desalination in which the primary RO concentrate from a first stage RO desalination is treated by APS with a subsequent secondary RO desalting (Fig. 7.3b). The analysis was conducted using the ROPRO simulator (Koch Membrane Systems) with input process specifications based on the analysis presented in Sections 6.2-6.4 and 7.3. For the single step APS-RO desalting process (Fig. 7.3a), a two stage membrane module configurations was utilized with the concentrate from the first RO stage desalted in a secondary RO stage. For the two-step APS-RO process (Fig. 7.3b) two different membrane stage configurations were considered: (a) a single stage RO (Fig. 7.4a), and (b) a two-stage RO module

design (Fig. 7.4b). In the two stage configuration (Fig. 7.4b) an inter-stage pump is used to allow operation of the second stage at a higher pressure in order to compensate for the osmotic pressure rise with increased recovery.

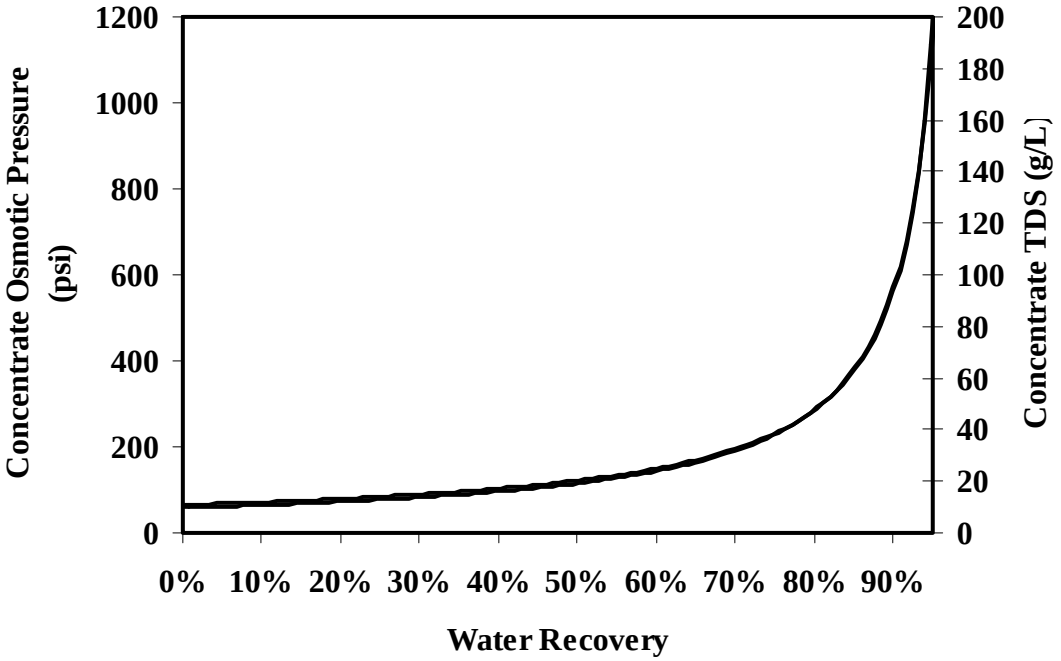


**7.1.** Dependence of osmotic pressure and total dissolved solids (TDS) of RO desalination concentrate on water recovery (assuming 97% salt rejection).

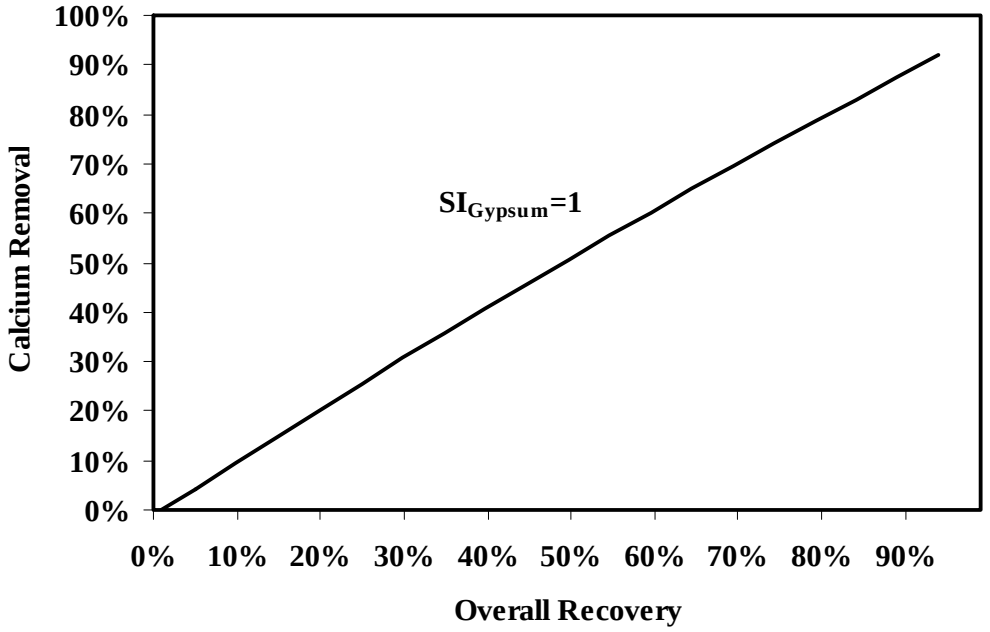


**7.2**. Calcium removal (as calcium carbonate) required to maintain gypsum at saturation

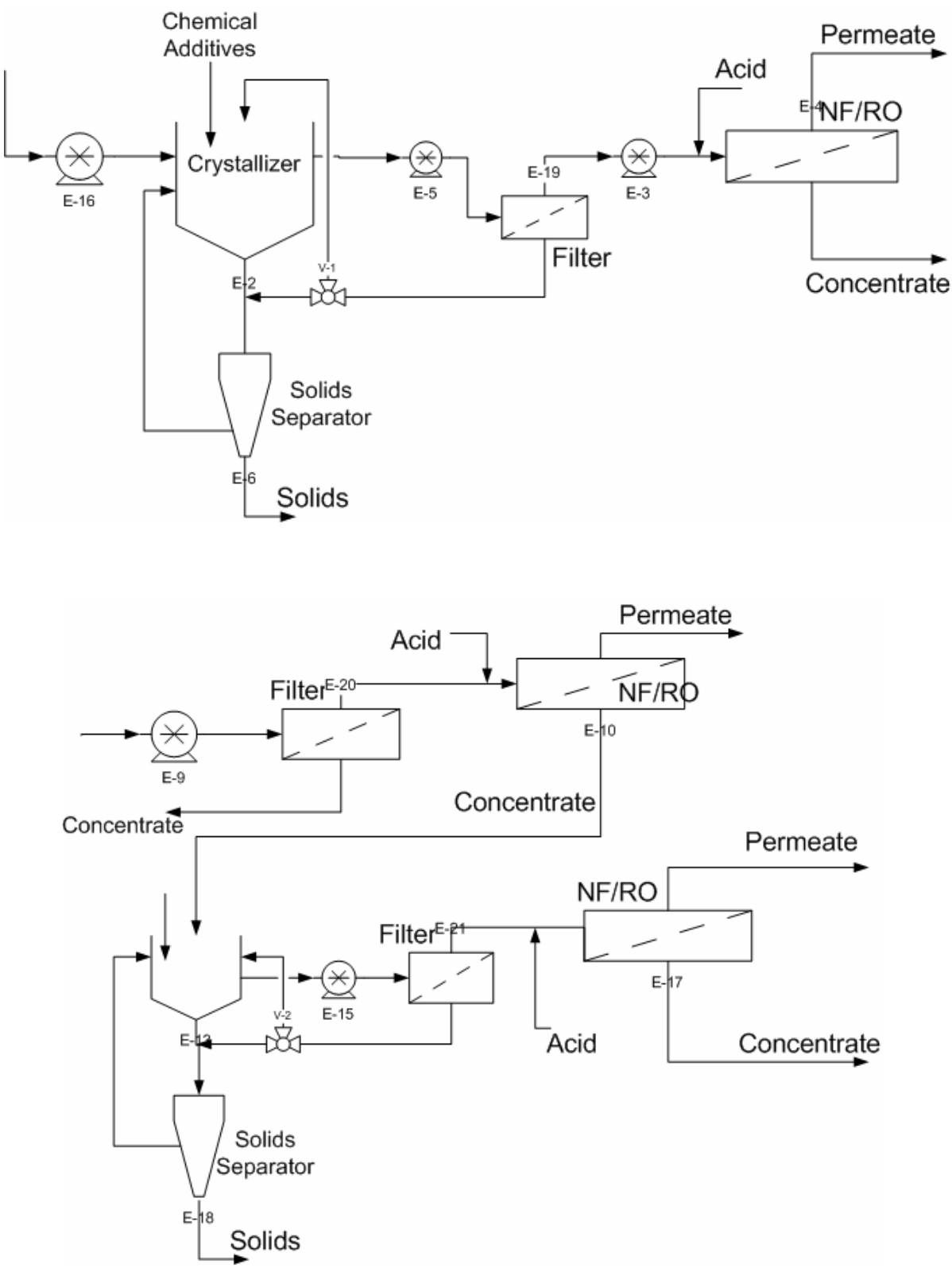


**Figure 7.3.** (a) Single step high recovery RO desalination, (b) two-step high recovery RO desalination.

ROPRO simulations were carried out for both the single-step and two-step strategies for a 5 MGD plant size for two overall recovery levels of 75% and 90%. The results are shown in Tables7.2 and 7.3. In all cases, the final permeate quality in terms of total dissolved solids (TDS) was within the recommended limit of 750 mg/L for agricultural water utilization. In order to prevent calcite scaling, the pH of the feed to the RO units was specified at a level that would keep the calcite saturation index at or just below unity. The single step desalting IAP (Fig. 7.3a) required feed pH of 6 to keep the solution undersaturated with respect to calcite. For all other cases the feed pH was specified at 6.5.

(a)

(b)

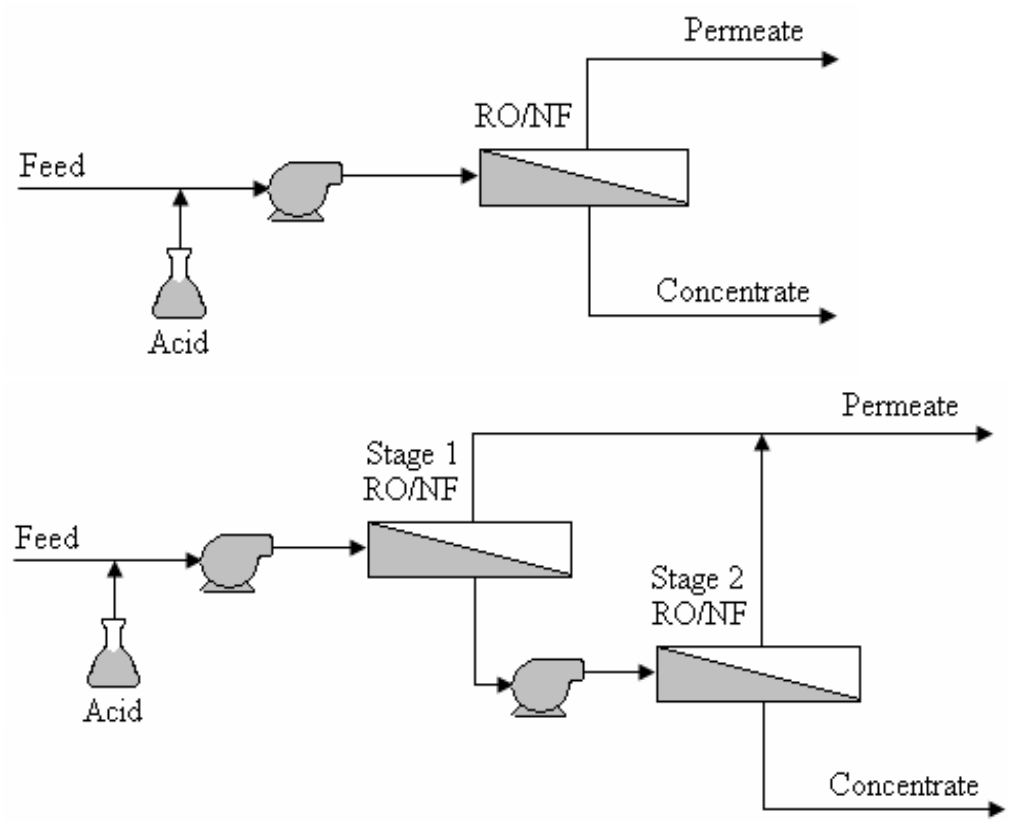


**Figure 7.4.** RO/NF designs: (a) Single-stage module configuration, (b) Two-stage RO module arrangement

### 7.4.2 Single Step APS-Membrane Desalting

In the single-step APS-RO desalting, accelerated precipitation softening (APS) treatment for calcium removal is applied to the total feed volume. In the first simulation APS treatment of the feed was specified for 76% calcium removal (Fig. 7.5a). This level of APS treatment enabled 75% product water recovery in the membrane desalting stage while maintaining the saturation index for gypsum below unity (Table 7.2). Recovery of 60% was attained in the first stage with 37.6% recovery obtained in the second stage. The use of low pressure high flux RO membrane (TFC-ULP for both stages) enabled operation at pressure that did not exceed 260 psi with a concentrate of about 35 g/L TDS.

In order to increase the product water recovery level a two-stage membrane desalting configurations was explored for RO desalting. Calcium removal from the feed (via APS) was specified at a level of 89% in order to meet the objective of 90% product water recovery (Fig., 7.5b and Table 7.2). The feed was first treated by APS so as to attain 89% calcium removal from the feed. However, in order to meet the target permeate TDS of 750 mg/L, extra high rejection RO (XR-RO) was used in both membrane stages, resulting in higher pressure requirements (430 psi for stage 1 and 560 psi for stage 2). Water recovery of 79.5% was obtained for the first stage and 51% was attained in the second stage. It is noted that the high permeate quality in the first stage compensates for the lower permeate quality in the second stage (due to extremely high TDS that must be handled during the second RO stage).

### 7.4.3 Two-Step APS-Membrane Desalting

In the two-step APS-RO process the feed was first desalted to achieve product water recovery of 54.3% (Table 7.3). This level of recovery is possible with the application of antiscalants since the saturation index for gypsum is 2.16 which is below the recommended limit of 2.5. Desalting was achieved with a single pass ULP module (which is essentially an NF membrane) to achieve permeate TDS was below 500 mg/L at operating pressure of 213 psi (Table 7.3).

In order to achieve 75% overall product water recovery the primary RO concentrate was desalted in a secondary RO treatment after first being treated by APS with specified 74% calcium removal (Fig. 7.6a). A single pass ULP module was also utilized operating at a pressure of 341 psi. Water recovery in this second desalting stage was at 45.3% with a concentrate TDS

of about 37,000 mg/L. It is noted that operation at a lower pressure is possible by decreasing the permeate flux and increasing the number of membrane modules.

Higher product water recovery can be achieved by utilizing a two-stage module configuration for the secondary desalting step. The primary desalting step was achieved with a TFC-ULP membrane operating at pressure of 213 psi at 54.3% product water recovery (Fig. 7.6b and Table 7.3). The primary membrane desalting concentrate (~20,500 mg/L TDS) is treated by APS to achieve a specified calcium removal of 89%. The high TDS of the primary RO concentrate required an extra high rejection RO membrane (TFC-XR) for both stages of the secondary membrane desalting step. Product water recovery of 63% and 40.5% were attained for the first and second stages, respectively, of the secondary desalting step. This enabled 90% overall product water recovery with the first and second stage secondary RO desalting units operating at pressures of 562 psi and 638 psi, respectively (Table 7.3). It is noted that the operating pressure can be decreased somewhat by increasing the number of elements which would allow operating at a lower flux.

It is important to note that the above simulations were conducted to demonstrate the possible process configurations and level of achievable recovery. The configurations and the operating conditions were not optimized with respect to process cost, recovery or product water quality. Notwithstanding, the present simulations clearly demonstrate that even for the most difficult source water (highest saturation with respect to gypsum), high recovery is possible provided that a chemical calcium removal step is integrated with membrane desalting.

In order to evaluate the feasibility of high recovery, a series of experiments were carried out, as described in Section 7.5, to evaluate the effectiveness of APS and antiscalants treatment to achieve the above levels of product water recovery. The experiments consisted of APS treatment with $Na_2CO_3$ and NaOH dosing and membrane scaling tests to evaluate antiscalants effectiveness.

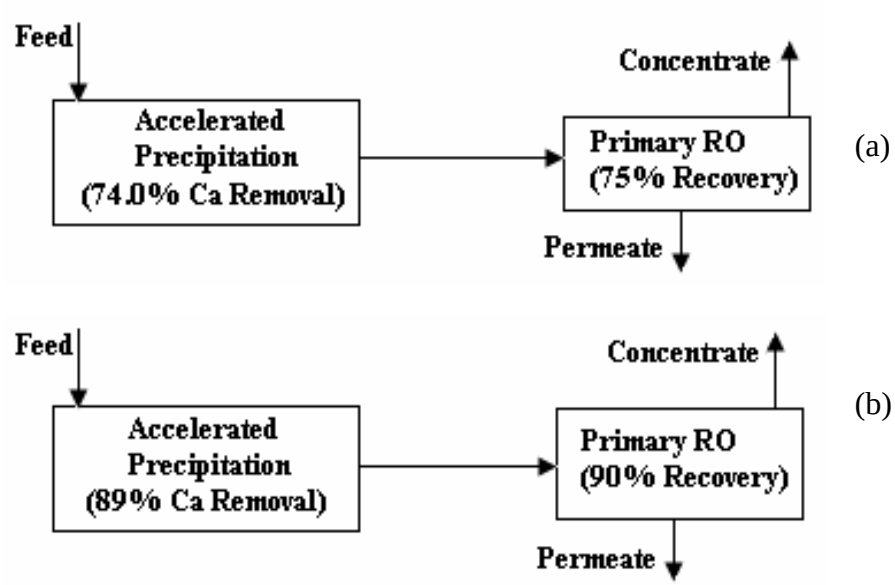


**Figure 7.5.** Single-step high recovery desalination with precipitation of the feed stream for calcium removal: (a) 75% Recovery, (b) 90% Recovery

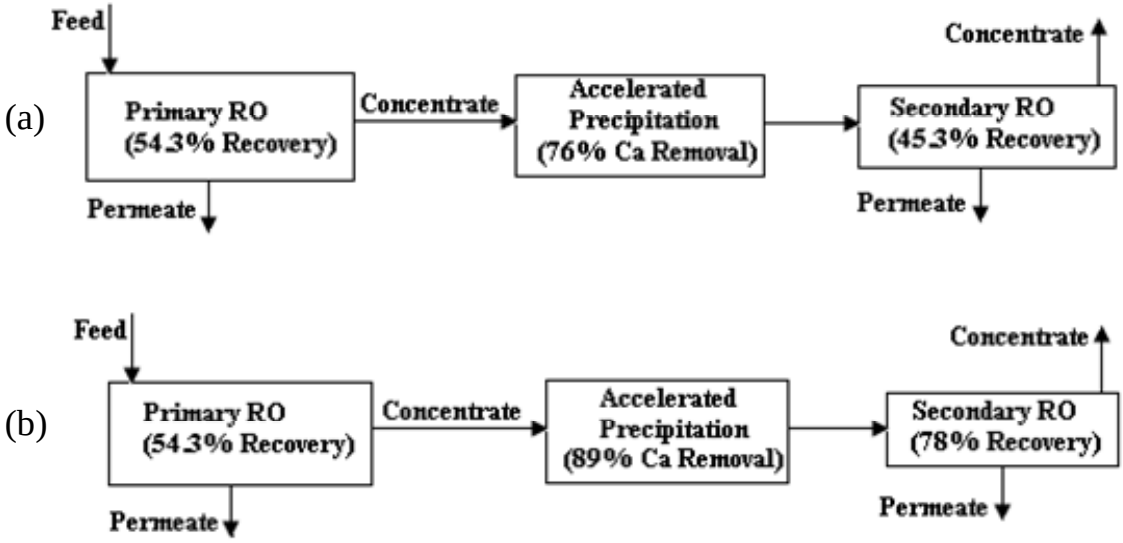


**Figure 7.6** Two-step high recovery desalination with inter-step precipitation for calcium removal: (a) 75% Recovery, (b) 90% Recovery

**Table 7.2.** Simulation results for a single step high recovery 5 MGD desalination of agricultural drainage water (OAS site). The primary RO feed is treated by accelerated precipitation softening.

| | **75% Recovery** | **90% Recovery** |
|---|---|---|
| **Membrane Stages** | Two Stages | Two Stages |
| **Element Type** | ULP-RO / NF | XR-RO / XR-RO |
| **Accelerated Precipitation** | | |
| % Calcium Removal | 76% | 89% |
| **Feed Flow Rate (MGD)** | 5 | 5 |
| **Stage 1** | | |
| Recovery | 60% | 79.5% |
| Pressure w/ FA (psig) | 228 | 430 |
| Elements per vessel | 4 | 5 |
| Element | | |
| Bank 1 | TFC 8823ULP-400 | TFC 8822XR-400 |
| Bank 2 | TFC 8823ULP-400 | TFC 8822XR-400 |
| Number of Vessels (Permeate Flux) | | |
| Bank 1 | 90 (16.9 GFD) | 114 (15 GFD) |
| Bank 2 | 43 (7.8 GFD) | 57 (4.9 GFD) |
| **Stage 2** | | |
| Recovery | 37.60% | 51% |
| Pressure w/ FA* (psig) | 254.9 | 563.9 |
| Elements per vessel | 5 | 7 |
| Element | | |
| Bank 1 | TFC 8923S-400 | TFC 8822XR-400 |
| Bank 2 | - | - |
| Number of Vessels (Permeate Flux) | | |
| Bank 1 | 34 (11 GFD) | 47 (4 GFD) |
| Bank 2 | - | - |
| **Step TDS (mg/L)** | | |
| Feed | 9,764 | 9,765 |
| Concentrate | 36,873 | 9,0763 |
| Permeate | 747 | 721 |
| **Overall Permeate TDS (mg/L)** | 747 | 721 |
| **Final Concentrate** | | |
| Flow Rate (MGD) | 1.25 | 0.50 |
| $SI_{Gypsum}$ | 0.976752 | 0.95 |
| $SI_{Calcite}$ (pH) | 0.43 (pH 7.0) | 0.27 (pH 6.9) |
| Osmotic Pressure (psi) | 220 | 539 |

* FA: Fouling Allowance = 15 % ; Feed pH was set to 6 by the addition of $H_2SO_4$

**Table 7.3. S**imulation results for a two-step high recovery 5 MGD desalination of agricultural drainage water (OAS site). The primary RO concentrate is treated by accelerated precipitation.

| | **Primary Step** | **Secondary Step** (75% Overall Recovery) | **Secondary Step** (90% Overall Recovery) |
|---|---|---|---|
| **Step Design** | Single Stage | Single Stage | Two Stages |
| **Element Types** | ULP-RO / NF | ULP-RO | XR-RO / HR-RO |
| **Accelerated Precipitation** | | | |
| % Calcium Removal | - | 74% | 89% |
| **Feed Flow Rate (MGD)** | 5 | 2.28 | 2.28 |
| **Water Recovery** | | | |
| Primary | 54.3% | 54.3% | 54.3% |
| Secondary | - | 45.3% | 78.0% |
| Overall | 54.3% | 75% | 90% |
| **Stage 1** | | | |
| Recovery | 54.3% | 45.3% | 63.0% |
| Pressure w/ FA (psig) | 213 | 341 | 562 |
| Elements per vessel | 4 | 6 | 5 |
| Element | | | |
| Bank 1 | TFC 8823ULP-400 | TFC 8823ULP-400 | TFC 8822XR-400 |
| Bank 2 | TFC 8923S-400 | - | TFC 8822XR-400 |
| Number of Vessels (Permeate Flux) | | | |
| Bank 1 | 63 (17.2 GFD) | 36 (12 GFD) | 40 (14.9 GFD) |
| Bank 2 | 43 (14.2 GFD) | - | 20 (6.2 GFD) |
| **Stage 2** | | | |
| Recovery | - | - | 40.50% |
| Pressure w/ FA* (psig) | - | - | 637.9 |
| Elements per vessel | - | - | 5 |
| Element | | | |
| Bank 1 | - | - | TFC 8822HR-400 |
| Bank 2 | - | - | TFC 8822HR-400 |
| Number of Vessels (Permeate Flux) | | | |
| Bank 1 | - | - | 34 (5 GFD) |
| Bank 2 | - | - | - |
| **Step TDS (mg/L)** | | | |
| Feed | 9651 | 20970 | 20906 |
| Concentrate | 20548 | 37461 | 91191 |
| Permeate | 481 | 1057 | 1065 |
| **Overall Permeate TDS (mg/L)** | 481 | 640 | 712 |
| **Final Concentrate** | | | |
| Flow Rate (MGD) | 2.285 | 1.25 | 0.50 |
| $SI_{Gypsum}$ | 2.16 | 1.02 | 0.96 |
| $SI_{Calcite}$ (pH) | 0.62 (pH 6.8) | 0.23 (pH 6.7) | 0.67 (pH 7.1) |
| Osmotic Pressure (psi) | 127 | 227 | 536 |

* FA: Fouling Allowance = 15 % ; Feed pH was set to 6 by $H_2SO_4$ addition.

## 7.5 Antiscalant Effectiveness

In order to assess the effectiveness of antiscalants treatment in enabling one to reach a reasonable recovery in primary RO desalting (Table 7.3), bulk crystallization tests were first conducted with a model OAS/E solution at 20$^{o}$C (Table 7.4). The crystallization induction time was determined following the approach described in Section 4.2). The crystallization induction time for the feed solution (without antiscalants addition) was determined to be about 40 minutes (Fig. 7.7a). Upon the addition of 3 ppm of the antiscalants Flocon 100, precipitation was not observed even after a period of seven days (Fig. 7.7b). The above results clearly indicate that the antiscalant should be effective in retarding bulk crystallization.

**Table 7.4.** Composition of OAS Model solutions representing primary RO desalination feed and concentrate (54.3 % recovery).

| | **Feed** (mM) | **Concentrate** (mM) |
|---|---|---|
| $Na_2SO_4$ | 49.28 | 107.61 |
| $MgSO4.7H_2O$ | 9.15 | 19.86 |
| $CaCl_2.2H_2O$ | 11.29 | 24.52 |
| $NaNO_3$ | 0.73 | 1.23 |
| $NaHCO_3$ | 2.91 | 4.39 |
| pH | 7.8 | 6.8* |
| $SI_{Gypsum}$ | 0.99 | 2.16 |
| $SI_{Calcite}$ | 3.98 | 0.61 |

* pH adjusted using HCl

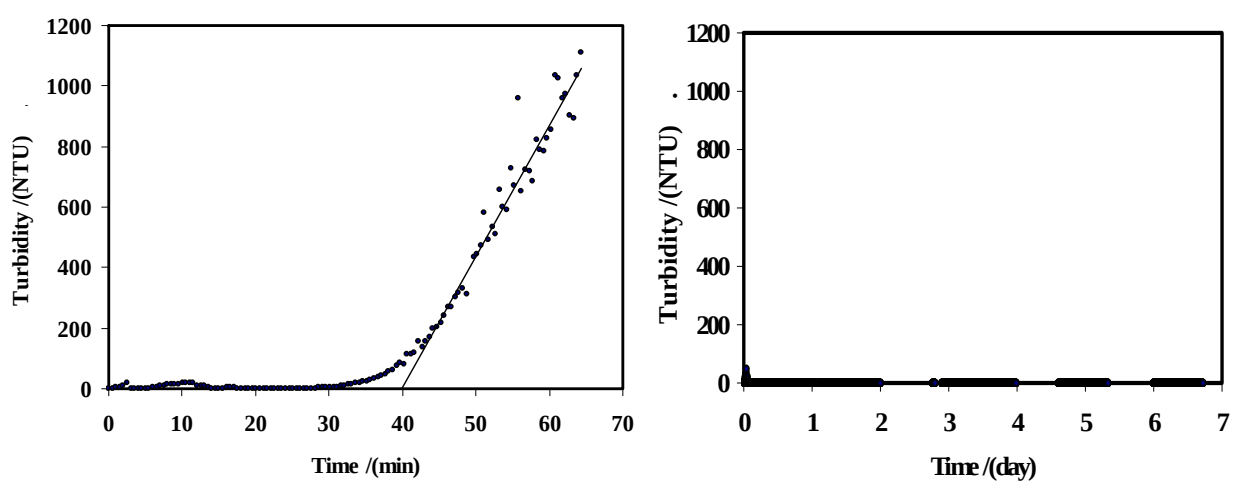


**Figure 7.7.** Bulk crystallization of OAS/E model solution at $SI_{gypsum}$ = 2.16 (Brine concentrate from primary Ro at recovery of 54.3 %: a) No Antiscalant b) 3 ppm Flocon 100.

Scaling due to surface crystallization was evaluated in a membrane scaling test with a model solution, dosed with 3 ppm antiscalants, using the dual cell plate-and-frame RO system (Fig. 5.1) following the procedure described in Section 5.4 and Section 5.8. The scaling test was conducted at feed crossflow velocity of 0.11 m/s and transmembrane pressure of 270 psi. At the above conditions, the average concentration polarization level (CP) was estimated to be 1.74 which resulted in an average saturation index of gypsum ($SI_{gypum}$) at the membrane surface of 1.96. It is noted that the above CP and $SI_{gypum}$ values represent average conditions since both these parameters increase in magnitude as the membrane channel exit is approached. The flux decline results shown in Fig. 7.8 indicate less than 2-3% flux decline over the 24 hour test period, which is well within the experimental error of the diagnostic test. The above results clearly suggest that the antiscalants treatment at a dose of 3 ppm was effective in mitigating scaling. Considering that the feed convective residence time in a commercial RO system is much shorter than the 24-hr test period (likely to be in on the order of minutes or less), it is possible that a lower antiscalants dose could be applied and further testing with actual field water samples may be warranted.

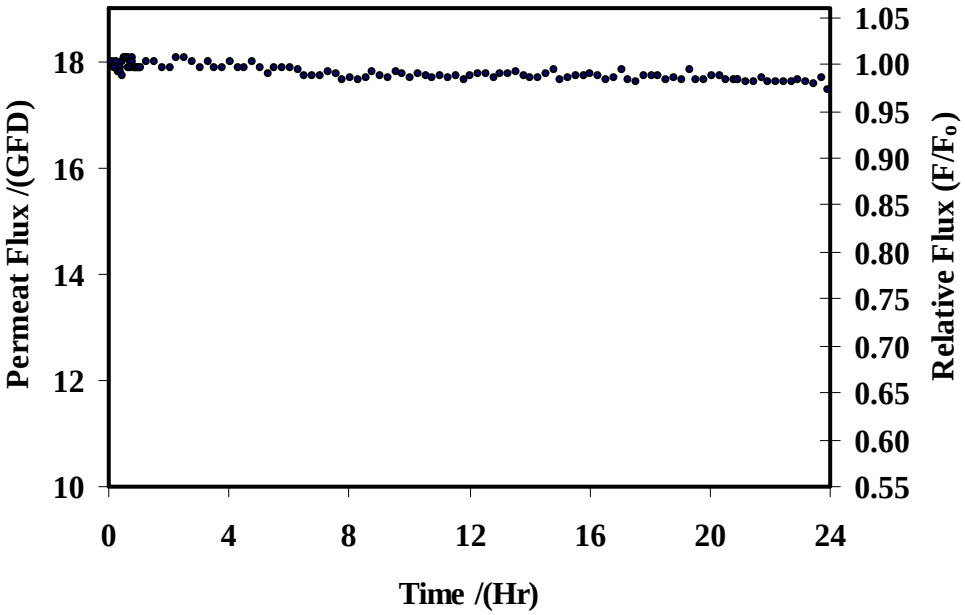


**Figure 7.8**. Membrane diagnostic scaling test of OAS/E model solution. Initial saturation index of gypsum at the membrane surface = 1.96, 3 ppm dosage of the antiscalants Flocon 100.

## 7.6 Calcium Removal by Accelerated Precipitation Softening

The feasibility of calcium removal via dosing with either $Na_2CO_3$ or NaOH was first evaluated via theoretical equilibrium calculations. The analysis was carried out for the primary RO model solution feed (Table 7.4) and for a primary RO concentrate obtained by RO desalting of the feed at 54.3% recovery. The theoretical results are depicted in Fig. 7.9 in which the alkali dose refers to the addition of either $Na_2CO_3$ or NaOH. The OAS/RO feed water is limited in terms of its carbonate concentration. Therefore, the addition of NaOH will result in calcium carbonate precipitation up to the point where the carbonate ion has been exhausted. Therefore, the addition of NaOH alone is insufficient and $Na_2CO_3$ addition is needed to increase the carbonate concentration. As demonstrated in Fig. 7.9, calcium removal can be achieved by either $Na_2CO_3$ dosing alone or in combination with NaOH.

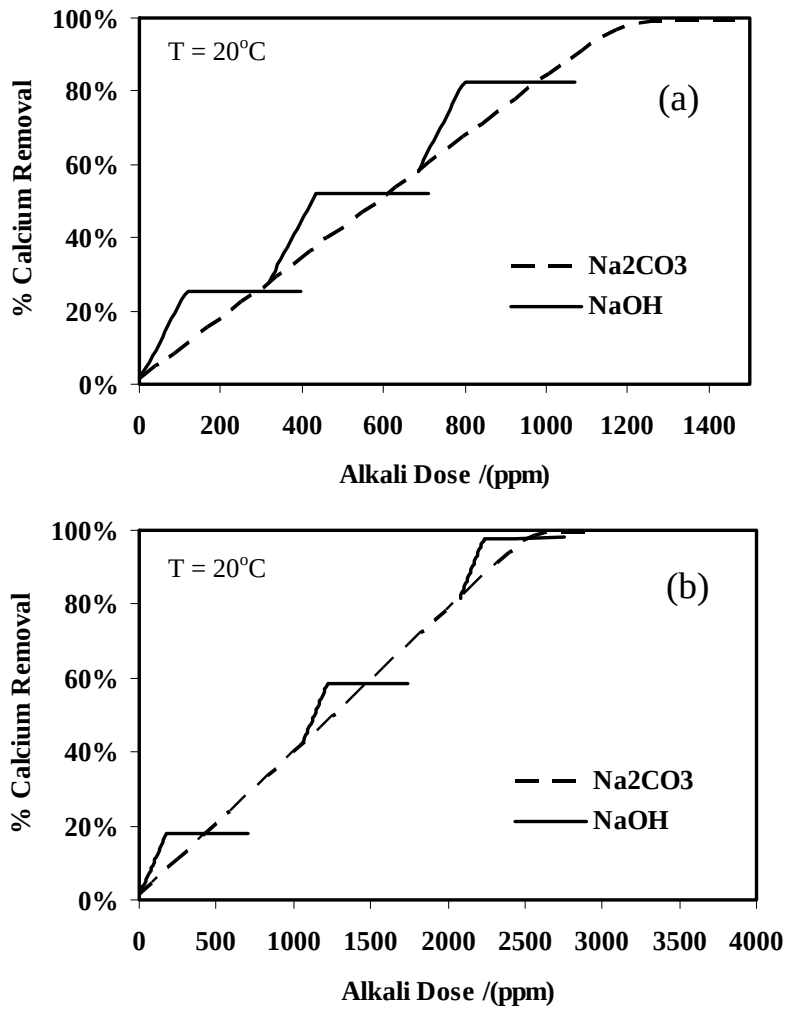


**Figure 7.9**. Theoretical equilibrium analysis of calcium by accelerated precipitation softening of OAS/E model solution: (a) primary RO feed, (b) primary RO concentrate from 54.3% recovery.

A series of experiments were conducted to verify the reliability of the equilibrium calculations. Accelerated precipitation experiments were carried out over a period of 30 hours. In the first set of studies the primary RO feed model solution (without antiscalants addition) was dosed with different amounts of $Na_2CO_3$ along with the addition of calcite seeds at a load of 1.4 g/L. Clearly, the experimental results (Fig. 7.10a) are in excellent agreement with the theoretical equilibrium analysis. In a second set of experiments the primary RO feed was dosed with 878 mg/L of $Na_2CO_3$ so as to obtain calcium removal of about 71%, followed by the addition of sodium hydroxide. As shown in Fig. 7.10b, the experimental percent removal of calcium was lower (especially at higher NaOH dose) than estimated based on the equilibrium analysis. It is believed that $CO_2$ exchange with the atmosphere in the present open precipitation system, an effect not considered in the theoretical analysis, contributed to the observed deviation.

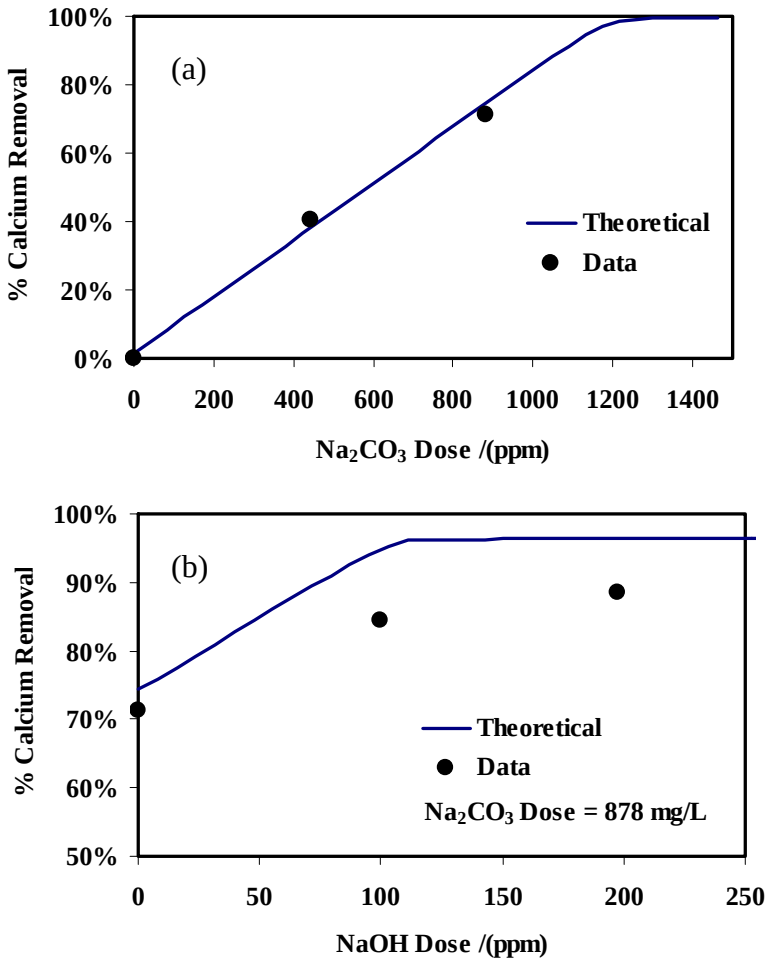


**Figure 7.10.** Calcium removal by accelerated precipitation softening of OAS/E model feed solution (Table 7.4). (a) $Na_2CO_3$ dosing with calcite seed load of 1.4 g/L, (b) NaOH dosing along with the initial addition of 878 mg/L $Na_2CO_3$ and calcite seed load of 1.4 g/L.
Equilibration period= 30 hr, T= 20$^o$C.

In order to evaluate the feasibility of calcium removal from the primary RO concentrate (produced via desalting at 54.3% water recovery), batch accelerated precipitation softening (APS) experiments were carried out with $Na_2CO_3$ and NaOH dosing along with calcite seeding. Antiscalant (Flocon 100) was added to the model primary RO concentrate solution (Table 7.4) at a dose of 6 ppm. The results of APS with $Na_2CO_3$ dosing are in excellent agreement with the equilibrium calculations (Fig. 7.11a). The experimental data confirmed that antiscalants in the concentrate did not adversely impact calcium removal by APS. In a second test, the model RO concentrate was first dosed with 2083 mg/L $Na_2CO_3$ to achieve about 78% calcium removal, followed by NaOH dosing to calcium removal in excess of 90% (Fig. 7.11b). The experimental calcium removal results followed the theoretical predictions, but were consistently over predicted (1%-6%), possibly due to $CO_2$ exchange with the atmosphere in the open experimental system.

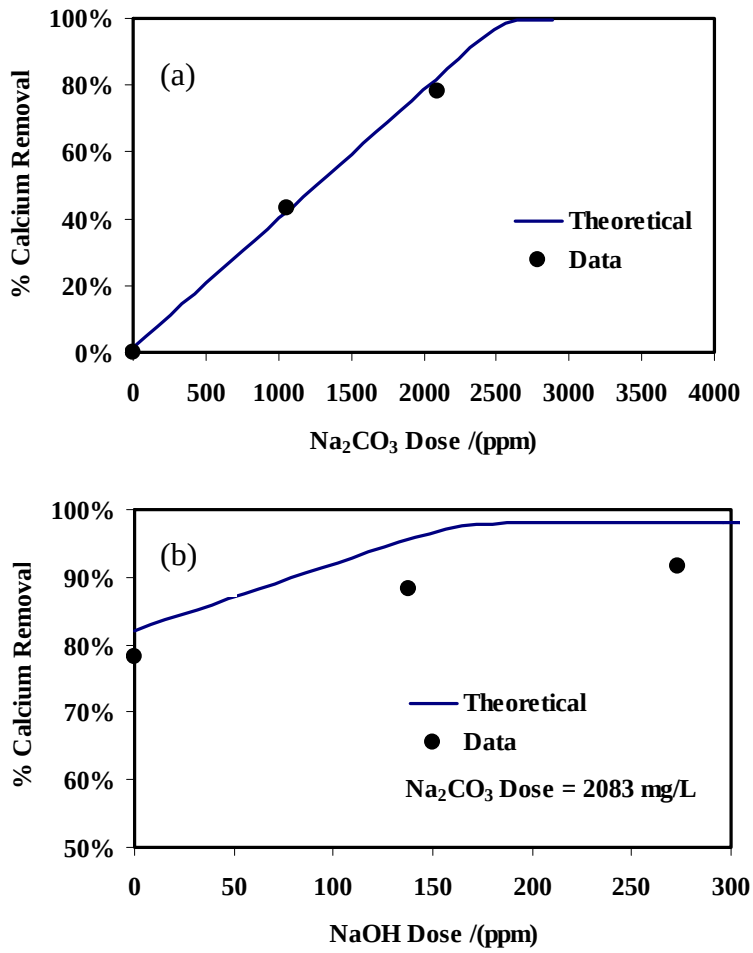


**Figure 7.11.** Calcium removal by accelerated precipitation softening of OAS/E model solution of primary RO concentrate obtained from RO desalting at recovery of 54.3%. (a) $Na_2CO_3$ dosing with calcite seed load of 1.4 g/L, (b) NaOH dosing along with the initial addition of 2083 mg/L $Na_2CO_3$ and calcite seed load of 1.4 g/L. Equilibration period= 30 hr, T= 20$^o$C.

As a final evaluation of the feasibility of APS, the precipitation kinetics was assessed using the OAS/E model solution for the primary RO feed and for the primary RO concentrate (produced at 54.4% recovery). These experiments were conducted in a 600 ml vessel in which the depletion of calcium was followed over the course of the precipitation process. Calcium concentrations at a given time, relative to the initial concentration, are plotted in Figs. 7. 12a and 7.12b for APS treatment of the primary RO and RO concentrate, respectively. Precipitation was induced by the addition of $Na_2CO_3$ and calcite seeding of 1.4 g/L. Steady state with respect to calcium precipitation was approached within ~10-20 minutes. It is noted that for APS treatment of the steady-state removal was closely predicted by the equilibrium prediction. For the primary RO concentrate, the time to reach steady state was longer than for the primary RO feed. It is noted that for the RO concentrate to which 6 ppm antiscalants was added, the experimental calcium concentration at pseudo-steady state was somewhat higher (~ 3%) than the equilibrium prediction. In other words, the experimental percent of calcium removal was lower than predicted. The above deviation is plausibly due to the presence of the antiscalants which complexes with calcium nuclei and also retards crystal growth. It is possible that over a longer period of time, the calcium concentration will decline and approach the predicted equilibrium level.

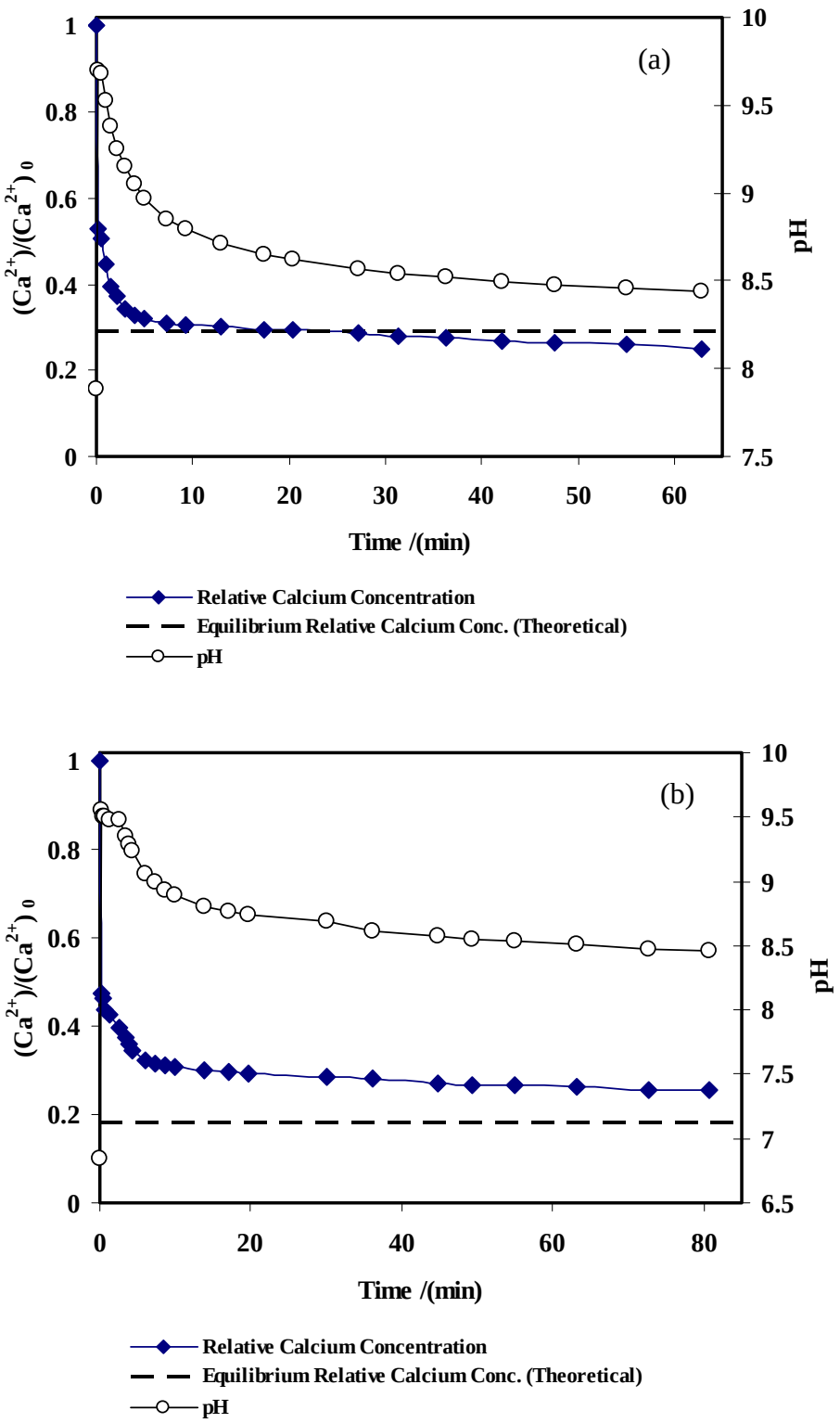


**Figure 7.12.** Kinetics of accelerated precipitation of OAS model solutions: (a) Primary RO feed (841 mg/L $Na_2CO_3$ dosage, 1.4 g/L calcite seed load, no antiscalant), (b) Primary RO concentrate (2068 mg/L $Na_2CO_3$ dosage, 1.4 g/L calcite seed load, 6 ppm antiscalant). T = 24°C.

# 8.0 Summary and Recommendations

A systematic approach was developed to assess product water recovery limits as imposed on RO desalination by mineral salt scaling. A number of key laboratory diagnostic protocols, in addition to thermodynamic and process analyses, were utilized to analyze potential strategies for increasing product water recovery in membrane RO desalting of brackish groundwater. The study consisted of the following elements: (a) ranking of antiscalant effectiveness and selection of candidate antiscalants for low pressure RO desalting, (b) optimization of antiscalant dose via the combination of bulk crystallization studies and diagnostic membrane scaling experiments, (c) mineral scale characterization and quantification of membrane scaling propensity, (d) thermodynamic analysis of mineral salt solubility in multi-electrolyte solutions to assess conservative limits on product water recovery imposed by mineral salt precipitation, (e) process analysis and diagnostic laboratory bench-scale assessment of the potential for increased product water recovery via a combination of precipitation softening and antiscalant feed treatment.

Technical feasibility assessment of the limit on product water recovery can be carried out via a combination of process calculations and diagnostic laboratory studies. Such an approach is imperative for the San Joaquin Valley (SJV) given the wide range of water quality in the region. Primary RO desalting of SJV brackish groundwater is likely to be limited to 50%-75%; this level of recovery can be accomplished through the combination of nanofiltration, low pressure RO desalting and antiscalant treatment. Increasing recovery up 90% or higher is possible through reduction of scaling propensity by accelerated precipitation softening, followed by secondary RO desalting. However, high TDS (10,000-20,000 mg/L) of the concentrate from primary membrane desalting could require operation at pressures as high as about 600 psi. Clearly, the choice of process configuration would have to be determined based on overall economics and product end use specifications. A pilot-scale field study would be useful to demonstrate the technical feasibility of various process alternatives. Such a field study should be designed and refined with respect to process conditions based on the approach presented in the present study. Given that there can be significant seasonal variation in the composition of brackish water across the San Joaquin Valley, process configuration should be of sufficient flexibility to adapt to changing water composition. This would be an important consideration for field implementation of RO desalting of brackish groundwater in the San Joaquin Valley.

# 9. References


[1] M. Al-Ahmad, F.A.A. Aleem, A. Mutiri, and A. Ubaisy, Biofuoling in RO membrane systems Part 1: Fundamentals and control, *Desalination*, 132 (2000) 173.

[2] R.W. Lee, J. Glater, Y. Cohen, C. Martin, K. Kovac, M.N. Milobar, and D.W. Bartel, Low-pressure RO membrane desalination of agricultural drainage water, *Desalination*, 155 (2003) 109.

[3] S.B.S. Ghayeni, P.J. Beatson, R.P. Schneider, and A.G. Fane, Adhesion of waste water bacteria to reverse osmosis membranes, *Journal of Membrane Science*, 138 (1998) 29.

[4] H.C. Flemming, G. Schaule, T. Griebe, J. Schmitt, and A. Tamachkiarowa, Biofouling - the Achilles heel of membrane processes, *Desalination*, 113 (1997) 215.

[5] H.C. Flemming, *Mechanistic aspects of reverse osmosis membrane biofouling and prevention*, in *Membrane Technology*, Z. Amjad, Editor. 1992, Van Nostrand Reinhold: New York. p. 163.

[6] P. Campbell, R. Srinivasan, T. Knoell, D. Phipps, K. Ishida, J. Safarik, T. Cormack, and H. Ridgway, Quantitative structure-activity relationship (QSAR) analysis of surfactants influencing attachment of a Mycobacterium sp to cellulose acetate and aromatic polyamide reverse osmosis membranes, *Biotechnology and Bioengineering*, 64 (1999) 527.

[7] J.S. Baker, and Dudley, L.Y., Biofouling in membrane systems-A review, *Desalination*, 118 (1998) 81.

[8] J.E. Kilduff, S. Mattaraj, J.P. Pieracci, and G. Belfort, Photochemical modification of poly(ether sulfone) and sulfonated poly(sulfone) nanofiltration membranes for control of fouling by natural organic matter, *Desalination*, 132 (2000) 133.

[9] A.G.I. Dalvi, R. Al-Rasheed, and M.A. Javeed, Studies on organic foulants in the seawater feed of reverse osmosis plants of SWCC, *Desalination*, 132 (2000) 217.

[10] C. Gabelich, T.I. Yun, J.F. Green, I.H. Suffet, and W.R. Chen, Evaluation of precipitative fouling for colorado river water desalination using reverse osmosis, U.S. Department of the Interior, Bureau of Reclamation, Denver, CO 80225, DWPR No. 85, December 2002.

[11] W.Y. Shih, A. Rahardianto, R.W. Lee, and Y. Cohen, Morphometric characterization of calcium sulfate dihydrate (gypsum) scale on reverse osmosis membranes, *Journal of Membrane Science*, 252 (2005) 253.

[12] I. Atamanenko, A. Kryvoruchko, and L. Yurlova, Study of the scaling process on membranes, *Desalination*, 167 (2004) 327.

[13] Y.A. Le Gouellec and M. Elimelech, Calcium sulfate (gypsum) scaling in nanofiltration of agricultural drainage water, *Journal of Membrane Science*, 205 (2002) 279.

[14] E.E.A. Ghafour, Enhancing RO system performance utilizing antiscalants, *Desalination*, 153 (2003) 149.

[15] W.Y. Shih, K. Albrecht, J. Glater, and Y. Cohen, A dual-probe approach for evaluation of gypsum crystallization in response to antiscalant treatment, *Desalination*, 169 (2004) 213.

[16] D. Hasson, A. Drak, and R. Semiat, Induction times induced in an RO system by antiscalants delaying CaSO4 precipitation, *Desalination*, 157 (2003) 193.

[17] M. Al-Shammiri, M. Safar, and M. Al-Dawas, Evaluation of two different antiscalants in real operation at the Doha Research Plant, *Desalination*, 128 (2000) 1.

[18] D. Hasson, R. SEmiat, D. Bramson, M. Busch, and B. Limoni-Relis, Suppression of $CaCO_3$ scale deposition by antiscalants, *Desalination*, 118 (1998) 285.
[19] Z. Amjad, Applications of antiscalants to control calcium sulfate scaling in reverse osmosis systems, *Desalination*, 54 (1985) 263.
[20] F.H. Butt, F. Rahman, and U. Baduruthamal, Identification of Scale Deposits through Membrane Autopsy, *Desalination*, 101 (1995) 219.
[21] W.-Y.C. Shih, Y., *Topology and Functionality Effects on Surface Scale Formation*, in *Annual Meeting, Austin Convention Center*. 2004, AIChE: Austin, TX.
[22] R.-W. Lee, *Low pressure reverse osmosis membrane treatment of agricultural drainage water and surface water*, in *Chemical Engineering Department*. 2003, University of California, Los Angeles: Los Angeles.
[23] B.E. Corporation, Desalination pilot report for Buena Vista Water Storage District, preliminary progress report, for the 2002 irrigation season, (2002).
[24] C.J. Gabelich, T.I. Yun, B.M. Coffey, and I.H. Suffet, Pilot-scale testing of reverse osmosis using conventional treatment and microfiltration, *Desalination*, 154 (2003) 207.
[25] C.J. Gabelich, T.I. Yun, M.R. Cox, C.R. Bartels, J.F. Green, and I.H. Suffet. *Evaluating ultra-low pressure reverse osmosis for surface water desalination*. in *AWWA Technology Conference*. 1999. Long Beach, CA.
[26] C.J. Gabelich, F.W. Gerringer, J. Franklin, J. Gao, Y. Cohen, and I.H. Suffet. *Reverse osmosis pretreatment: challenges with conventional treatment*. in *2004 AWWA ACE, Orlando, Florida*. 2004.
[27] A. Rahardianto, Y. Cohen, and D.M. Williams, *Enhanced water recovery from primary membrane desalination concentrate by precipitative softening and secondary RO desalting*, in *AIChE 2004 Annual Meeting*. 2004, AIChE: Austin, TX.
[28] C.W. Li, J.C. Jian, and J.C. Liao, Integrating membrane filtration and a fluidized-bed pellet reactor for hardness removal, *Journal American Water Works Association*, 96 (2004) 151.
[29] J.H. Kweon and D.F. Lawler, Fouling mechanisms in the integrated system with softening and ultrafiltration, *Water Research*, 38 (2004) 4164.
[30] O. Kedem and G. Zalmon, Compact accelerated precipitation softening (CAPS) as a pretreatment for membrane desalination.1. Softening by NaOH, *Desalination*, 113 (1997) 65.
[31] Y. Cohen, J. Gao, A. Rahardianto, and J. Glater, *Enhanced Water Recovery from Membrane RO Concentrate: Process Evaluation, Membrane Scaling and Precipitation Kinetics*, in *AIChE 2003 Annual Meeting*. 2003, AIChE: San Francisco, CA.
[32] J. Gilron, D. Chaikin, and N. Daltrophe, Demonstration of CAPS pretreatment of surface water for RO, *Desalination*, 127 (2000) 271.
[33] Y. Oren, V. Katz, and N.C. Daltrophe, Compact accelerated precipitation softening (CAPS) with submerged filtration: Role of the $CaCO_3$ "cake" and the slurry, *Industrial & Engineering Chemistry Research*, 41 (2002) 5308.
[34] Y. Oren, V. Katz, and N.C. Daltrophe, Improved compact accelerated precipitation softening (CAPS), *Desalination*, 139 (2001) 155.
[35] G.J.G. Juby and C.F. Schutte, Membrane life in a seeded-slurry reverse osmosis system, *Water Sa*, 26 (2000) 239.
[36] G.J.G. Juby, C.F. Schutte, and J. van Leeuwen, Desalination of calcium sulphate scaling mine water: design and operation of the SPARRO process, *Water Sa*, 22 (1996) 161.

[37] W. Pulles, G.J.G. Juby, and R.W. Busby, Development of the slurry precipitation and recycle reverse-osmosis (SPARRO) technology for desalinating scaling mine waters, *Water Science And Technology*, 25 (1992) 177.
[38] S. Seewoo, R. Van Hille, and A. Lewis, Aspects of gypsum precipitation in scaling waters, *Hydrometallurgy*, 75 (2004) 135.
[39] S.L. He, J.E. Oddo, and M.B. Tomson, The seeded growth of calcium-sulfate dihydrate crystals in NaCL solutions up to 6-M and 90-degrees-C, *Journal of Colloid and Interface Science*, 163 (1994) 372.
[40] A.L. Zydney, Stagnant film model for concentration polarization in membrane systems, *Journal Of Membrane Science*, 130 (1997) 275.
[41] OLI, *OLI Analyzer 2.0*. 2005, OLI Systems, Morris Plains, NJ.
[42] J. Gilron and D. Hasson, Calcium-sulfate fouling of reverse-osmosis membranes - flux decline mechanism, *Chemical Engineering Science*, 42 (1987) 2351.
[43] M. Brusilovsky, J. Borden, and D. Hasson, Flux decline due to gypsum precipitation on RO membranes, *Desalination*, 86 (1992) 187.
[44] S. Lee, J. Kim, and C.H. Lee, Analysis of $CaSO_4$ scale formation mechanism in various nanofiltration modules, *Journal of Membrane Science*, 163 (1999) 63.
[45] J. Borden, J. Gilron, and D. Hasson, Analysis of RO flux decline due to membrane-surface blockage, *Desalination*, 66 (1987) 257.
[46] J. Gilron and D. Hasson, Calcium sulfate fouling of reverse osmosis membranes, *J. Chem. Eng. Japan*, 42 (1987) 2351.
[47] Hydranautics, Chemical Pretreatment of RO/NF, Application Bulletin, No. 111, Rev. B, 2003.